SAPIENZA
UNIVERSITÀ DI ROMA

Dipartimento di Chimica e Tecnologie del Farmaco

PhD Thesis

NMR Spectroscopy: A Versatile Tool for the Investigation of Organic Reaction Mechanisms and Metabolomics Analyses

by Deborah Quaglio

Supervisor:
Prof. Bruno Botta

Dottorato di Ricerca in Scienze Farmaceutiche – XXIX Ciclo

To my family

“Somewhere, something incredible is waiting to be known”

Carl Sagan

Abstract

This Ph.D. thesis focuses on two main topics:

Part A. Resorc[4]arene ω-Undecenyl Ester in the *Chair* Form as Macrocyclic Synthon for Olefin Metathesis

Olefin metathesis has become a powerful tool for the formation of carbon-carbon bonds and, therefore, for the synthesis of a number of molecules. This progress was recognized in 2005 with the award of NOBEL Prize in Chemistry to Yves Chauvin, Robert Grubbs and Richard Schrock for their work in this area. While the series of [2+2]cycloadditions and retro[2+2]cycloadditions that make up the pathways of ruthenium-catalysed metathesis reactions is well-established, the exploration of mechanistic aspects of alkene metathesis is going on. At first, we reported the tetramerization of (*E*)-2,4-dimethoxycinnamic acid ω-undecenyl ester with ethereal BF_3. The reaction gave three stereoisomers **1a**, **1b**, and **1c**, which were assigned as the *chair*, *cone*, and *1,2-alternate* conformations, respectively. Undecenyl resorc[4]arene **1a**, which featured the simplest pattern of substituent, was submitted to olefin metathesis using the second generation Grubbs complex as the catalyst. Depending on the reaction conditions, different products were isolated: a bicyclic alkene **2a**, a linear dimer **3a**, and a cross-linked homopolymer **P1a**. Moreover, we detected for the first time the formation of a ruthenium-carbene-resorc[4]arene complex during the metathesis reaction of resorc[4]arene olefin **2a** with the first generation Grubbs catalyst in $CDCl_3$. We developed an NMR analytical protocol which proved capable of yielding both qualitative and quantitative information. In the first case, we were able to identify the complex **3a[Ru]** as a key intermediate in the ROM-CM sequence of reactions, giving us a definitive proof of the previously hypothesized mechanism. As a further feedback of the pathway, we performed a quantitative analysis using benzene in the place of $CDCl_3$, due to the poor stability of the catalyst in such a solvent. The reaction allowed the isolation of decomposition products of the

ruthenium-carbene-resorc[4]arene complex **2a[Ru]** such as compound **4a**, which, due to the presence of still reactive alkene functions, proved to behave as propagating alkylidene species leading to further decomposition products.

Part B. Metabolomics Studies by NMR Spectroscopy

Metabolomics provides a direct measure of the state of the cell or biological system, where changes in the metabolome capture how the system responds to environmental or genetic stress. Specifically, a drug or an active chemical lead would be expected to perturb the metabolome of a cell or tissue upon treatment. The two leading analytical approaches to metabolomics are mass spectrometry (MS) and nuclear magnetic resonance (NMR) spectroscopy. In particular, NMR technique accounts for high reproducibility, quantitative determination of a wide dynamic range, and the capability to determine the structure of unknown metabolites.

Cells of high-grade tumors, including medulloblastoma (MB) and glioblastoma (GBM), must similarly balance energy metabolism with the need to synthesize the macromolecules essential for tumor growth. Cells with large ATP requirements are likely to be disadvantaged by aerobic glycolysis because glycolysis generates less ATP per molecule of glucose than oxidative phosphorylation. Proliferating cells, however, may use aerobic glycolysis to satisfy the competing needs for both energy generation and the accumulation of biomass. Recently, it has been demonstrated that Sonic Hedgehog (SHH) pathway activation in granule cell progenitors (GCPs), responsible of MB development, induces transcription of hexokinase 2 (HK2) and pyruvate kinase M2 (PKM2), two key gatekeepers of glycolysis. The process is mediated by the canonical activation of the GLI transcription factors and causes a robust increase of extracellular lactate concentration.

Glabrescione B (GlaB), an isoflavone naturally found in the seeds of *Derris glabrescens* (Leguminosae), turned out to be an efficient inhibitor of the growth of HH/GLI-dependent tumors and cancer

stem cells *in vitro* and *in vivo*. Here, we reported the GlaB activity on both human MB DAOY and murine glioma GL261 cell models *in vitro* and *in vivo*. In order to evaluate how the GlaB-treatment affects cell metabolism as a consequence of GLI1 inhibition, untargeted NMR metabolomics analyses of cellular lysates and conditioned media were performed in both cell lines. For this purpose, a simple, fast, and reproducible sample preparation protocol was developed. To reduce bias in the interpretation of the experiments, it was decided to produce from five to seven biological replicates for each treated and untreated group. The 1D ^{1}H NMR spectra were acquired to determine the metabolic fingerprints of the treated and untreated cancer cells. Notably, the NMR metabolomics approach revealed a typical *endo*-metabolic phenotype of the cells under investigation. Both the *exo*- and *endo*-metabolome of the DAOY and GL261 cell lines resulted to be completely changed after 24 h and 48 h of GlaB administration, respectively. The levels of most metabolites decreased after treatment, consistently with possible apoptosis phenomenon.

Contents

Part B

Metabolomics Studies by NMR Spectroscopy

Part A

Resorc[4]arene ω-Undecenyl Ester in the *Chair* Form as Macrocyclic Synthon for Olefin Metathesis

The present part of the thesis deals with a research activity carried out at the Dipartimento di Chimica e Tecnologie del Farmaco at Sapienza Università di Roma, under the supervision of Prof. Bruno Botta.

Chapter A1
General Introduction

A1.1 Emerging class of macrocyclic receptors

A1.1.1 Calixarenes

Calixarenes are macrocyclic molecules containing phenolic rings bridged by methylene groups and are among the most ubiquitous host molecules in supramolecular chemistry (Arduini et al., 2001; Casnati et al., 2003; Gutsche, 1998; Katsuhiko and Toyoki, 2006; Ludwig, 2005; Mandolini and Ungaro, 2000). The basic molecular scaffolds are, in general, simple to prepare in high yields from cheap starting compounds: they derive from the condensation of phenols and formaldehyde. These compounds are characterized by an hydrophobic cavity which allows the interactions with neutral molecules (Arduini et al., 2001), but they can also be derivatized in the lower rim or in para positions on the aromatic nuclei (upper rim) with catalytic centers or other functional groups which favor interactions with ions (Figure 1.1) (Dalla Cort and Mandolini, 2000).

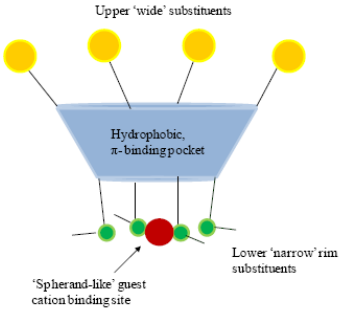

Figure 1.1. Anatomy of a calix[4]arene in the *cone* conformation.

The parent calixarenes are flexible during their high temperature synthesis, the rotation of the phenolic moieties about the bridging CH_2 groups possible, but the smallest members of the class "freeze out" upon cooling to ambient temperatures (Steed and Atwood, 2009). This is an important consideration when working with calix[4]arenes, macrocyclic molecules consisting of four phenol units connected via methylene bridges in the *ortho* position with respect to the hydroxyl group. They exist in different conformers that are hard to interconvert and become immobilized in a particular case if substituents are bound in the lower rim, even if re-heated to relatively high temperatures. Four principal conformers are observed at room temperature (Figure 1.2). If all four upper rim substituents are in the same orientation, then a *cone* conformer results, which is the average C_{4v} symmetry structure resulting from a

fast equilibrium between two equivalent C_{2v} *flattened cone* conformers (Abis et al., 1988). If one phenolic group is inverted with respect to the others, a *partial cone* conformer is found. Finally, two possibilities exist when two phenol rings are inverted: *1,3-alternate* and *1,2-alternate*. Similar descriptions exist also for larger calixarenes, although these compounds are often conformationally dynamic and only frozen out in the solid state or in low temperature experiments.

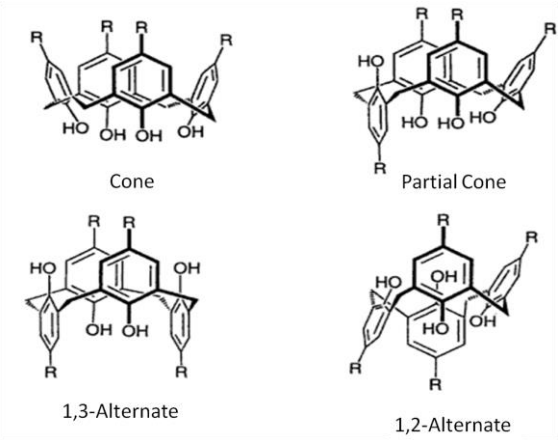

Figure 1.2. Calix[4]arene conformers.

A1.1.2 Resorcarenes

Condensation products obtained from the reaction between aliphatic aldehyde and resorcinol were first reported in the XIX century (Baeyer, 1872a**;** Baeyer, 1872b), but only in 1968 their

structure was finally proved by Erdtman and co-workers by a single crystal X-ray analysis (Erdtman et al., 1968). A suitable trivial name for these molecules was not found earlier, but recently the term resorc[4]arene (or resorcarene, in a shorter version) seems to be generally accepted to indicate cyclic tetramers made by resorcinol units connected with methylene bridges. A simplified general structure of a resorcarene is shown in Figure 1.3 with typical atoms (Botta et al., 2005).

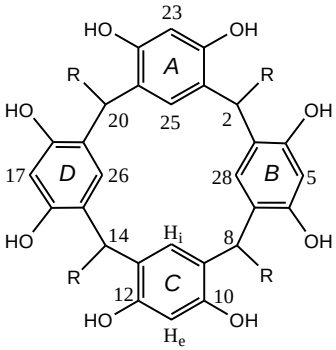

Figure 1.3. General structure of resorcarenes.

❖ *Conformations of resorcarenes*

The stereochemistry of resorcarenes may be defined as the combination of three elements (Timmerman et al., 1996):

1. The conformation of the macrocyclic ring, which can adopt five extreme symmetrical arrangements: *crown* or *cone* (C_{4v} symmetry), *boat* or *flattened cone* (C_{2v}), *diamond* or *1,2-alternate* (C_s), *saddle* or *1,3-alternate* (D_{2d}), and *chair* (C_{2h}). The five architectures are presented both in 3D (Figure 1.4) and in sketched representations (Figure 1.5). The most common conformation of resorc[4]arenes (*cone*) is very close in solution to the one of calixarenes, but it is, in reality, the result of the equilibrium between two equivalent forms (Högberg, 1980a, Högberg, 1980b). Only one form (namely, *flattened cone*) characterizes the structure of the macrocycle in solid (Erdtman et al., 1968) and gas (Botta et al., 1994) phases.

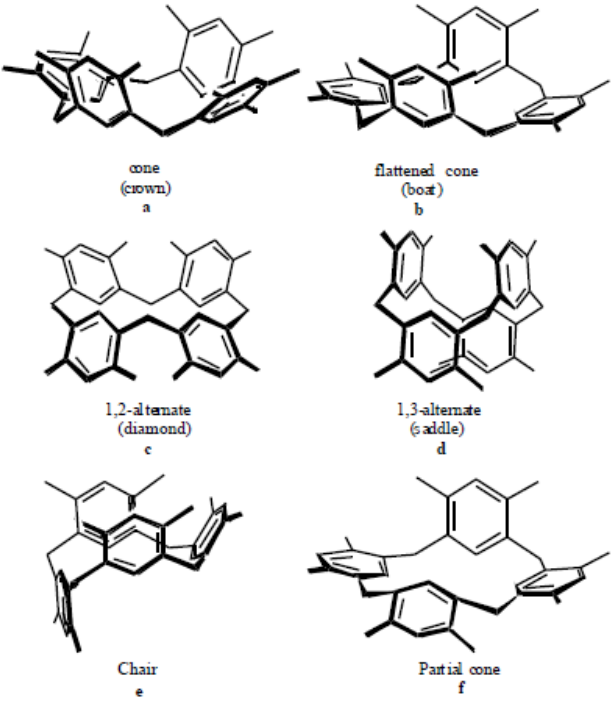

Figure 1.4. Principal conformations (and symmetry) for the resorc[4]arene.

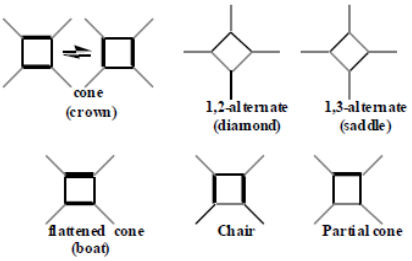

Figure 1.5. Sketched conformations.

Octamethoxyresorcarenes have also been found in two different *chair*-like forms, named *flattened partial cone 1* (**f**) (Botta et al., 1994) and *flattened partial cone 2* (Botta et al., 1997), coincident with the previously reported "*chair*" (**e**) (Abis et al., 1988).

2. The relative configurations of the side chains at the methylene bridges: the arrangements of the substituents were ruled by Högberg (Figure 1.6), who took as a reference the side chain on the C-2 methine (*r*) and considered the relative positions (*cis* or *trans*, i.e. *c* or *t*) of the other CH in the sequence (C-8, C-14, C-20). The substituents of the *cone* and 1,3-*alternate* forms are all cis (or *rccc*). The substitution pattern of *1,2-alternate* is *rctc*, where it is evidenced the anomalous position of the C-14 substituent. The substitutions found for *flattened partial cone* 1 and *chair* were *rccc* and *rctt*, respectively, but other arrangements cannot be excluded.

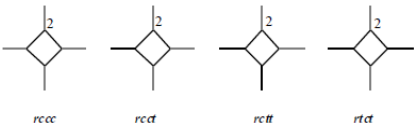

Figure 1.6. Substituents distribution pattern.

3. The individual configuration of the substituents at the methylene bridge, which, in conformations of the macrocycle with C symmetry, may be axial or equatorial. In the sketched structures of Figure 1.5, axial substituents are represented with a dotted line.

❖ ***Synthesis of resorcarenes***

Condensation of resorcinol with aldehydes

The acid-catalyzed condensation reaction between resorcinol and an aliphatic or aromatic aldehyde (Scheme 1.1) is generally carried out by heating the constituents to reflux in a mixture of ethanol and concentrated HCl for several hours (Egberink et al., 1992; Tunstad et al., 1989; Thoden van Velzen et al., 1994). Each aldehyde, in an almost unlimited range of R options, requires different optimal conditions, while unsubstituted resorcinol (1,3-dihydroxybenzene, X=H) is the mostly used counterpart. 2-Methylresorcinol (X=Me) (Konishi et al., 1990) or pyrogallol (1,2,3-trihydroxy benzene, X=OH) (Cometti et al., 1992) have been preferentially used in the reaction with formaldehyde to obtain better yields. A number of different 5,11,17,23-tetrahydroxyresorc[4]arenes (pyrogallo[4]arenes) have been obtained *via* acidic condensation of 2-hydroxyresorcinol with the appropriate aldehyde in mixtures of HCl, ethanol, and water. Tetra-*n*-nonyl-, tetra-*n*-octyl-, tetra-isobutyl-, tetraethyl-, tetramethyl-, and tetrakis(biphenylyl)-hydroxyresorcarenes has been prepared in this way (Gerkensmeier et al., 2001). The substituents, with some exceptions, presented an axial all-*cis* configuration, which forced the cyclic tetramer to assume a bowl-like shape and form polarity-induced double layers (Gerkensmeier

et al., 2001), in the solid state. Resorcinol derivatives carrying electron-withdrawing substituents, like NO_2 or Br at C-2 or featuring partially alkylated hydroxyl groups do not give cyclization. The resorcarenes synthesized throughout the years till the end of 1994 are listed in a review by Reinhoudt and co-workers (Timmerman et al., 1996).

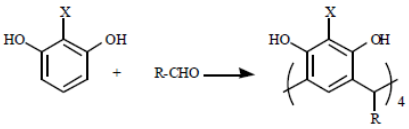

Scheme 1.1. Classical synthesis of resorcarenes X=H, Me,OH.

Tetramerization of resorcinol dimethyl ether derivatives by Lewis acid

It has been seen that treatment of (*E*)-2,4-dimethoxycinnamic acid esters (R = COOMe, COOEt, COOiP) with $BF_3{\cdot}Et_2O$ in $CHCl_3$ at reflux (Scheme 1.2) gives after 15 min the corresponding octamethylated resorcarene (R=COOMe, COOEt, COOiP) in 75% overall yield, as a mixture of *cone*, *1,2-alternate* and *1,3-alternate* forms (Botta et al., 1992).

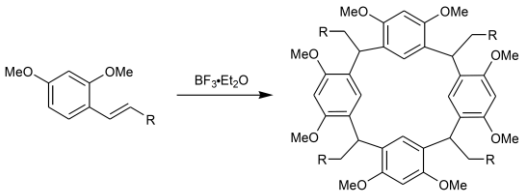

Scheme 1.2. Tetramerization of cinnamic acid derivatives.

Indeed, this simple reaction allows the design of several new structures: the versatility of the reaction does not depend only on the variability of R group in the monomer, but also on the possible modifications of the side chains, CH_2R. Each new structure is a potential owner of features that may introduce into a novel research avenue.

As an example Botta *et al.* synthesized double-spanned resorc [4]arenes treating octamethylated resorc[4]arenes with glutaroyl, adipoyl and pimeloyl dichlorides in the presence of triethylamine (Botta *et al.*, 1997). The insertion of two polymethylene bridges led to the formation of a cavity-shaped architecture resembling a basket which gave the name to these molecules (Fig 1.7). NMR characterization showed a C_{2v} symmetry with two parallel bridges: the formation of the bridge froze one of the two *flattened cone* conformations, which are normally in fast equilibrium to get the *cone* conformation as average (Figure 1.7).

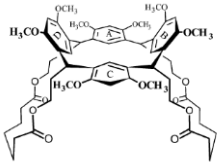

Figure 1.7. Chemical structure of a basket resorc[4]arene with two polymethylene bridges.

Analogously, when 2,4-dimethoxybenzyl alcohol was treated with trifluoroacetic acid (5% in $CHCl_3$), the unsubstituted resorcarene **a** was obtained in 95% yield (Scheme 1.3) (Falana et al., 1994). Notably, compound **a** cannot be synthesized by the acid-catalyzed condensation of resorcinol and formaldehyde, since this reaction gives only polymeric products (Gutsche, 1983; Gutsche, 1989; Gutsche, 1995; Böhmer, 1995; Mandolini and Ungaro, 2000; Asfari et al., 2001). Lewis acid catalyzed also the condensation (Scheme 1.3) of 1,3-dimethoxybenzene with isovaleraldehyde, to give **b**; in particular, $SnCl_4$ led to selective formation in high yield of the *rccc* isomer.

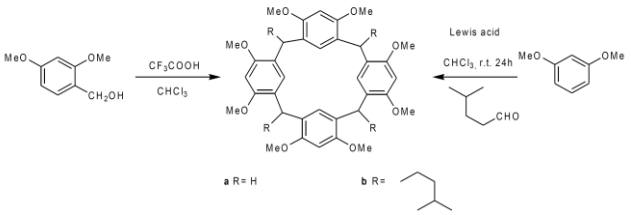

Scheme 1.3. Octamethoxyresorcarenes by Lewis acid catalyzed reaction.

A1.2 The metathesis reactions: from a historical perspective to recent developments

Metathesis, with its multiple aspects, has become one of the most important chemical reactions and is now extremely useful. This area has gone beyond the research stage in inorganic and organometallic chemistry to develop in organic, medicinal, polymer and materials chemistry to such an extent that it has now become a familiar tool for the specialists of these fields (Astruc, 2005).

A1.2.1 Metathesis: fragments changing place

The etymology of the word metathesis comes from the Greek μεταθεσιζ (metathesis) that means transposition. Thus, metathesis is invoked when, for instance, ions are exchanged in a solution containing two ion pairs in order to produce the most stable ion pairs [eqn. (1)] (Loupy et al., 1992). In the same way, two carbenes of an olefin can be exchanged to give, if they are different, another recombination leading to the two symmetrical olefins [eqn. (2)] or the two carbynes of an alkyne to give the two symmetrical alkynes [eqn. (3)].

$$A^+B^- + C^+D^- \rightleftharpoons A^+D^- + C^+B^- \qquad (1)$$

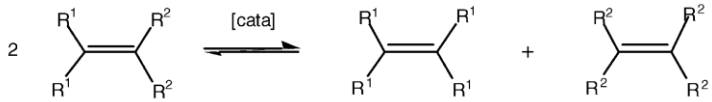

(2)

(3)

Although the name metathesis was given for the first time to this reaction by Calderon in the seventies (Calderon, 1967; Calderon, 1972) the first observation of the metathesis of propene at high temperature was reported in 1931. Twenty years later, industrial chemists at Du Pont, Standard Oil and Phillips Petroleum reported that propene led to ethylene and 2-butenes when it was heated with molybdenum (in the form of the metal, oxide or $[Mo(CO)_6]$ on alumina) (Banks and Bailey, 1964; Rouhi, 2002). The first polymerization of norbornene by the system $WCl_6/AlEt_2Cl$ was independently reported in 1960 by Eleuterio (Eleuterio, 1960; Eleuterio, 1991) and by Truett (Truett et al., 1960), but it was recognized only in 1967 that ROMP (*ring opening metathesis polymerization*) and the disproportionation of acyclic olefins were the same reaction. A detailed historic account was reported by Eleuterio (Eleuterio, 1991). The metathesis reactions are in principle under thermodynamic control, that is they are equilibrated, which

clearly is an inconvenience. In fine chemical synthesis, this problem can be circumvented by choosing to carry out metathesis of a terminal alkene or alkyne. The formation of ethylene (or respectively, acetylene) displaces the reaction towards the product. This strategy also applies to olefins terminated by an ethylidene group, because metathesis then produces 2-butenes whose volatility also displaces the reaction towards the products. Operating under reduced pressure insures elimination of the volatile olefin in order to displace the metathesis reaction [eqns. (4) and (5)]. In fact, many metathesis reactions are under kinetic control. Notably alkene metathesis is most often complicated by the formation of both Z and E isomers [eqn. (4)], whereas this problem does not exist in alkyne metathesis [eqn. (5)], disclosed for the first time by Blanchard, Mortreux and coworkers (Blanchard and Mortreux, 1972; Blanchard and Mortreux, 1975; Mortreux et al., 1977; Mortreux et al. 1978; Mortreux et al., 1995; Bunz, 2002; Bunz, 2003; Grela and Ignatowska, 2002; Zhang et al., 2003; Zhang et al., 2004; Zhang and Moore 2004).

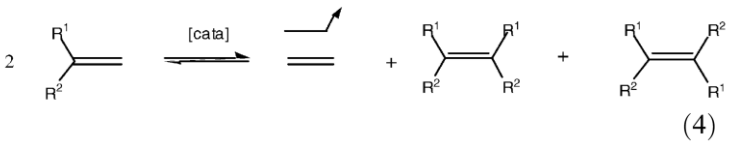

(4)

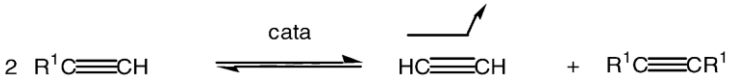

(5)

A1.2.2 The Chauvin mechanism

At the end of the 1960's, the metathesis reaction was very mysterious. Catalytic systems were either oxides such as WO_3/ SiO_2 used in industry for the transformation of propene to ethylene and butenes or Ziegler–Natta derived systems such as WCl_6 (or $MoCl_5$) + AlX_nR_{3-n} or (SnR_4). Mechanistic ideas had appeared, but they did not match the results of some metathesis experiments. In the process of thinking about the metathesis mechanism, Yves Chauvin from the Institut Français du Pètrole, had taken into account the report of Fischer on the synthesis of a tungsten-carbene complex (Fischer, 1964), that of Natta on the polymerization of cyclopentene by ring opening catalyzed by a mixture of WCl_6 and $AlEt_3$ (Natta, 1964) and that of Banks and Bailey on the formation of ethylene and 2-butene from propene catalyzed by [$W(CO)_6$] on alumina (Banks and Bailey, 1964). Consequently, Chauvin and his student Jean-Louis Hérisson

published their proposition of metathesis mechanism in 1971 (Scheme 1.4) (Hérisson and Chauvin, 1971). The latter involves a metal-carbene species (or more precisely metal-alkylidene), the coordination of the olefin onto the metal atom of this species, followed by the shift of the coordinated olefin to form the metallocyclobutane intermediate, and finally the topologically identical shift of the new coordinated olefin in the metallocyclobutane in a direction perpendicular to the initial olefin shift. This forms a metal-alkylidene to which the new olefin is coordinated, then liberated. This new olefin contains a carbene from the catalyst and the other carbene from the starting olefin. The new metalalkylidene contains one of the two carbenes of the starting olefin and it can re-enter into a catalytic cycle of the same type as the first one. In fact, depending on the orientation of the coordinated olefin, the new catalytic cycle can give two different metallacyclobutenes, one leading to the symmetrical olefin and the other one leading the starting olefin. This latter cycle is said to be degenerate olefin metathesis. Thus, the catalytic cycles alternatively involves both metal-alkylidene species resulting from the combination of the metal with each of the two carbenes of the starting olefin. Hérisson and Chauvin not only suggested the metallacyclobutane mechanism, but also published several experiments to confirm it.

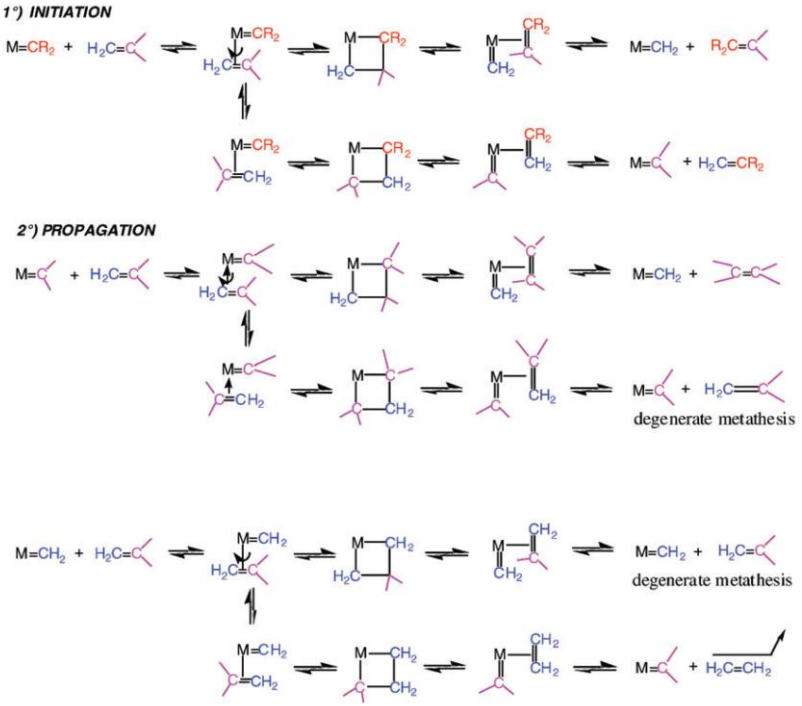

Scheme 1.4. Chauvin's mechanism, proposed in 1971, for the catalyzed olefin metathesis involving metal alkylidene and metallacyclobutane intermediates.

Chauvin's mechanism introduced several new ideas. First, it proposed the implication of a metal-carbene complex to initiate the catalysis of the metathesis reaction. This idea first suggested that one could just synthesize metal-alkylidene complexes and let them react as catalysts with olefins to carry out the metathesis reaction.

It was in 1980 that Dick Schrock's group at MIT reported a tantalum-alkylidene complex, [Ta(=CH–*t*-Bu)Cl(PMe_3)(O–*t*-Bu)$_2$], which catalyzed the metathesis of cis-2-pentene (Schrock et al., 1980). This provided the very first proof for Chauvin's mechanism of olefin metathesis with a well-defined high oxidation state alkylidene complex, almost a decade after Chauvin's proposal. Molybdenum and tungsten, however, were obviously the most active metals in alkene metathesis and, around 1980, Schrock and his group considerably increased their efforts in the search for stable molecular alkylidene and alkylidyne complexes of these metals that would catalyze the metathesis of unsaturated hydrocarbons. This search was successful (Wengrovius et al., 1980) and eventually produced a whole family of molybdenum- and tungsten-alkylidene complexes of the general formula [M(=CHCMe_2Ph)(=N–Ar)(OR_2], R being bulky groups. These compounds presently are the most active alkene metathesis catalysts (Figure 1.8) (Schrock et al., 1990; Bazan et al., 1990; Bazan et al., 1991).

The advantage of Schrock's catalysts, whose most efficient members were reported in 1990, was that even though they are extremely active, they are molecular (without additives) and also provided a commercial catalyst and chiral versions for the first examples of asymmetric metathesis catalysis (Aeilts et al., 2001; Teng et al., 2002; Tsang et al., 2003a; Tsang et.al., 2003b).

Schrock's closely related Mo-alkylidyne complexes do not react with olefins, but they selectively and efficiently metathesize alkynes without the need for a co-catalyst.

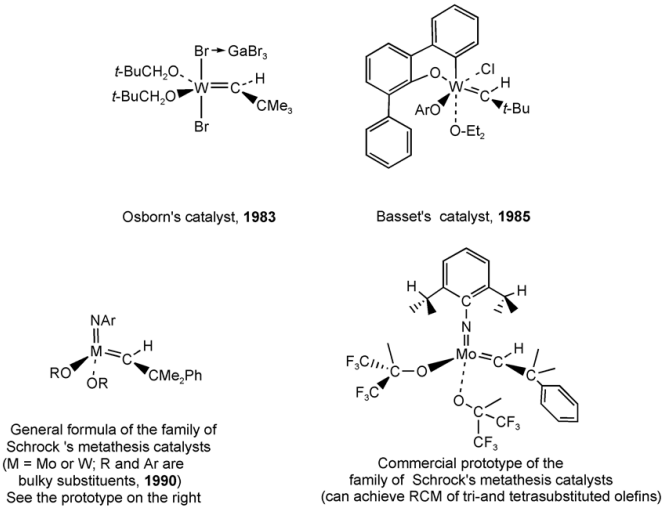

Figure 1.8. Main families of molecular Mo and W metathesis catalysts.

A1.2.3 Transition metal catalysts

Two classes of metal-alkylidene complexes are usually distinguished: those containing a nucleophilic carbene of the Schrock type and those with an electrophilic carbene of the Pettit type (Guerchais and Astruc, 1985). A related Fischer-type ruthenium complex, $[RuCp\{=C(Me)OMe\}(CO)(PCy_3)][PF_6]$, stabilized by a methoxy group on the carbene carbon, was synthesized by Malcolm Green's group at Oxford in 1971. This was the first reported

ruthenium-carbene complex (Green et al., 1971). The reactivity of this type ruthenium complexes towards olefins is again cyclopropanation, because of the strongly electrophilic character of the carbene ligand due to the positive charge, further increased by the electron-withdrawing carbonyl ligands (Figure 1.9). Grubbs had been interested for a long time in the metathesis reaction, as indicated by his mechanistic proposal of a metallocyclopentane intermediate (Grubbs, 1972). He had noticed Natta's publication on the catalysis by $RuCl_3$ of the polymerization of cyclobutene and 3-methylcyclobutene by ring opening (Natta et al., 1965; Grubbs and Tumas, 1989). This process (in butanol) had been developed by Norsorex. In this context, the Ziegler–Natta polymerization of olefins under mild conditions obviously had a considerable impact on polymer chemistry. The delineation of a new polymerization mechanism, however, was not a simple task. Wellinspired by this approach, Grubbs published in 1988 the polymerization of 7-oxanorbornene into a high molecular weight monodisperse polymer ($Mw = 1.3 \times 10^6$ g mol^{-1}; $Mw/Mn = 1.2$) by $RuCl_3$ or $[Ru(H_2O)_6](OTs)_2$ (OTs = toluene sulfonate). This catalysis was all the more remarkable as it was conducted in water (Novak and Grubbs, 1988).

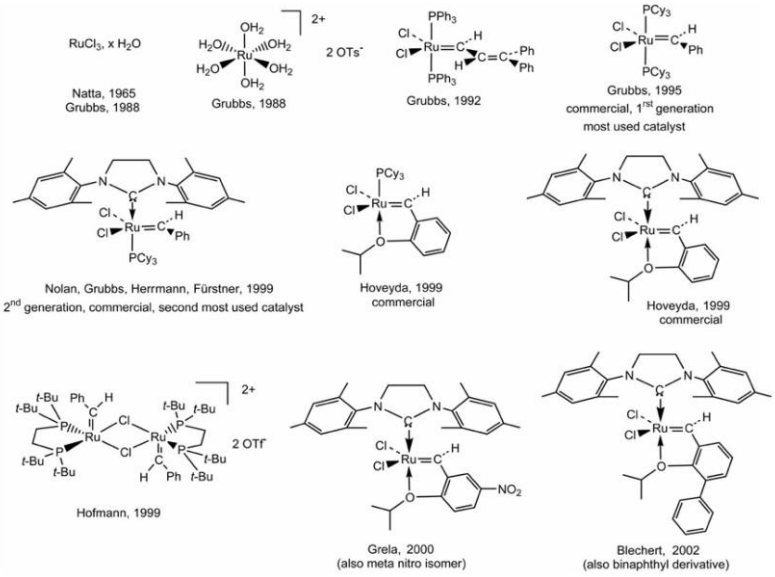

Figure 1.9. Grubbs-type (or derived) ruthenium metathesis catalysts, air-stable and compatible with most functional groups.

Shortly afterwards, he could show, in the course of the same reaction, the formation of a Ru-alkylidene intermediate, then the polymerization of cyclooctene, an olefin with little constraints, when the alkylidene ligand source was ethyl diazoacetate added to the aqueous solution of $[Ru(H_2O)_6](OTs)_2$ (France, 1993; Nguyen, 1992; Schwab et al., 1998). Consecutively and according to the same logic, a great step forward was accomplished by Grubbs in 1992. He reported the first molecularly well-defined ruthenium-carbene complex that promoted the ROMP of low-strain olefins as well as the catalytic *ring-closing metathesis* (RCM) of functionalized dienes.

Grubbs showed that these vinylidene complexes, $[RuCl_2(PR_3)(=CH–CH=CPh_2)]$ (R = Ph or Cy), were efficient molecular catalysts for these polymerization reactions (Scheme 1.5) and other metathesis reactions such as those involving ring closing of terminal diolefins.

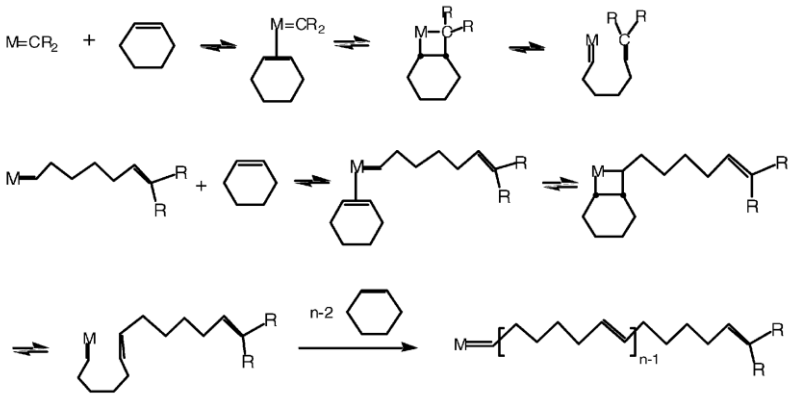

Scheme 1.5. Metathesis mechanism for the ring-opening metathesis polymerization (ROMP) of a cyclic olefin.

In 1995, the new molecularly well-defined catalysts $[Ru(=CHPh)Cl_2(PR_3)_2]$, R = Ph or Cy, whose structures are closely related to the vinylidene ones published three years earlier, appeared and were commercialized with R = Cy (Figure 1.9). $[Ru(=CHPh)Cl_2(PCy_3)_2]$ is now known as the **first generation Grubbs catalyst (G_1ST)** and is still today the most used metathesis catalyst by organic chemists, because of its stability to air and compatibility with a large variety of functional groups (except for amines and nitriles and basic media).

Fine mechanistic studies with this catalyst led Grubbs' group to conclude that the mechanism first involved the dissociation of one phosphine to generate the reactive 14-electron ruthenium intermediate. In order to accelerate this dissociative step, Grubbs introduced, in place of one phosphine, one of Arduengo's cyclic bis-amino carbene ligands that are relatively stable, even in the free forms obtained by deprotonation of the corresponding imidazolium cation (Arduengo, 1999; Herrmann and Köcher, 1997; Bourissou et al., 2000; Wetskamp et al., 1998). It is Herrmann's group that first synthesized ruthenium complexes with two such carbene ligands in the context of the catalysis of olefin metathesis, but their catalytic activity was shown to be modest. In **G_1STs** containing only one such ligand, they increase the electron density at the ruthenium center, however, and their trans effect labilizes the ruthenium-phosphine bond, favoring phosphine dissociation. Thus, the **second generation Grubbs catalysts (G_2ND)** $[RuCl_2\{C(N(mesityl)CH_2)_2\}(PCy_3)(=CHPh)]$ and its catalytic activity in metathesis were successively proposed within a few months by the groups of Nolan (Ackermann et al., 1999), Grubbs (Scholl et al., 1999a; Scholl et al., 1999b; Trnka et al., 2003; Love et al., 2003; Chatterjee et al., 2003; Morril and Grubbs, 2003), and Fürstner and Herrmann (Ackermann et al., 1999). It is presently the most used catalyst for efficient cross-metathesis reactions, although it is not tolerant to amines and nitriles (for

instance, with acrylonitrile, Schrock's catalyst is efficient, in contrast to the ruthenium catalysts). On the contrary, this new, commercially available, catalyst is even more active although it is also more thermally stable than the first one. Along this line, Hoveyda (Kingsbury et al., 1999; Grela et al., 2002), Hofmann (Hansen et al., 1999; Volland et al., 2004), Grela and Blechert (Connon et al., 2002; Wakamatsu and Blechert, 2002a; Wakamatsu and Blechert, 2002b; Dunne et al., 2003) reported other related, very active, stable and functional- group tolerant ruthenium metathesis catalysts. The first Hoveyda metathesis catalyst is derived from Grubbs' first generation catalysts. It bears only one phosphine and a chelating carbene ligand. The second one bears, in addition, Arduengo's carbene instead of the phosphine. Both catalysts are now commercially available, although expensive. Grela recently reported variations of the Hoveyda catalyst with increased efficiency (active even at 0 °C) when the aryl group of the benzylidene ligand bears a nitro group in the meta or para positions or two methoxy substituents (Figure 1.9). Grela's successful idea was to destabilize the Ru–O(ether) bond in order to favor the ether decoordination that generates the catalytically active 14-electron species (Grela et al., 2002). The family of Hoveyda catalysts, whose activity compares with that of the second generation Grubbs catalyst, are especially useful for difficult cases of metathesis of polysubstituted olefins and

selective cross metathesis (CM) in which homo-coupling needs be avoided (Kingsbury et al., 1999; Honda et al., 2004). The most successful variation of these Ru-benzylidene catalysts so far was reported by Blechert whose strategy to sterically destabilize the Ru–O(ether) bond was to introduce an aryl (phenyl or naphthyl) substituent on the benzylidene aryl in the ortho position relative to the O(ether) (Connon et al., 2002; Wakamatsu and Blechert, 2002a; Wakamatsu and Blechert, 2002b; Dunne et al., 2003). The catalytic efficiency and stability of Blechert complexes surpasses those of all the other Ru catalysts, although it has been shown several times that the catalytic efficiency depends on the type of metathesis reaction examined and the tolerance towards the required functional group.

A1.2.4 Intra- and intermolecular olefin metathesis

Olefin metathesis is a metal-catalyzed transformation, which acts on carbon-carbon double bonds and rearranges them via cleavage and reassembly. According to the mechanism, first introduced by Chauvin, the coordination of an olefin to a metal carbene catalytic species leads to the reversible formation of a metallacyclobutane (Scheme 1.6). This intermediate then proceeds by cycloreversion via either of the two possible paths: 1) non-productive—resulting in the re-formation of the starting materials or 2) product-forming—

yielding an olefin that has exchanged a carbon with the catalyst's alkylidene. Since all of these processes are fully reversible (Scheme 1.6), only statistical mixtures of starting materials as well as all of possible rearrangement products are produced in the absence of thermodynamic driving forces.

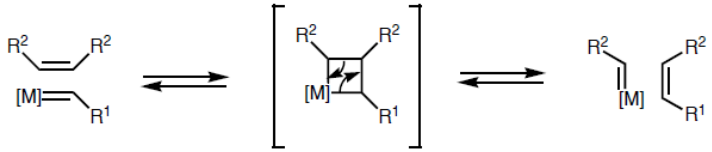

Scheme 1.6. General mechanism of olefin metathesis.

The most important olefin metathesis subtypes are presented in Scheme 1.7. They are currently employed in the synthesis of a large varierty of small, medium and polymeric molecules, as well as novel materials.

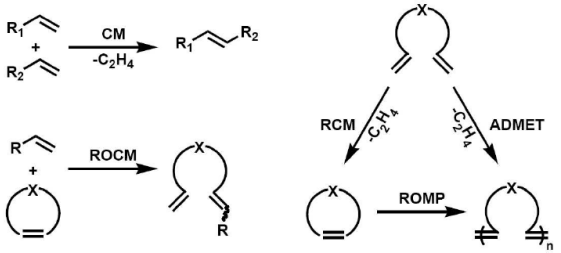

Scheme 1.7. Different types of olefin metathesis, all proceeding according to the Chauvin mechanism and catalyzed by Schrock-type or Grubbs-type catalysts.

Ring-Closing Metathesis (RCM)

Construction of rings is one of the fundamental processes in organic synthesis. Of the various strategies available, cyclization is the most straightforward way of obtaining rings. Commonly employed cyclization methods involve reactions of cationic, anionic or radical species. Common rings such as 5–7 membered ones are easily available by these methods. However, formation of medium or large rings by these methods either proceeds with low yields or does not proceed at all due to unfavourable enthalpic and entropic factors. In recent years, olefin metathesis has emerged as a powerful tool for carbon–carbon bond formation and has enabled the synthesis of rings of different sizes (Ghosh et al., 2006). The construction of macrocycles by ring-closing metathesis (RCM) is often used as the key step in the synthesis of natural products containing large rings (Conrad and Fogg, 2006). The Chauvin mechanism for olefin metathesis (Hérisson and Chauvin, 1971) involves a sequence of [2+2] cycloadditions and retroadditions, in which the key intermediate is a metallacyclobutane species. Each step of the catalytic cycle is in principle reversible, resulting in an equilibrium mixture of olefins unless a bias can be exerted to drive the reaction in a chosen direction. Ring-closing metathesis of dienes is entropically favoured by the formation of two olefinic products from a single diene precursor (Scheme 1.8). When both olefinic

groups in the diene are terminal, one equivalent of ethylene is formed for each cycloalkene, and ring-closing is driven by the loss of volatile ethylene.

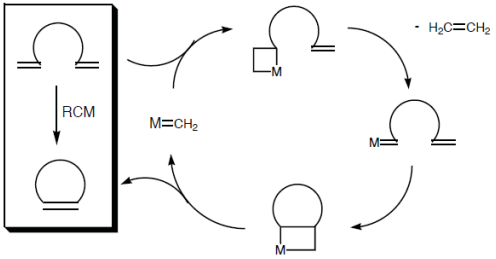

Scheme 1.8. Intramolecular RCM metathesis of a diene to form a cyclic olefin.

Steric parameters favour metathesis of α,ω-olefins over internal olefins, as does the decreased volatility and increased solubility (Atiqullah et al., 1998) of olefinic coproducts heavier than ethylene. The rate, products, and selectivity of RCM processes are determined by a subtle interplay of substrate and catalyst parameters. Substrate parameters, of course, determine whether a target reaction is thermodynamically feasible. Reaction rates and product selectivity are determined by the interaction of catalyst and substrate properties: the structure-activity relationships are very complex and remain poorly understood.

Cross-metathesis (CM) *and Ring-Opening Cross-Metathesis (ROM-CM)*

Olefin cross-metathesis (CM) can be formally described as the intermolecular mutual exchange of alkylidene (or carbene) fragments between two olefins promoted by metal-carbene complexes (Grubbs and Chang, 1998; Randall and Snapper, 1998). There are two main variations on this theme (Scheme 1.9): a) "pure" cross-metathesis (CM) and b) ring-opening cross-metathesis (ROM-CM).

CM is not yet in such widespread laboratory use as the more entropically favorable RCM reaction. However, the development of a second generation of active and robust ruthenium catalysts (see Section A1.2.3), which combine the high activity previously only associated with molybdenum-based catalysts with an impressive functional-group tolerance, has recently allowed many groups to breathe new life into what were previously in many cases little more than unselective mechanistic curiosities (Hérisson and Chauvin, 1971).

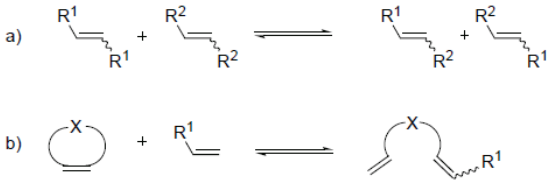

Scheme 1.9. Variations of cross-metathesis (CM).

A general mechanistic scheme for the CM of two symmetrically substituted olefins (in the practice, this is quite difficult) is presented in Scheme 1.10. The first step in the catalytic cycle (after the first catalyst turnover to produce A) is a [2+2] cycloaddition reaction between olefin B and a transition metal carbene A to give a metallacyclobutane C. The latter undergoes subsequent collapse in a productive fashion to afford a new olefin product D and a new metal carbine (alkylidene) E, which carries the alkylidene fragment R1. Similarly, E can react with a molecule of F via G to yield D and A, which then re-enters the catalytic cycle. The net result is that D is formed from B and F with A and E as catalytic intermediates.

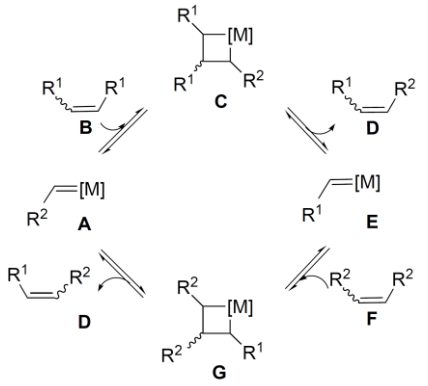

Scheme 1.10. General mechanistic scheme for the CM of the two symmetrically substituted olefins B and F.

The highly efficient and atom-economic ROM–CM reaction has been the subject of much recent investigation. The presumed catalytic cycle for this reaction is shown in Scheme 1.11.

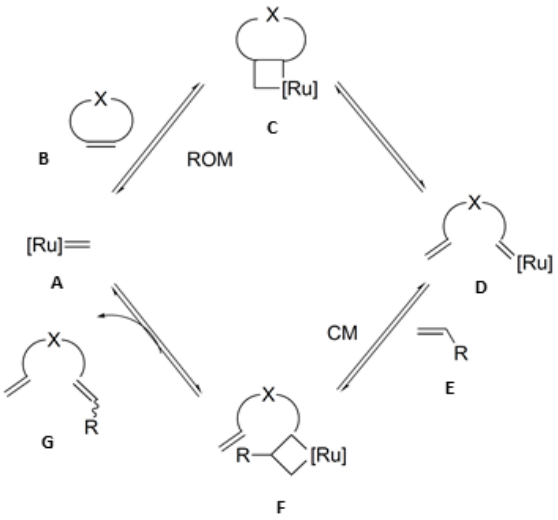

Scheme 1.11. ROM–CM catalytic cycle.

The reaction of ruthenium methylidene A and olefin substrate B furnishes metallacyclobutane intermediate C, which on collapse gives ring-opened alkylidene D. This step is most efficient for highly strained cyclic olefin substrates, in which relief from ring strain provides an energetic counterweight to the entropically favored reverse *ring-closing* reaction (D→A). It is hardly surprising, therefore, that norbornenes, oxanorbornenes, (Schneider and

Blechert, 1996; Schneider et al., 1997) and cyclobutenes (Randallet al., 1995; Tallarico et al., 1997; Snapper et al., 1997) are generally excellent substrates for ROM–CM reactions. CM between D and terminal olefin E (internal olefins may also serve as CM partners) then affords ROM–CM product G via intermediate F with loss of the ruthenium methylidene, which then reenters the catalytic cycle. An important condition for ROM–CM to be efficient is that CM between D and E must be faster than the reaction between D and B (a competing ROMP pathway), a factor which very much depends on the nature of the cyclic olefin B and the CM partner E used. However, in the majority of cases, ROM–CM competes effectively with ROMP, particularly under high dilution conditions.

Acyclic diene metathesis polymerization (ADMET)

Traditionally, acyclic diene metathesis (ADMET) is considered to be a step-growth polycondensation-type polymerization, which makes strictly linear chains from unconjugated dienes (Allcock et al., 2001; Wagener et al., 1997).

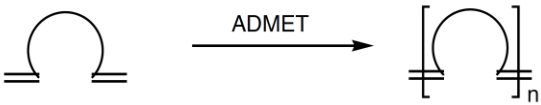

As such, ADMET requires very high monomer conversion rates to produce polymer chains of considerable size. Therefore, the more active second generation catalysts are usually better suited for ADMET than bisphosphine ones. Since the loss of ethylene is the main driving force behind the cross metathesis of terminal olefins, the efficient removal of this volatile gas from the reaction vessel is also crucial. Consequently, although olefin metathesis with ruthenium catalysts is, in general, very mild and does not require stringent air removal, ADMET greatly benefits from conditions which promote the diffusion and expulsion of ethylene (i.e., higher reaction temperatures, application of vacuum, and rigorous stirring). In addition, the use of concentrated or even neat solutions of monomers is usually helpful to polycondensation reactions but, in the case of ADMET, a very viscous solution might be detrimental to efficient stirring and ethylene removal. Furthermore, as a consequence of the poor molecular weight control of stepgrowth reactions, the polydispersity index (PDI) of polymers obtained by this method is usually quite large. However, an important advantage of ADMET is that it allows a large variety of monomers to be polymerized since terminal olefins are quite easy to install. Many functional groups and moieties of interest can be incorporated into such polymers directly through monomer design, due to the excellent tolerance of ruthenium catalysts.

Ring-Opening Metathesis Polymerization (ROMP)

Ring opening metathesis polymerization (ROMP) exhibits very different reaction kinetics from the ADMET approach to polymeric materials. ROMP is a chain-growth type polymerization which relies on monomer ring strain and, thus, it can be efficiently controlled by catalyst loading.

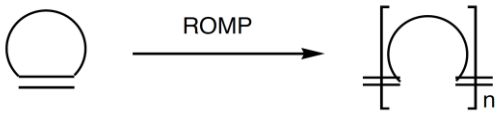

The equilibrium molecular weight of the resulting polymer chains is, therefore, essentially independent of the extent of conversion. Moreover, a variety of olefin metathesis catalysts effect ROMP and sufficiently fast initiating ones can even lead to a living polymerization of appropriately chosen monomers. For example, the polymerization of norbornenes with the fast initiating bispyridine species produces well-defined polymers with PDIs close to 1.0 (Choi and Grubbs, 2003). The employment of these strained, bi-cyclic alkenes as monomers ensures that both depolymerization via competing RCM and chain fragmentation via “back-biting” of the catalyst into the growing chain are significantly suppressed. However, the limited availability of suitable monomers is the main disadvantage of this method. Although a variety of backbones can be created through monomer functionalization, such alterations

sometimes negatively affect the ring strain and, thus, success of ROMP.

A1.3 Key processes in ruthenium-catalysed olefin metathesis

The elucidation of the mechanism of metathesis reaction catalyzed by Grubbs catalysts has been the subject of intense experimental (Dias et al., 1997; Ulman and Grubbs, 1998; Hinderling et al., 1998; Adlhart et al., 2000a; Adlhart and Chen, 2000; Adlhart et al., 2000b; Sanford et al., 2001; Conrad et al., 2007) and theoretical (Cavallo, 2002; Adlhart and Chen, 2004; Occhipinti et al., 2006; Urbina-Blanco et al., 2013) investigations. Key processes (Scheme 1.12) in the ruthenium-catalysed homogeneous alkene metathesis reaction include: the study of pre-catalyst initiation, during which a stable precatalyst (typically 16-electron Ru^{II}) becomes an active 14-electron species; the study of how the ancillary ligand affects reactivity; the partitioning between intra- and inter-molecular metathesis pathways; the study and understanding of the key steps that occur during metathesis reactions, the development of Z-selective metathesis pre-catalysts; and the study of catalyst decomposition.

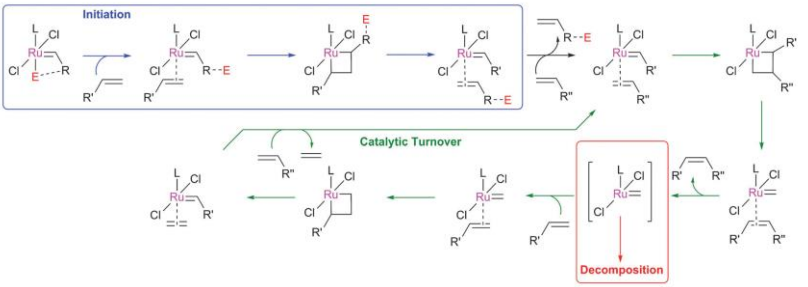

Scheme 1.12. Key stages of alkene metathesis reactions. (Reproduced from Nelson et al., 2014)

In the specific case of olefin metathesis, it has been proposed that carbenes and metallocyclobutanes (MCBs) are the key intermediates of the reaction (Hérisson and Chauvin, 1971). The first step to clarify the mechanism of the metathesis reaction has been the direct identification of the two above-mentioned ruthenium complexes by NMR technique. In 1992, Grubbs reported the first NMR spectroscopic evidence of a carbene intermediate produced during the reaction of a strained olefin with a well-defined Ru(II)-complex (Nguyen et al., 1992). Notably, Ru(II)-complex was able to polymerize norbornene in a 1:8 mixture of CH_2Cl_2/C_6H_6 at room temperature to yield polynorbornene. A new signal, attributed to H_α of the propagating carbene, was observed by ^1H NMR spectroscopy at 17.79 ppm. Its identity and stability were confirmed by Grubbs and collaborators by preparing a block

polymer with 2,3-dideuterionorbornene and perprotionorbornene (Scheme 1.13).

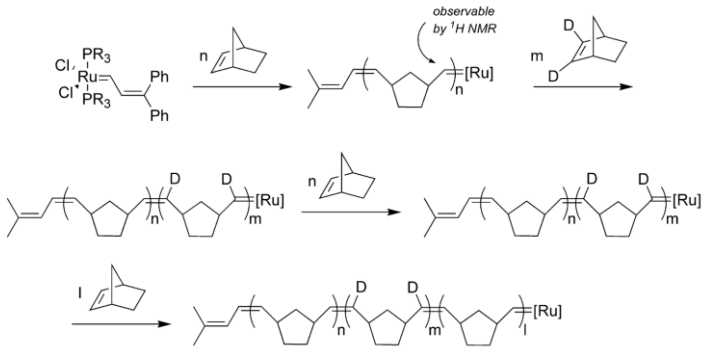

Scheme 1.13. The block copolymerization of 2,3-dideuterionorbornene and perprotionorbornene by a well-defined Ru alkylidene complex.

Later on, the selectivity and reactivity in ROM reactions was investigated by another research group by means of ^{1}H and ^{31}P NMR studies of the ruthenium alkylidenes formed during the reaction of cyclobutene-containing substrates (Randall et al., 1995; Tallarico et al., 1997a; Tallarico et al., 1997b). The factors behind the chemo-, regio- and stereoselectivities of ROM were examined and the mechanistic models suggested were supported by stoichiometric studies of the ruthenium alkylidenes formed during the ROM of various cyclobutene-containing substrates. The utility and limitations of ^{1}H NMR methods for monitoring the progress of ring-

closing metathesis (RCM) reactions were also examined (Monfette et al., 2010).

A significant advance in MCBs intermediate detection was made when Piers and co-workers developed rapidly-initiating 14-electron ruthenium carbene complexes such as **Piers1** and **Piers2** (Romero et al., 2004; Dubberley et al., 2006; Leitao et al., 2010). This class of compounds has enabled the preparation, observation and study of MCB species using modern low-temperature NMR spectroscopic techniques (Romero and Piers, 2005). In the first report of this reactivity, Piers demonstrated that the reaction of **Piers2** with 2.2 equiv. of ethene yielded quantitative conversion to MCB **b** (Scheme 1.14).

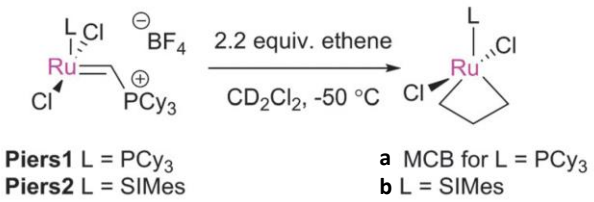

Scheme 1.14. Formation of MCBs using Piers-type complexes. (Adapted from Nelson et al., 2014)

The NMR data suggested a bottom-bound MCB geometry, while H_α exhibited a resonance at 6.6 ppm and H_β at -2.6 ppm.

$^1J_{CH}$ Coupling constants suggested a 'kite-shaped' MCB. First generation analogue **Piers1** yielded no observable MCB, consistent with DFT calculations that suggest that first generation MCBs are less stable than their second generation analogues (Cavallo, 2002). As an extension of their work, the same authors have shown the formation of ruthenacyclobutane and ruthenium carbene intermediates in RCM reaction (van der Eide et al., 2008), and provided a direct spectroscopic characterization of them.

Recently, we submitted to olefin metathesis reaction undecenyl resorc[4]arene macrocycles, with the aim to synthesize macrocyclic compounds capable of behaving as pre-organized hosts for the supramolecular recognition of appropriate molecular guests. The *chair* stereoisomer proved to be suitable substrate to yield cyclic alkenes by both intra- and intermolecular metathesis. In particular, the reaction performed on the *chair* substrate **1a** led mainly to the formation of the resorc[4]arene bicyclic olefin **2a**, along with the dimer **3a**. The latter proved to develop from two molecules of **2a** reacting together via a ring opening-cross metathesis (ROM-CM) sequence, according to an hypothesized mechanism (Ghirga et al., 2013).

The key role played by resorc[4]arene bicyclic olefin **2a** as monomeric building block for the construction of more complex architectures prompted us to investigate more deeply the

mechanism of the ROM-CM sequence of reactions. Typically, ROM-CM reactions are most successful when using highly strained substrates that show a good propensity to undergo a ring opening, which is the initial step then followed by CM. In the presence of reactive metal carbenes, also unstrained olefins proved to be suitable substrates for ROM-CM reactions (Ulman et al., 2000; Randl et al., 2001) by effecting ring-expansion reactions leading to a variety of macrocycles whose ring sizes can be modulated by using appropriate cyclic olefins (Lee et al., 2002). We report here the direct observation of a ruthenium-carbene-resorc[4]arene complex produced during a metathesis reaction of a resorc[4]arene bicyclic olefin with the G_1ST catalyst.

Chapter A2
Synthesis of Resorc[4]arene ω-Undecenyl Esters 1a–1c

A2.1 Results and discussion

A2.1.1 Synthesis of resorc[4]arene ω-undecenyl esters 1a–1c

The preparation of C-alkylated resorc[4]arenes by tetramerization in the presence of ethereal BF_3 of opportunely substituted 2,4-dimethoxycinnamates has prompted our group to study both the versatility of the reaction and the chemical and physical properties of the new macrocycles obtained, as depending on the variation of the side chains (Botta et al., 1992; Botta et al., 1997; Botta et al., 2005). In this Phd thesis i planned to synthesize resorc[4]arenes featuring long aliphatic side chains ending with a vinylidene group which provides the possibility for cross-linking reactions.

(*E*)-2,4-Dimethoxycinnamic acid was quantitatively converted into the corresponding acid chloride (Scheme 2.1) by reaction with thionyl chloride in dry dichloromethane (DCM), and then converted into the corresponding ester by reaction with ω-undecenyl alcohol in dry THF, in the presence of diisopropylethylamine (DIPEA). Purification by silica gel column chromatography (chloroform as eluent) yielded the ω-undecenyl ester as a yellow oil (yield 81%). Treatment of (E)-2,4-dimethoxycinnamic acid ω-undecenyl ester with BF_3•Et_2O (molar ratio 1:2) in chloroform at reflux afforded in 60% yield three stereoisomeric resorc[4]arene ω-undecenyl esters, which were shown to be in the *chair* (**1a**), *cone* (**1b**), and *1,2-*

alternate (**1c**) configuration. The structure of stereoisomers **1a–1c** was confirmed by ^{1}H and ^{13}C NMR spectroscopy and by electrospray ionization high-resolution mass spectrometry (ESI-HRMS).

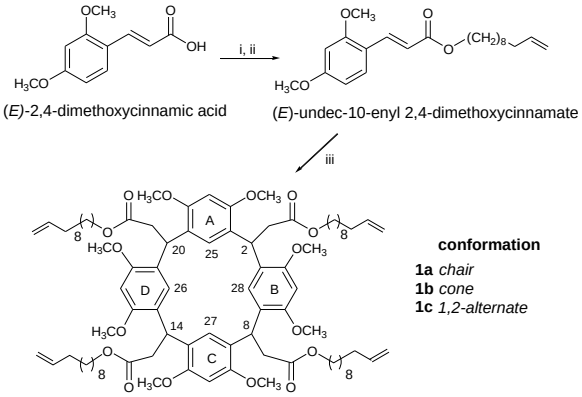

Scheme 2.1. Synthesis of resorc[4]arene ω-undecenyl esters 1a–1c. Reagents and conditions: (i) thionyl chloride, dry DCM, reflux, 2 h and 40 min; (ii) 10-undecen-1-ol, DIPEA, dry THF, reflux, 3 h. (iii) $BF_3 \bullet Et_2O$ (molar ratio 1:2), $CHCl_3$ (stabilized with amylene), reflux, 20 min.

Conformation in solution of resorc[4]arenes **1b** (*cone* with a C_{4v} symmetry) and **1c** (*1,2-alternate* with a C_s symmetry) could easily be assigned by the distribution pattern of NMR spectral data (Abis et al., 1988). On the contrary, the NMR spectral data of resorc[4]arene **1a** were in agreement with both the D_{2d} symmetry of the *1,3-alternate* conformation (Botta et al., 2005) and the C_{2h} symmetry of a *chair* conformer (Högberg, 1980a; Högberg, 1980b). This ambiguity was solved by X-ray diffraction analysis of a crystal of

resorc[4]arene **1a** (solvent, ethyl acetate): the results obtained fit very likely with a *chair* conformation (vide infra).

In the three forms, the side chains have different arrangements, i.e., two cis and two *tran*s (rctt) in the *chair* **1a**, all-*cis* (rccc) in the *cone* **1b**, three *cis* and one *trans* (rctc) in the *1,2-alternate* **1c** (Figure 2.1).

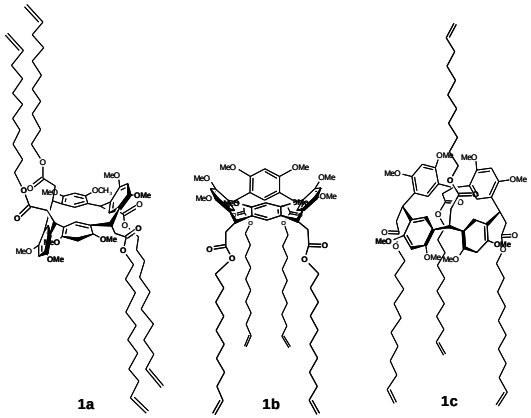

Figure 2.1. Chemical structures of resorc[4]arene ω-undecenyl esters **1a** (*chair*), **1b** (*cone*), and **1c** (*1,2-alternate*).

A2.1.2 X-Ray diffraction analysis of resorc[4]arene 1a

The molecular structure of resorc[4]arene **1a** is illustrated in Figure 2.2. Taking as a reference the weighed least squares plane, namely R, passing through the four bridging carbon atoms of the macrocycle, the calculated dihedral angles δ values (Perrin and

Oehler, 1991) (collected in Table 2.1) show that the B and D aromatic rings are almost coplanar with the plane R, whereas A and C are almost orthogonal to it, but on opposite sides.

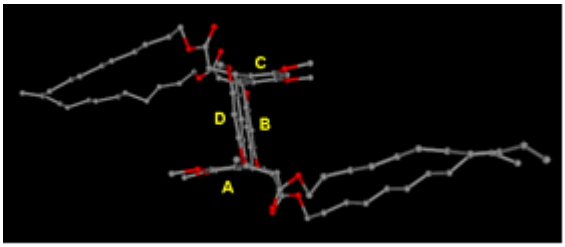

Figure 2.2. X-Ray structure of undecenyl resorc[4]arene **1a** showing the *chair* conformation adopted by the macrocycle. Colors are as follows: C, grey; O, red. Hydrogen atoms are omitted for clarity.

Following a procedure already adopted, (Botta et al., 2007) the molecular conformation of the macrocycle was given by the conformational parameters ϕ and χ, which account without ambiguities for the reciprocal orientations between adjacent aromatic rings (see Table 2.1).

Table 2.1. Dihedral angles (δ) and conformational parameters (ϕ and χ) for resorc[4]arene **1a**.

Rings	δ [°][a]	Rings	ϕ [°][a]	χ [°][a]
R^A	90.23 (3)	A–B	76.8 (4)	-151.4 (2)
R^B	178.02 (4)	B–C	-147.9 (2)	78.3 (1)
R^C	270.48 (4)	C–D	-70.3 (1)	152.2 (2)
R^D	177.13 (4)	D–A	145.9 (1)	-75.5 (1)

[a] Estimated standard deviations (ESD) are reported in parentheses. R is the weighed least squares plane passing through the four bridging carbon atoms of the macrocycle.

The sequence of signs (+-,+-,-+,-+) of the calculated values of ϕ and χ fits very likely with a *chair* conformation. The four ester chains attached to the bridging methine groups of the aromatic pocket point towards the exterior of the macrocycle and are segregated in pairs on opposite sides of the R plane. Such arrangement in the solid state makes resorc[4]arene **1a** a preorganized synthon undergoing a peculiar type of self-assembly which produces zigzag one-dimensional ribbons as those depicted in Figure 2.3.

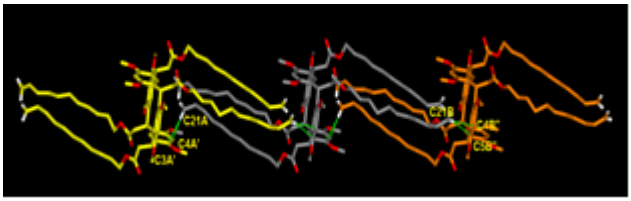

Figure 2.3. Perspective view of a zigzag one-dimensional ribbon in resorc[4]arene **1a** showing CH/π interactions (green lines) occurring between the terminal

methylene hydrogen atoms of one molecule and the π systems of two adjacent molecules.

In the novel "secondary structure", two pairs of aliphatic arms from two neighbouring resorcarenes are inserted as in a sandwich by two pairs of aromatic methoxyl groups. The driving force for such self-assembly seems to be CH/π interactions between the terminal methylene hydrogen atoms of one molecule and the π systems of two adjacent molecules (evidenced by green lines in Figure 2.3). In such a way, resorc[4]arene **1a** can behave at the same time as donor and acceptor of CH/π interactions, whose geometrical parameters are collected in Table 2.2.

Table 2.2. Geometrical parameters for the CH/π interactions in resorc[4]arene **1a**.

Carbon number	C•••C_π (Å)[a]	H•••C_π (Å)[a]	CH•••C_π (°)[a]
C21A-H···C3A'	3.509 (3)	2.716 (2)	136.6 (2)
C21A-H···C4A'	3.248 (3)	2.797 (2)	108.4 (2)
C21B-H···C5B''	3.197 (3)	2.955 (3)	94.7 (2)
C21B-H···C4B''	3.199 (3)	2.619 (2)	117.0 (2)

[a] Estimated standard deviations (ESD) are reported in parentheses.

As it can be seen, strong CH/π interactions could be expected, as judged by three intermolecular distances (i.e., 2.619 (2), 2.716, (2) and 2.797 (2) Å) significantly shorter than the corresponding value of 3.6 Å found by high-level *ab initio* calculations on a benzene-ethylene complex (Tsuzuki et al., 2000). Drawing inspiration from these findings, we envisaged to carry out high-level ab initio

calculations when resorcinol replaced benzene in the complex with ethylene. To this purpose, interaction energies were calculated using 6-311++G**, aug-cc-pVDZ, and aug-cc-pVTZ basis sets, for each of the two model complexes shown in Figure 2.4, namely (A) and (B), where resorcinol and ethylene are in the same two reciprocal orientations observed in the crystal structure, i.e., at the same intermolecular distances [2.797 and 2.716 Å in complex (A), and 2.619 and 2.955 Å in complex (B)].

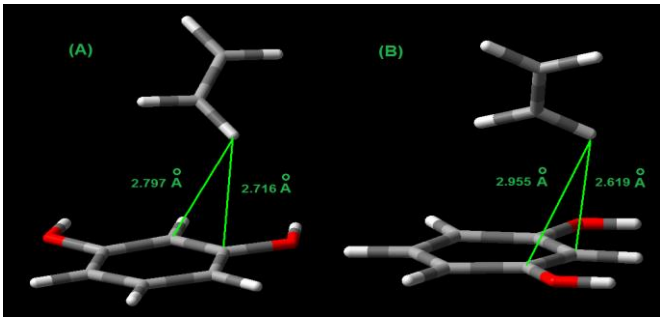

Figure 2.4. Resorcinol-ethylene complexes (A) and (B) considered for high-level *ab initio* calculations of CH/π interactions. The intermolecular distances are the same as those found in the crystal structure of resorc[4]arene **1a**.

The calculated interaction energies of (A) and (B) complexes (summarized in Table 2.3) proved to be dependent on the basis set used, becoming more negative (the mutual attraction increases) as the set is enriched with correlation-consistent polarized basis sets. Moreover, reciprocal resorcinol-ethylene attraction is always larger (the interaction energy is more negative) in complex (A) than in

complex (B), where ethylene is tilted with respect to the resorcinol plane. In any case, the calculations were in agreement with the experimentally observed short contacts in the crystal of resorc[4]arene **1a** and support the hypothesis of a pivotal role exerted by the CH/π interactions in the detected self-assembly.

Notably, along each ribbon, polar surfaces (due to the resorcarene core, the calculated dipole moment being 3.046 D) are alternated to apolar surfaces (due to the aliphatic chains). A peculiar "tertiary structure" was indeed detected in the crystal lattice for resorc[4]arene **1a**, where a lamellar-type crystalline organization is built-up by the face-to-face exposition of polar-with-polar and apolar-with-apolar surfaces. The result is a multilayer structure containing hydrophilic (ca 7 Å thick) and hydrophobic (ca 6 Å thick) layers intercalated. Such structure might give a chance of intercalating resorc[4]arene **1a** inside biological membranes.

Table 2.3. Calculated interaction energies (kJ mol^{-1}) of the resorcinol-ethylene complexes (A) and (B).

Basis set	(A)[a]	(B)[a]
MP2/6-311++G** (290)[b]	–4.52	–0.72
MP2/aug-cc-pVDZ (320)[b]	–7.14	–4.60
MP2/aug-cc-pVTZ (690)[b]	–8.41	–6.48

[a] The geometry of complexes (A) and (B) is shown in Fig. 3. [b] Basis functions are given in parentheses.

A2.2 Experimental section

NMR measurements

NMR spectra were recorded at 300 K on a Bruker AVANCE AQS600 spectrometer operating at the proton frequency of 600.13 MHz and equipped with Bruker a multinuclear z-gradient inverse probe head capable of producing gradients in the z-direction with a strength of 55.4 G cm^{-1}. ^{1}H and ^{13}C NMR spectra were always referenced to residual $CHCl_3$ signal (^{1}H, δ = 7.26 ppm; ^{13}C, δ = 77.20 ppm). The ^{1}H NMR spectra were acquired using the following experimental conditions: number of scans 16–32, recycle delay 5 s, π/2 pulse 9.0 μs, and 32K data points. ^{1}H diffusion filter-edited NMR spectra were obtained using a double stimulated echo pulse sequence incorporating a longitudinal eddy current delay (Jerschow and Mueller, 1997) with a Δ of 160 ms, a δ of 2.6 ms, and a longitudinal eddy current delay of 25 ms. A gradient pulse recovery time of 0.1 ms, 2% and 60% of the maximum gradient intensity were used. Sixty-four scans were accumulated in time domain with 32768 points.

A2.2.1 Synthesis of ω-undecenyl (*E*)-2,4-dimethoxycinnamate

A solution of (*E*)-2,4-dimethoxycinnamic acid (6.0 g, 28.8 mmol) in

dry DCM (60 mL) was treated with $SOCl_2$ (3.1 mL, 42.6 mmol) and the mixture was held at reflux for 2 h and 40 min. After removing the solvent under vacuum, the residue was dissolved in dry THF (32 mL) and diisopropylethylamine (DIPEA; 5.4 mL, 31.2 mmol) was added under nitrogen. After 20 min stirring at room temperature, 10-undecen-1-ol (7.0 mL, 34.1 mmol) was added to the solution and the mixture was heated under reflux for 3 h. Purification of the crude residue by silica gel chromatography with chloroform as eluent afforded the title compound (8.4 g, 81%, yellow oil). ^{1}H NMR (600 MHz, $CDCl_3$, 300 K): δ (ppm) = 7.89 (d, *J* = 16 Hz, 1H, H-α), 7.43 (d, *J* = 8.6 Hz, 1H, H-6), 6.49 (dd, *J* = 8.6, 2.4 Hz, 1H, H-5), 6.44 (d, *J* = 2.4 Hz, 1H, H-3), 6.42 (d, *J* = 16 Hz, 1H, H-β), 5.80 (m, 1H, =CH), 4.98 (br d, *J* = 17 Hz, 1H, $=CH_AH_B$), 4.91 (br d, *J* = 10 Hz, 1H, $=CH_AH_B$), 4.16 (t, *J* = 6.7 Hz, 2H, ω-CH_2), 3.86, 3.83 (s, 3H each, 2 $\times$ OCH_3), 2.03 (q, *J* = 7.5 Hz, 2H, α-CH_2), 1.68 (m, *J* = 7 Hz, 2H, θ-CH_2), 1.36 (m, 2H, η-CH_2), 1.28 (m, 8H, 4 $\times$ CH_2); ^{13}C NMR (100 MHz, $CDCl_3$, 300 K): δ (ppm) = 168.0 (s, C=O), 162.6, 159.8 (s each, C-4, C-2), 139.9 (d, CH-α), 139.2 (d, =CH), 130.4 (d, CH-6), 116.7 (s, C-1), 116.2 (d, CH-β), 114.1 (t, $=CH_2$), 105.2 (d, CH-5), 98.4 (d, CH-3), 64.4 (t, ω-CH2), 55.5 (q, OCH_3), 33.8 (t, α-CH2), 29.5–29.1 (t, 4 $\times$ CH_2), 28.9 (t, β-CH_2), 28.8 (t, θ-CH_2), 26.0 (t, η-CH_2). HRMS (ESI): *m/z* calcd for $C_{22}H_{32}O_4$ + Na^+: 383.21928 $[M + Na]^+$ (monoisotopic mass); found: 383.21910.

A2.2.2 Synthesis of resorc[4]arene ω-undecenyl esters 1a–1c

BF_3•Et_2O (1.5 mL; 11.25 mmol) was added to a solution of ω-undecenyl (*E*)-2,4-dimethoxycinnamate (2.0 g, 5.55 mmol) in $CHCl_3$ (stabilized with amylene, 5 mL) under stirring and the mixture was held under reflux for 20 min. After addition of ice-water, the stirring was continued until the chloroform phase turned to fuchsia. The chloroform layer was dried over Na_2SO_4 and the solvent was removed under vacuum. The residue was purified by silica gel column chromatography (DCM and DCM-ethyl acetate, 97:3) to yield resorc[4]arene ω-undecenyl esters, in the order of elution, **1b** (130 mg, 26%), **1a** (120 mg, 24%), and **1c** (45 mg, 9%).

*Resorc[4]arene ω-undecenyl ester **1a** (chair)*

White solid, 24% overall yield. Mp: 137 ± 0.3 °C. ^{1}H and ^{13}C NMR signals are reported in Table 2.4. HRMS (ESI): *m/z* calcd for $C_{88}H_{128}O_{16}$ + Na^+: 1463.90946 [*M* + Na]$^+$ (monoisotopic mass); found: 1463.91035. FT-IR (KBr): 2918, 2852, 1734, 1612, 1585, 1468, 1299, 1201 cm^{-1}. In Fig. 2.5 is reported a rapresentative ^{1}H NMR spectrum of resorc[4]arene **1a**.

Table 2.4. ^{1}H NMR and ^{13}C NMR signals* of undecenyl resorc[4]arene **1a** (*chair*).

Carbon	^{13}C	^{1}H
C=O	172.4	-
C_{Ar}–O	156.6 155.8	-
=CH	139.2	5.82 ddt (17.2, 10.2, 6)
CH_i (26,28) CH_i (25,27)	126.6 125.7	6.19 s 6.82 s
C_{Ar}–C	125.3 122.6	-
$=CH_2$	114.3	4.99 br d (17.2) 4.92 br d (10.2)
CH_e (5,17) CH_e (11,23)	97.1 95.3	6.47 s 6.39 s
OCH_2	64.3	3.98 br t 3.92 t
OMe	56.0 56.0	3.88 s 3.64 s
CH_2-(CO)	39.6	2.73 dd (14.5, 10.5) 2.65 dd (14.5, 6.5)
CH_2-(CH=)	34.0	2.05 q (6)
CH	33.0	5.04 dd (10.5, 6.5)
CH_2-(CH_2-CH=)	29.1	1.46 m
CH_2-(CH_2O)	28.7	1.38 m
$CH_2 \times 5$	29.6 29.6 29.5 29.3 26.0	1.24 br m

* 600 MHz (^{1}H) and 100 MHz (^{13}C), $CDCl_3$, *T* = 300 K; coupling constants *J* (Hz) are given in parentheses.

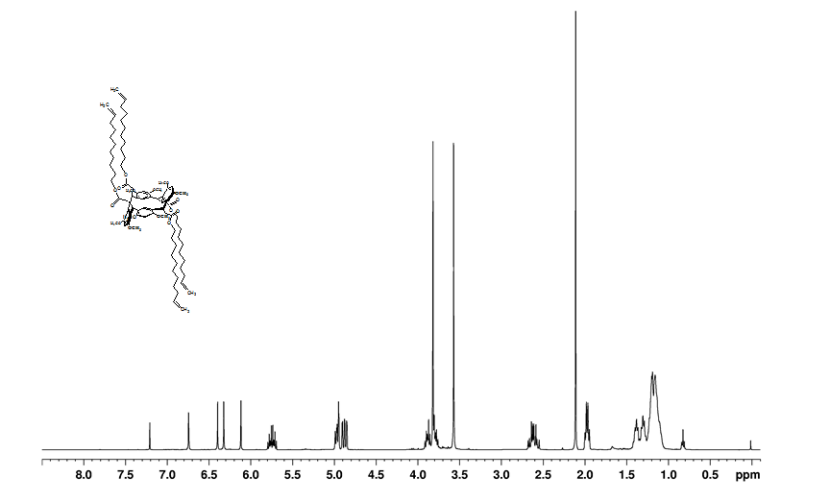

Figure 2.5. ^{1}H NMR spectrum of undecenyl resorc[4]arene **1a** (*chair*). 600 MHz, $CDCl_3$, 300 K.

*Resorc[4]arene ω-undecenyl ester **1b** (cone)*

Yellow solid, 26% overall yield. Mp: 101 ± 0.9 °C. ^{1}H and ^{13}C NMR signals are reported in Table 2.5. HRMS (ESI): *m/z* calcd for $C_{88}H_{128}O_{16}$ + Na^+: 1463.90946 $[M + Na]^+$ (monoisotopic mass); found: 1463.91035. FT-IR (KBr): 2918, 2852, 1734, 1612, 1585, 1468, 1299, 1201 cm^{-1}. In Fig. 2.6 is reported a rapresentative ^{1}H-NMR spectrum of resorc[4]arene **1b**.

Table 2.5. ^{1}H NMR and ^{13}C NMR signals* of undecenyl resorc[4]arene **1b** (*cone*).

Carbon	^{13}C	^{1}H
C=O	172.5	-
C_{Ar}–O	156.2	-
=CH	139.3	5.82 ddt (17.2, 10.2, 6.5)
CH_i (25,26,27,28)	126.0	6.51 s
C_{Ar}–C	124.2	-
$=CH_2$	114.3	4.99 br d (17.2) 4.93 br d (10.2)
CH_e (5,11,17,23)	96.4	6.30 s
OCH_2	64.4	3.95 t (6.8)
OMe	56.0	3.63 s
CH_2-(CO)	39.2	2.83 d (7.6)
CH_2-(CH=)	34.0	2.03 m (6.5)
CH	33.2	4.96 t (7.6)
CH_2-(CH_2-CH=)	29.1	1.35 br m
CH_2-(CH_2O)	28.8	1.49 br m
$CH_2 \times 5$	29.7 29.6 29.5 29.3 26.0	1.27 br m

* 600 MHz (^{1}H) and 100 MHz (^{13}C), $CDCl_3$, *T* = 300 K; coupling constants *J* (Hz) are given in parentheses.

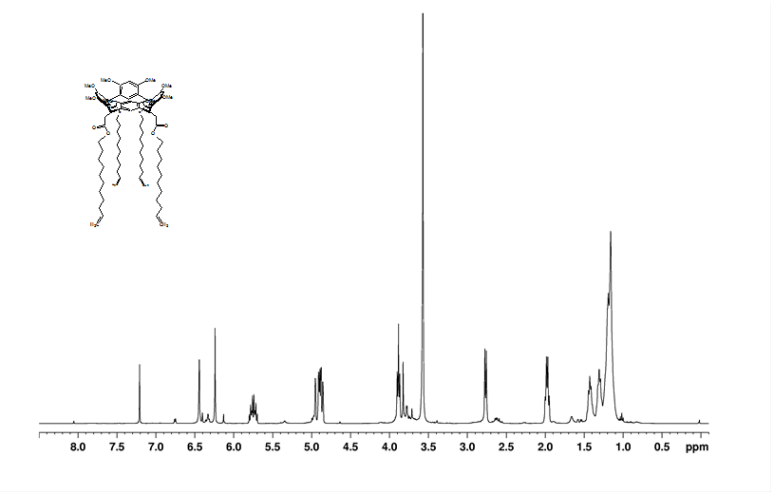

Figure 2.6. ^{1}H NMR spectrum of undecenyl resorc[4]arene **1b** (*cone*). 600 MHz, $CDCl_3$, 300 K.

*Resorc[4]arene ω-undecenyl ester **1c** (1,2-alternate)*

Yellow solid, 9% overall yield. Mp: 86 ± 0.9 °C. ^{1}H and ^{13}C NMR signals are reported in Table 2.6. HRMS (ESI): *m/z* calcd for $C_{88}H_{128}O_{16}$ + Na^+: 1463.90946 [*M* + Na]$^+$ (monoisotopic mass); found: 1463.91035. FT-IR (KBr): 2918, 2852, 1734, 1612, 1585, 1468, 1299, 1201 cm^{-1}. In Figure 2.7 is reported a rapresentative ^{1}H-NMR spectrum of resorc[4]arene **1c**.

Table 2.6. ^{1}H NMR and ^{13}C NMR signals* of undecenyl resorc[4]arene **1c** (*1,2-alternate*).

Carbon	^{13}C	^{1}H
C=O	172.7 × 2 172.3 172.2	-
C_{Ar}–O (6,22) C_{Ar}–O (4,24) C_{Ar}–O (10,18) C_{Ar}–O (12,16)	156.4 156.3 156.1 156.1	-
=CH	139.2	5.79 ddt (17.2, 10.2, 6.5)
CH_i (25,28) CH_i (26,27)	127.6 126.5	7.25 s 6.36 s
C_{Ar}–C (7,21) C_{Ar}–C (1,3) C_{Ar}–C (13,15) C_{Ar}–C (9,19)	124.7 124.4 124.0 123.4	-
$=CH_2$	114.4	4.97 br d (17.2); 4.91 br d (10.2)
CH_e (11,17) CH_e (5,23)	96.7 96.0	6.38 s 6.40 s
OCH_2 (2) OCH_2 (14) OCH_2 (8,20)	64.4 63.1 64.4 × 2	4.00 t (7.0) 3.97 t (7.0) 3.91 t (7.0)
OMe	56.4; 56.1; 55.9; 55.9	3.83 s; 3.82 s; 3.75 s; 3.64 s
CH_2-(CO) (2) CH_2-(CO) (14) CH_2-(CO) (8,20)	41.2 40.3 39.4 × 2	2.87 d (8.0) 2.33 d (8.0) 2.88 dd (15.1)
CH_2-(CH=)	34.0	2.03
CH (2) CH (14) CH (8,20)	34.0 33.6 34.0 × 2	5.46 t (8.0) 5.10 t (8.0) 5.06 dd (9.6, 6.5)
CH_2-(CH_2-CH=)	29.1	1.38 br m
CH_2-(CH_2O)	28.8	1.45 br m
CH_2 × 5	29.7; 29.7; 29.7; 29.6; 26.0	1.27 br m

* 600 MHz (^{1}H) and 100 MHz (^{13}C), $CDCl_3$, *T* = 300 K; coupling constants *J* (Hz) are given in parentheses.

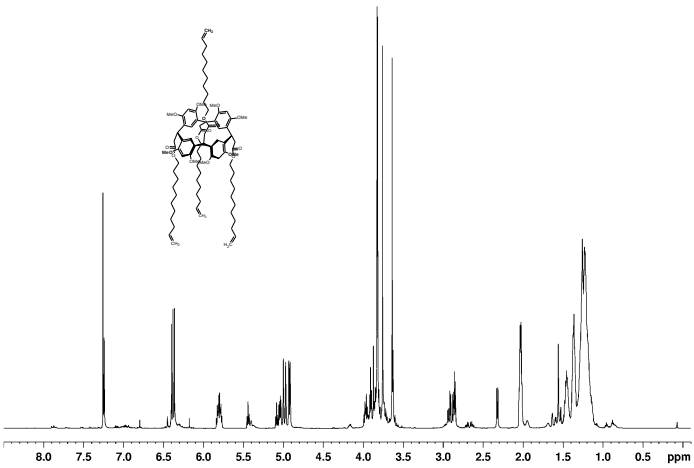

Figure 2.7. ^{1}H NMR spectrum of undecenyl resorc[4]arene **1c** (*1,2-alternate*). 600 MHz, $CDCl_3$, 300 K.

A.2.2.3 Crystallographic data of resorc[4]arene 1a

Chemical formula	$C_{88}H_{128}O_{16}$
Formula weight	1441.97
crystal system	triclinic
space group	*P1*
a (Å)	12.297(5)
b (Å)	17.946(5)
c (Å)	10.559(5)
α (°)	100.610(5)
β (°)	102.440(5)
γ (°)	105.110(5)
V (Å^3)	2124(1)
Z	1
ρ_{calcd} (g × cm^{-3})	1.127
μ (mm^{-1})	0.6 (Cu-K$_\alpha$)
Data Collection and Refinement	
2θ max for data collection (°)	139.98
Temperature (K)	293
Data collected (*h*, *k*, *l*)	(-14, -21, -12) to (14, 21, 12)
Total reflections	8039
Unique reflections	7989 (R_{int} = 0.0)
Observed reflections	2598 [*Fo*>4.0σ(*Fo*)]
Goodness-of-fit S on F^2 [a]	1.040
Final R indices (obs. data)[b]	R_1 = 0.0639, wR_2 = 0.143
Largest diff. peak and hole (e/Å^{-3})	0.16/-0.12

[a] Goodness-of-fit S = $[\Sigma w(Fo^2\text{-}Fc^2)^2/(n\text{-}p)]^{1/2}$, where *n* is the number of reflections and *p* the number of parameters. [b] $R_1 = \Sigma \; || Fo|-|Fc||/\Sigma|Fo|$, $wR_2 = [\Sigma w(Fo^2\text{-}Fc^2)^2/\Sigma wFo^4]^{1/2}$.

Chapter A3
Metathesis Reaction of Resorc[4]arene ω-Undecenyl Ester 1a

A3.1 Results and discussion

A3.1.1 Olefin metathesis reaction on resorc[4]arene 1a

The field of olefin metathesis is currently in a period of renaissance, largely because of the development in the early 1990s of well-defined ruthenium catalysts (Scholl et al., 1999). When we started our investigation on olefin metathesis, we faced with the problem of the selection of the appropriate catalyst. Second-generation Grubbs and Grubbs-Hoveyda complexes were tested, with a starting catalyst loading of 10 mol% (Figure 3.1).

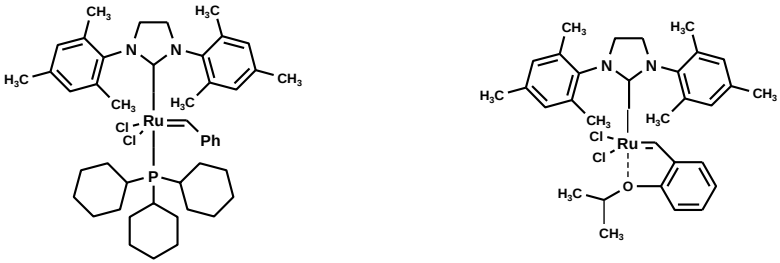

Figure 3.1. The structure of the second-generation Grubbs (left) and Grubbs-Hoveyda (right) complexes.

To ascertain the optimal reaction conditions, several experiments (summarized in Table 3.1) were run with resorc[4]arene **1a** as the substrate, in which a variation in the substrate concentration and the catalyst loading was performed. After some trials under TLC

plate checking, we observed that when the reaction was performed under high substrate concentration (i.e., 1.0×10^{-2} M in DCM), a large quantity of undesired products (polymers, presumably) was obtained, as revealed by the thickness of the baseline in the TLC plate system. Under high dilution conditions (i.e., 3.0×10^{-4} M), a less complicated TLC pattern was obtained, but the starting material did not completely disappear (except in the case of second-generation Grubbs catalyst at 10 mol%). An intermediate concentration (3.0×10^{-3} M) was afterward chosen, since it allowed the formation of a series of interesting compounds to be isolated and characterized (vide infra). The two catalysts proved to be almost equally effective, but the second left a 10% of starting material at a lower catalyst loading (i.e., 1 mol%). Finally, a combination of temperature (reflux) and reaction time (20 min) was evaluated as the best for the complete disappearance of **1a** on the TLC plate, as compared with room temperature and longer times. On the other hand, as we previously showed, thermal-induced conformational changes from the chair to other stereoisomers do not occur, unless ethereal BF_3 is involved (Botta et al.,1994).

Table 3.1. Summary of results obtained for olefin metathesis reactions of resorc[4]arene **1a**.[a]

	Catalyst (loading)	Yield (%)		
		2a	**3a**	**P1a**
3×10^{-3} M	Grubbs 2nd (10%)	46	5	44
	Grubbs-Hoveyda (10%)	30	trace	50
	Grubbs 2nd (1%)	43	trace	n.f.
	Grubbs-Hoveyda (1%)	30[b]	trace	n.f
3×10^{-4} M	Grubbs 2nd (10%)	60	n.f	n.f
	Grubbs-Hoveyda (10%)	40[b]	n.f	n.f
	Grubbs 2nd (1%)	30[b]	n.f	n.f
	Grubbs-Hoveyda (1%)	10[b]	n.f	n.f

[a] Reactions in DCM at reflux temperature and 20 min reaction time. [b] Starting material **1a** was present. n.f. = not formed.

The crude reaction mixture obtained under the optimal conditions (see first row of Table 3.1) was treated with a QuadraSil AP metal scavenger (amine-modified silica gel) to remove residual ruthenium by filtration (McEleney et al., 2006). The soluble (DCM) part of the filtrate was purified by silica gel chromatography eluting with DCM/ethyl acetate mixtures of increasing polarity (see A3.2.1

Section). The following products (Scheme 3.1) were isolated: **2a** (white powder, 46% yield) and **3a** (white powder, 5% yield). The insoluble (in most organic solvents, including DMSO) fraction **P1a** (85 mg, 44%) was obtained in two fractions: the first, as a precipitate (40 mg) and the second, as the material (45 mg) recovered by the top of the chromatographic column. The structure of compounds **2a** and **3a** was assigned by NMR spectroscopy and by electrospray ionization high-resolution mass spectrometry (ESI-HRMS). With regard to **2a**, the comparison of its NMR spectral data with those of the parent resorc[4]arene **1a** evidenced the following points. Proton and carbon signals (AB part of an ABM system) for the terminal methylene group of **1a** are absent, while the signal for an olefinic double bond (M part in **1a**) is still present (slightly shifted upfield) in **2a** and linked with a methylene group of the chain, as shown by TOCSY spectra. These evidences support the formation of a new double bond between two chains with the elimination of one molecule of ethylene, as required by a ring-closing metathesis. As a confirmation, the sodium adduct $[M + Na]^+$ in the ESI mass spectrum of **2a** was found at *m/z* 1407.84543, that is 56 *m/z* ($2 \times C_2H_4$) less than the corresponding $[M + Na]^+$ peak of **1a** (*m/z* 1463.91035). As expected for a long hydrocarbon chain derivative, both the peaks originated a series of ions decreasing in intensity by losses of a methylene unit (14 *m/z*). Moreover, the resonance at δ 5.34 (*br* t, *J*

= 3 Hz) for the =CH methine is flanked by a minor signal (*br* t, *J* = 4 Hz) at δ 5.32. The two peaks, in approximate integrated ratio of 3:1, were correlated (by TOCSY data) to methylene signals at δ 2.01 and 2.03, as well as to the corresponding carbon resonances (by HSQC) at δ 32.0 and 26.8, respectively. The two peaks were thus assigned to *trans* and *cis* olefinic protons, respectively, in agreement with the expected highfield carbon value of the α-CH_2 in the *cis* configuration. Furthermore, whereas the signal at δ 5.34 showed a strong spatial correlation (by NOESY data) with the protons of both α- and β-methylene groups, the minor signal at δ 5.32 ppm was NOE-correlated only to the protons of the geminal methylene nucleus, as required for *trans* and *cis* olefinic protons, respectively. Two predictable RCM thus occurred independently between two neighbour chains (e.g. C-2/C-20 or C-8/C-14) on opposite faces of the planar aromatic rings. As a result, two bridges, featuring an inner double bond, were formed, leading to a bicyclic alkene structure for **2a**. The geometrical isomerism of the double bond did not apparently influence the NMR resonances of the remaining methylene groups. Only two small satellite peaks at δ 6.85 and 6.18 appeared in the ^{1}H NMR spectrum of **2a** and were attributed to the H-25/27 and H-26/28 protons of the *cis* form, respectively. Though formally the whole molecule may have a *tt* (55%), *tc* (35%) or *cc* (10%) double bonds distribution pattern, actually the compound can

be described as a *E*/*Z* (3:1) mixture of two independent moieties (for the sake of clarity, we reported in Scheme 3.1 just the *Z* stereoisomer of **2a**).

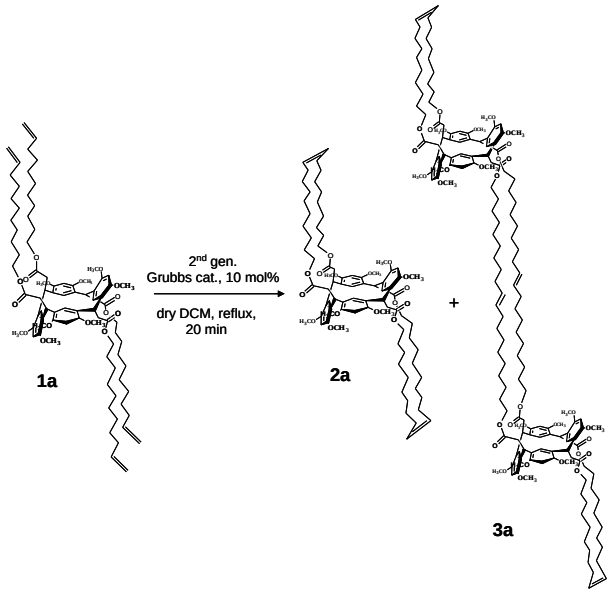

Scheme 3.1. Olefin metathesis reaction on undecenyl resorc[4]arene **1a**.

Catalytic hydrogenation (10% Pd/C) of **2a** led to the unique reduction compound **2ar**, which showed the expected $[M + Na]^+$ peak at 1411.87772 *m/z* and clean signals without satellite peaks in the ^1H and ^{13}C NMR spectra.

With regard to the minor product **3a**, the ^1H NMR spectral data (see Table 3.3 of Section A3.2) are almost coincident with those of **2a**,

except for the signals of a new =CH-CH_2-CH_2 sequence, belonging to a second disubstituted *trans* double bond, again with a minor 1:3 *cis* partner. Two diagnostic peaks at 2792.69337 and 1407.84371 *m*/*z* in the ESI mass spectrum, which were attributed to $[M + Na]^+$ and $[M + 2Na]^{2+}$ sodium adducts, respectively, revealed a molecular weight of 2769.7 Da and a molecular formula $C_{168}H_{240}O_{32}$. The two ions were flanked by the expected peaks corresponding to serial losses of CH_2 (14 and 7 *m/z*, respectively). These findings suggested the presence of two new intermolecular eleven carbon chains, while two intramolecular bridges as in **2a** were still remaining: in summary, the formation of a linear dimer **3a**, as depicted in Scheme 3.1. The novel chain could have been originated by a double cross-metathesis (CM) intermolecular closure of the neighbour chains of two different molecules of **1a**, but, more likely, it derives from the reaction between two molecules of **2a**. The role of bicyclic alkene **2a** as a key intermediate in the pathway leading to the linear dimer **3a** was stressed by submitting an aliquot of pure **2a** to the same olefin metathesis conditions (time, temperature and catalyst) as those used for **1a** (see A3.2.2 Section). As a result, derivative **3a** was obtained in a comparable 10% yield as the main product, among a series of more polar compounds which were not isolated. Around 34% of unreacted starting bicycle **2a** was recovered, but only traces of polymeric products were noticed on the TLC baseline.

A3.1.2 ADMET-like polymerization

Besides bicycle **2a** and dimer **3a**, olefin metathesis of undecenyl resorc[4]arene **1a** afforded the insoluble (in most organic solvents, including DMSO) fraction **P1a** (85 mg, 44%) as an amorphous solid, which was characterized by solid state ^{13}C CPMAS NMR spectroscopy. Solid state NMR, in fact, is a powerful method to understand macrostructure and morphology of synthetic polymers (Yu and Guo, 1990). The ^{13}C CPMAS NMR spectrum of **P1a** is shown in Fig. 3.2. The signals obtained, although typically broadened, perfectly match the corresponding signals of **2a** recorded in solution (see Table 3.2 of section A3.2.1), including the disappearance of the terminal methylene signal, which confirmed that a metathesis reaction had occurred. However, the quality of the double bond (whether intra or intermolecular) could not be established.

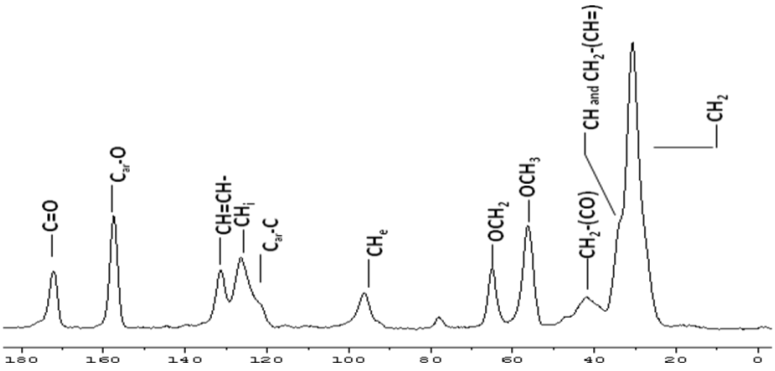

Figure 3.2. Solid state ^{13}C CPMAS NMR spectrum of **P1a** measured at 100.63 MHz with the contact time 6 ms (room temperature).

Fourier-Transform IR spectrum of **P1a** showed a broad absorption band at 3444 cm^{-1} and identical sharp peaks as those obtained for the parent undecenyl resorc[4]arene **1a**, as well as for bicycle **2a** and dimer **3a**. This means that, in the polymer, the typical functional groups are still present. The huge band around 3444 cm^{-1} is indicative of intermolecular hydrogen bonding interactions occurring into the labyrinthic framework of the polymer. Unfortunately, the insolubility of **P1a** in most organic solvents prevented the resort to both gel permeation chromatography (GPC) and MALDI-TOF mass spectrometry to obtain molecular weight distribution; however, elemental analysis of the sample was in satisfactory agreement with the molecular formula $(C_{84}H_{120}O_{16})_n$, where $C_{84}H_{120}O_{16}$ is the monomer (with n =1), if we assume that **P1a** is a homogeneous polymer. We afterwards hypothesized that **P1a** is a cross-linked polymer formed by an ADMET-like reaction, even though in different conditions. The ADMET polymerization is the result of the reversible condensation of highly pure dienes into linear polymers (Wagener et al., 1991a; Wagener et al., 1991b; Tindall et al., 1998). The presence of two isolated undecenoxy groups with active sites quite far from the bulky constituent in the core of the molecule (Allcock et al., 2001) and from any “negative neighboring group” effect (Wagener et al., 1997) makes resorc[4]arene **1a** particularly suitable for such reaction. The ring

closure between two vicinal chains is competitive in the CM conditions and, possibly, will complicate the inner structure of the polymer. When the ADMET reaction is carried out under solvent-free conditions with constant (or intermittent) vacuum (Wagener and Smith, 1991; Smith and Wagener, 1993), the competitive intramolecular CM reaction does not work and the conditions are thus favorable for linear polymers to be formed. Therefore, we submitted resorc[4]arene **1a** to a previously reported ADMET polymerization procedure; again, an insoluble polymer was obtained with a solid state ^{13}C CPMAS NMR spectrum coincident with that of **P1a**, resulting from the olefin metathesis of the same precursor. The insolubility of both the products obtained by classical olefin metathesis and ADMET polymerization of resorc[4]arene **1a** suggests the formation of a complex polymeric architecture with ramifications due to the competitive intramolecular CM reaction and/or the intermolecular link between two distant molecules. We can reasonably expect that a polymeric line will be formed from a chain reaction of two side chains of different molecules A, B, C and so on, but the two free terminal methylene groups of any unit (e.g., A) will react not necessarily with one of the neighbour molecule (e.g., B), rather with any other mobile member of the polymeric line. The structure represented in Figure 3.3 is only a possible formal representation of the constitutional repeating unit of the

polymer, that is $(C_{84}H_{120}O_{16})_n$, and the presence of chains with terminal alkene can be considered negligible. In such a way, bicycle alkene **2a** can be considered as the monomer (n = 1, molecular weight 1385 Da) and compound **3a** the corresponding dimer (n = 2, molecular weight 2770 Da).

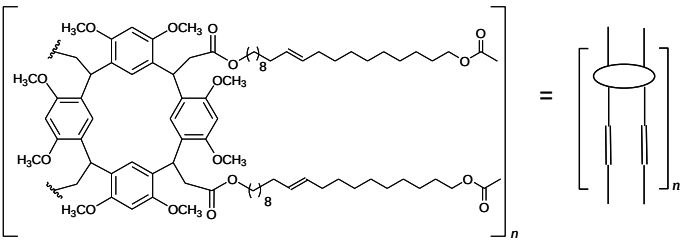

Figure 3.3. Formal representation of the constitutional repeating unit, i.e., $(C_{84}H_{120}O_{16})_n$ of polymer **P1a**.

A3.2 Experimental section

General procedures and materials

All manipulations were performed using a combination of glovebox and high vacuum under a nitrogen atmosphere. HPLC grade solvents were dried and degassed by standard procedures. Second-generation Grubbs and Grubbs-Hoveyda catalysts were purchased from Sigma Aldrich, together with QuadraSil AP silica gel.

NMR measurements

NMR spectra were recorded at 300 K on a Bruker AVANCE AQS600 spectrometer operating at the proton frequency of 600.13 MHz and equipped with Bruker a z-gradient inverse probe head capable of producing gradients in the z-direction with a strength of 55.4 G cm^{-1}. ^{1}H and ^{13}C NMR spectra were always referenced to residual $CHCl_3$ signal (1H, δ = 7.26 ppm; ^{13}C, δ = 77.20 ppm). The ^{1}H NMR spectra were acquired using the following experimental conditions: number of scans 16–32, recycle delay 5 s, $\pi/2$ pulse 9.0 µs, and 32K data points. ^{1}H diffusion filter-edited NMR spectra were obtained using a double stimulated echo pulse sequence incorporating a longitudinal eddy current delay with a Δ of 160 ms, a δ of 2.6 ms, and a longitudinal eddy current delay of 25 ms. A gradient pulse

recovery time of 0.1 ms, 2% and 60% of the maximum gradient intensity were used. Sixty-four scans were accumulated in time domain with 32768 points. 2D NMR experiments, namely $^{1}H–^{1}H$ TOCSY, $^{1}H–^{1}H$ NOESY, $^{1}H–^{13}C$ HSQC and $^{1}H–^{13}C$ HMBC,35 were performed using the following experimental conditions: $^{1}H–^{1}H$ TOCSY and $^{1}H–^{1}H$ NOESY were acquired in phase sensitive mode using TPPI selection, a 6 kHz spectral width in both dimensions, a 1.8 s relaxation delay, a 80 ms contact time for TOCSY and a 400 ms mixing time for NOESY, 2048 data points in f2 and 512 increments in f1. Zero filling in f1 to 1024 real data points and unshifted sinusoidal window functions in both dimensions were applied before Fourier transformation. The $^{1}H–^{13}C$ gradient-selected HSQC experiment was acquired in phase-selective mode with the following parameters: 13.8 μs π/2 ^{13}C hard pulse and 73 μs for composite pulse GARP ^{13}C decoupling sequence (GARP, Globally optimized Alternating-phase Rectangular Pulses), 6 and 30 kHz spectral widths in the proton and carbon dimensions, respectively, 2.5 s relaxation delay, 1024 data points in f2 and 512 increments in f1. Linear prediction up to 1024 point and unshifted squared cosine window functions were applied in the f1 dimension before Fourier transformation. The $^{1}H–^{13}C$ HMBC spectrum was obtained with a 2 s relaxation delay, π/2 pulse of 13.8 μs for ^{13}C, 6 and 30 kHz spectral widths in the proton and carbon dimensions, respectively, 1024 data points in f2, 512

increments in f1, linear prediction up to 1024 points in f1, processed with the use of unshifted sinusoidal window functions in both dimensions.

A3.2.1 Olefin metathesis reaction on undecenyl resorc[4]arene 1a

Resorc[4]arene ω-undecenyl ester **1a** (0.2 g, 0.14 mmol) was dissolved in dry DCM (46 mL) to reach a final substrate concentration of 3.0×10^{-3} M. The solution was heated at reflux temperature and then exposed to a solution of the $[(H_2IMes)(PCy_3)(Cl)_2Ru{=}CHPh)]$ catalyst (0.012 g, 0.014 mmol, 10 mol%) in dry DCM (4 mL), previously prepared into the glovebox. The reaction mixture was kept at reflux under stirring and nitrogen atmosphere for 20 min and afterwards treated with QuadraSil AP metal scavenger (aminopropyl silica gel, 4 g). After 5 min, the mixture was cooled to room temperature and left under stirring overnight. After filtration and evaporation, the residue was suspended in DCM and the soluble part was applied onto a silica gel column to give compound **2a** (88 mg, 46%, with DCM/ethyl acetate, 97:3) and product **3a** (10 mg, 5%, with DCM/ethyl acetate, 93:7). The yield of the insoluble portion **P1a** (85 mg in total, of which 45 mg recovered from the top of the column) was 44%.

*Bicyclic alkene **2a***

White powder, 46% yield. Mp: 190.9 ± 0.5 °C. ^{1}H and ^{13}C NMR signals are reported in Table 3.2. HRMS (ESI): *m/z* calcd for $C_{84}H_{120}O_{16}$ + Na^{+}: 1407.84686 $[M + Na]^{+}$ (monoisotopic mass); found: 1407.84543. FT-IR (KBr): 2921, 2850, 1728, 1583, 1506, 1301, 1201 cm^{-1}. In Figure 3.5 is reported a representative ^{1}H-NMR spectrum of bycyclic alkene **2a**.

Table 3.2. ^{1}H NMR and ^{13}C NMR signals* of bicyclic alkene **2a**

Carbon	^{13}C	^{1}H
C=O	172.5	-
C_{Ar}–O	156.5 155.6	-
CH= (*trans*) CH= (*cis*)	130.8 [130.1]	5.34 br t (3) [5.32 br t (4)]
CH_i (26,28) CH_i (25,27)	126.3 125.3	6.17 br s [6.18 br s] 6.84 br s [6.85 br s]
C_{Ar}–C	125.3 122.6	-
CH_e (5,17) CH_e (11,23)	97.4 95.5	6.48 s 6.40 s
OCH_2	64.3	3.95 dd (11.5, 7) 3.89 m
OMe	56.1 55.9	3.64 s 3.90 s
CH_2-(CO)	39.7	2.69 dd (14.5, 7) 2.64 dd (14.5, 7)
CH_2-(CH=)	32.0 [26.8]	2.01 m [2.03 m]
CH	32.8	5.05 t (7)
CH_2-(CH_2-CH=)	28.9	1.35 m
CH_2-(CH_2O)	28.6	1.50 m
$CH_2 \times 5$	29.5 29.3 29.1 28.1 25.9	1.24 br m

* 600 MHz (^{1}H) and 100 MHz (^{13}C), $CDCl_3$, *T* = 300 K; coupling constants *J* (Hz) are given in parentheses. Proton and carbon resonances for the *cis* form, not coincident or overlapped by those of the *trans* form, are indicated by square brackets.

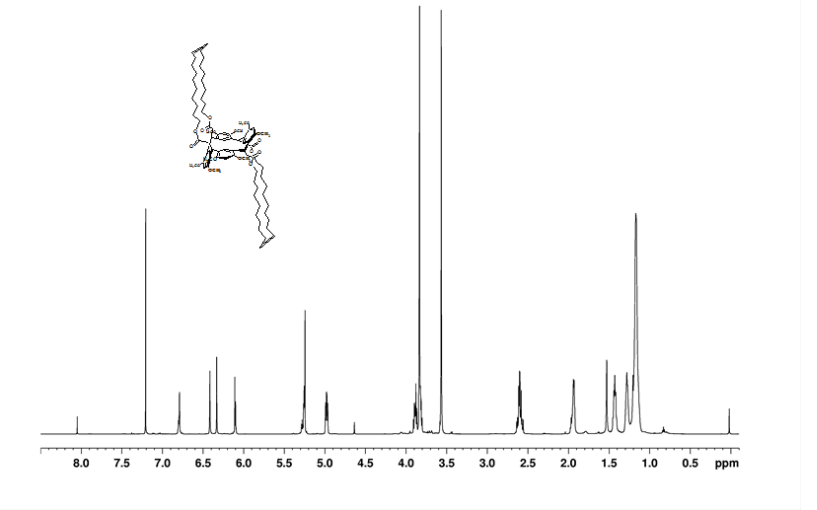

Figure 3.5. ^{1}H NMR spectrum of bicyclic alkene **2a.** 600 MHz, $CDCl_3$, 300 K.

*Dimer **3a***

White powder, 5% yield. Mp: 166.9 ± 0.5 °C. ^{1}H and ^{13}C NMR signals are reported in Table 3.3. HRMS (ESI): *m/z* calcd for $C_{168}H_{240}O_{32}$ + Na^{+}: 2792.70450 $[M + Na]^{+}$ (monoisotopic mass) and for $C_{168}H_{240}O_{32}$ + Na^{2+}: 1407.84686 $[M + 2Na]^{2+}$ (monoisotopic mass); found: 2792.69337 and 1407.84371. FT-IR (KBr): 2923, 2852, 1736, 1508, 1458, 1300, 1203 cm^{-1}. In Fig. 3.6 is reported a representative ^{1}H NMR spectrum of dimer **3a**.

Table 3.3. ^{1}H NMR and ^{13}C NMR signals* of linear dimer **3a**

Carbon	^{13}C	^{1}H
C=O	172.5	-
C_{Ar}–O	156.5 155.6	-
CH= (*trans*) CH= (*cis*)	130.8 130.3 [130.1] [129.8]	5.33 tt (3,1) 5.38 tt (3,1) [5.35 m] [5.36 m]
CH_i (26,28) CH_i (25,27)	126.3 125.3	6.18 br s 6.87 br s
C_{Ar}–C	125.3 122.6	-
CH_e (5,17) CH_e (11,23)	97.4 95.5	6.49 s 6.41 s
OCH_2	64.3	3.92 m 3.87 m
OMe	56.1 55.9	3.60 s 3.88 s
CH_2-(CO)	39.7	2.67 m
CH_2-(CH=)	32.6 32.0 [26.7] [26.8]	1.96 m 2.02 m [2.03 m] [2.03 m]
CH	32.8	5.04 t (7.5)
CH_2-(CH_2-CH=)	29.4 28.9	1.32 m 1.35 m
CH_2-(CH_2O)	28.6	1.50 m
$CH_2 \times 5$	29.5; 29.3; 29.1; 28.1; 25.9	1.24 br m

* 600 MHz (^{1}H) and 100 MHz (^{13}C), $CDCl_3$, *T* = 300 K; coupling constants *J* (Hz) are given in parentheses. Proton and carbon resonances for the *cis* form, not coincident or overlapped by those of the *trans* form, are indicated by square brackets.

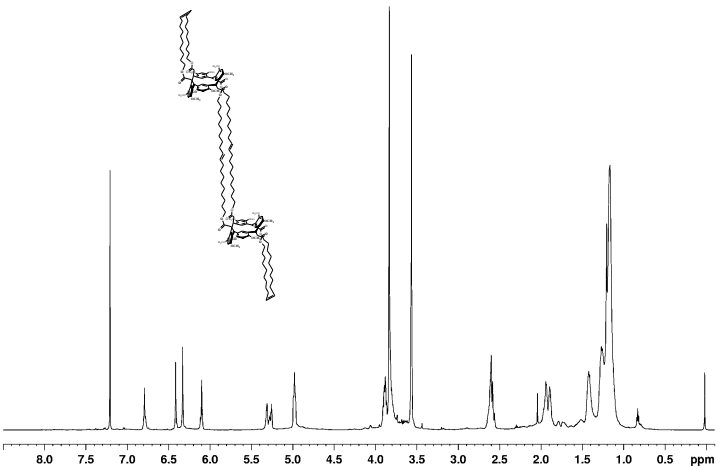

Figure 3.6. ^{1}H NMR spectrum of linear dimer **3a.** 600 MHz, $CDCl_3$, 300 K.

*Polymer **P1a***

White amorphous solid, 44% yield, which did not melt, nor soften (visually) under 300 °C. Solid state ^{13}C CPMAS NMR: δ 172.4 (C=O), 157.7 (C_{Ar}-O), 131.4 (CH=CH-), 126.4 (CH_i), 124.3 (C_{Ar}-C), 96.4 (CH_e), 65.0 (OCH_2), 56.3 (OCH_3), 41.9 (CH_2-C=O), 30.7 (CH and CH_2-CH=), 30.6 (CH_2). FT-IR (KBr): 3444 (broad), 2925, 2848, 1729, 1614, 1504, 1466, 1301, 1202 cm^{-1}. Elemental analysis (%): found: C 73.9 $\pm$ 0.69, H 8.79 $\pm$ 0.05. If we assume that **P1a** is a homogeneous polymer and $C_{84}H_{120}O_{16}$ is the molecular formula of the monomer, it requires C 72.8, H 8.73.

A3.2.2 Olefin metathesis reaction on compound 2a

Compound **2a** (0.070 g, 0.05 mmol) was dissolved in dry DCM (17 mL) to reach a final substrate concentration of 3.0×10^{-3} M. The solution was heated at reflux temperature and then exposed to a solution of the [$(H_2IMes)(PCy_3)(Cl)_2Ru$=CHPh)] catalyst (0.0045 g, 0.005 mmol, 10 mol%) in dry DCM (3 mL), previously prepared into the glovebox. The reaction mixture was kept at reflux under stirring and nitrogen atmosphere for 60 min and afterwards treated with QuadraSil AP metal scavenger (aminopropyl silica gel, 1.5 g). After 5 min, the mixture was cooled to room temperature and left under stirring overnight. After filtration and evaporation, the residue was purified by silica gel chromatography with DCM/ethyl acetate, 93:7 (v/v) as eluent, to give compound **3a** (7 mg, 10%) and more polar compounds which were not isolated. The starting bicyclic alkene **2a** was recovered unreacted from the column eluting with DCM/ethyl acetate, 97:3 (46 mg, 34% by weight).

A3.2.3 Catalytic hydrogenation of 2a

After two vacuum/nitrogen cycles to replace the air inside the reaction tube, compound **2a** (42 mg, 0.030 mmol) and 10% Pd/C (10 mg) in dry THF (5 mL) were vigorously stirred at room temperature under 1 atm of hydrogen for 24 h. The reaction mixture was filtered

through a membrane filter (Millipore, Millex-LH, 0.45 mm) and the filtrate was concentrated. Purification of the residue by silica gel chromatography (DCM : ethyl acetate = 99 : 1 → 97 : 3) gave compound **2ar** (white solid, 42 mg, 0.030 mmol, quantitative yield). Mp: 184.3 ± 0.5 °C. ^{1}H NMR (400 MHz, $CDCl_3$, 300 K): δ (ppm) 6.81 (br s, CH_i-25,27), 6.45 (s, CH_e-5,17), 6.39 (s, CH_e-11,23), 6.21 (br s, CH_i-26,28), 5.03 (t, J = 7 Hz, 4H, CH), 3.92 (dd, J = 11.5 Hz, J = 7 Hz, 4H, OCH2), 3.87 (s, 12H, OMe), 3.91 (m, 4H, OCH_2), 3.64 (s, 12H, OMe), 2.69 (dd, J = 14.5 Hz, J = 7 Hz, 4H, CH_2–CO), 2.66 (dd, J = 14.5 Hz, J = 7 Hz, 4H, CH_2–CO), 1.49 (m, 8H, CH_2– CH_2O), 1.26 (br m, 16H, 8 6 CH_2); 13C NMR (100 MHz, $CDCl_3$, 300 K): δ (ppm) 172.4 (s, C=O), 156.5, 155.8 (s each, C_{Ar}–O), 126.6 (d, CH_i 26,28), 125.8 (d, CH_i 25,27), 125.1, 122.8 (s each, C_{Ar}–C), 97.3 (d, CH_e 5,17), 95.6 (d, CH_e 11,23), 64.2 (t, OCH_2), 56.1, 55.9 (q each, OMe), 39.6 (t, CH_2–CO), 32.8 (d, CH), 29.7, 29.3, 29.0, 28.9, 28.8, 28.5, 28.3, 28.2, 25.7 (t each, 9 x CH_2). HRMS (ESI): *m/z* calcd for $C_{84}H_{124}O_{16}$ + Na^+: 1411.87816 $[M + Na]^+$ (monoisotopic mass); found: 1411.87772.

A3.2.4 ADMET reaction on undecenyl resorc[4]arene 1a

According to a literature method (Allcock et al., 2001), resorc[4]arene ω-undecenyl ester **1a** (0.5 g, 0.35 mmol) was added under a dry, nitrogen atmosphere to a previously evacuated and

flame dried, high-vacuum valve equipped flask. The [(H_2IMes)(PCy_3)($Cl)_2$Ru=CHPh)] catalyst (7.5 mg, 8.8×10^{-3} mmol, 2.5 mol%) was dissolved in dry DCM (0.5 mL) into the glovebox under a nitrogen atmosphere. Such solution was *vacuum* transferred to the flask and the resulting mixture heated at 60 °C under full vacuum and magnetic stirring. After 1 h and evaporation of all the solvent, the temperature was gradually increased to 80 °C to maintain fluidity and facilitate stirring. Immobilization of the stirrer bar and discoloration of the catalyst occurred within an additional half an hour. The reaction mixture was filtered on paper and washed with DCM to give AD-1 fraction (223 mg). The washings were concentrated and the residue was suspended in a small volume of DCM. The insoluble gelly fraction was separated, washed with *n*-hexane/DCM mixtures to give a second AD-2 fraction (12 mg) for an overall 49% yield. Both AD-1 and AD-2 fractions were insoluble in most organic solvents (including DMSO), as well as in 1 N or 12 N HCl. Solid state ^{13}C CPMAS NMR of fraction AD-1: δ 172.8 (C=O), 157.9 (C_{Ar}-O), 131.8 (CH=CH-), 126.7 (CH_i), 124.5 (C_{Ar}-C), 96.6 (CH_e), 65.4 (OCH_2), 56.6 (OCH_3), 42.2 (CH_2-C=O), 31.1 (CH and CH_2-CH30.8 (CH_2). Solid state ^{13}C CPMAS NMR of fraction AD-2: δ 172.2 (C=O), 157.4 (C_{Ar}-O), 131.2 (CH=CH-), 126.3 (CH_i), 124.0 (C_{Ar}-C), 96.1 (CH_e), 64.9 (OCH_2), 56.1 (OCH_3), 41.7 (CH_2-C=O), 31.5 (CH and CH_2-CH=),

30.5 (CH_2). Elemental analysis of AD-1 fraction: calcd (%) for $(C_{84}H_{120}O_{16})_n$: C 72.8, H 8.73; found: C 73.5 $\pm$ 0.69, H 8.94 $\pm$ 0.16

Chapter A4
NMR Detection of a Ruthenium-Carbene-Resorc[4]arene Complex

A4.1 Results and discussion

Chapter A3 reported that undecenyl resorc[4]arene **1a** (in the *chair* conformation), due to the relatively simple arrangement of its chains, may give different metathesis products by exposure to Grubbs catalysts. Under optimized reaction conditions, two major products were isolated, namely, the bicyclic alkene **2a** (46%) and the dimer **3a** (5%) (See A3.1.1 Section). The synthesis of compound **2a** occurs by two almost contemporary RCM reactions, driven by the elimination of two molecules of ethylene (Scheme 4.1), which proved to be a powerful driving force for intra- and intermolecular metathesis (Monfette and Fogg, 2009). The reaction was also reported for *p*-tert-butylcalix[4]arenes, characterized by two similar but shorter chains ending with a terminal alkene, which gives the corresponding cyclic alkenes (Yang et al., 2007).

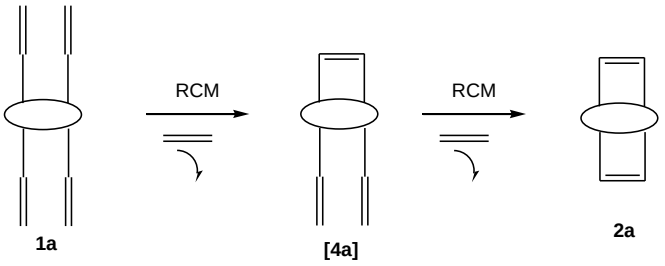

Scheme 4.1. Proposed reaction mechanism for the formation of bicyclic alkene **2a** starting from undecenyl resorc[4]arene **1a**.

Furthermore, we clearly demonstrated that the dimer **3a** is formed by reaction of two molecules of **2a** (Scheme 4.2) by submitting **2a** to the same reaction conditions (namely, time, temperature and catalyst) as those used for the starting terminal olefin **1a**. Accordingly, the mechanism was supposed to imply the two following steps: (i) the ROM of **2a**, and (ii) the concerted double CM between the ruthenium-carbene-resorc[4]arene complex **2a[Ru]** and a second molecule of **2a**, passing through the carbene complex **3a[Ru]**.

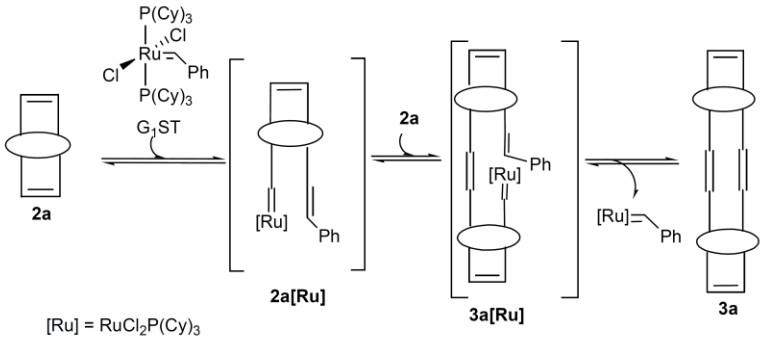

Scheme 4.2. Proposed mechanism for the dimerization of resorc[4]arene bicyclic olefin **2a**.

A4.1.1 Detection of a ruthenium-carbene-resorc[4]arene complex during the progress of a metathesis reaction

In the current study, we have decided to monitor the formation of such ruthenium-carbene-resorc[4]arene complexes by high-

resolution (600 MHz) ^{1}H and ^{31}P NMR spectroscopy, in order to get an exhaustive picture of the mechanism involved. For this purpose, resorc[4]arene bicyclic olefin **2a** was supposed to react with the metathesis catalyst directly into the NMR tube, using a proper deuterated solvent.

The first problem we faced was the choice of the suitable catalyst generation: Grubbs and co-workers proposed a general mechanism for ruthenium-catalyzed olefin metathesis where dissociation of an organophosphine ligand is a critical step in forming a 14-electron ruthenacarbene intermediate, which reacts with the olefin to generate a four-coordinate intermediate (Sanford et al., 2001). We needed a catalyst that had a reduced catalytic activity towards our substrate, in order to be able to monitor the reaction step by step. It is widely accepted that exists an inverse relationship between organophosphine dissociation (i.e., catalyst production) and catalytic activity for the two Grubbs catalyst generations: in the bis-phosphine systems (namely, G_1ST), the 14-electron intermediate is formed faster than in the second-generation catalysts (G_2ND), but they show a much lower catalytic activity. The different rates of catalyst production in G_1ST and G_2ND precatalysts have been quantitatively attributed to the different energy barriers for the rotation of carbene, which also play a key role in the olefin binding step (Yang et al., 2011). We therefore decided to use G_1ST as the

catalyst for the metathesis reaction of resorc[4]arene bicyclic olefin **2a**, since we expected a plausible scenario where the inactive rotamer would have been more favored.

A first experiment was done using a 1:1 resorc[4]arene **2a**/G_1ST ratio, in $CDCl_3$. The ^1H NMR spectrum of the catalyst shows a sharp singlet centered at 19.98 ppm (see Figure S1 of Section A4.2.7), which can be ascribed to the alkylidene proton. The corresponding ^{31}P NMR spectrum shows the expected signal at 53.37 ppm.

With regard to the kinetic analysis, the ^1H NMR spectrum of the freshly prepared reaction mixture shows two well-separated signals centered at 19.98 and 19.26 ppm (see Figure S2 of Section A4.2.7), due to the native form of the catalyst and the supposed intermediate ruthenium complex **3a[Ru]**, respectively. In the 1D TOCSY spectrum, the signal centered at 19.26 ppm gave scalar correlations to the methylene protons directly bound to the oxygen of the resorc[4]arene bridges (Figure 4.1). In addition, a correlation with a signal at 2.75 ppm is detected, attributed to the allylic methylene protons. These results indicate that a ruthenium species containing phosphorous ligands has been linked to the resorc[4]arene core.

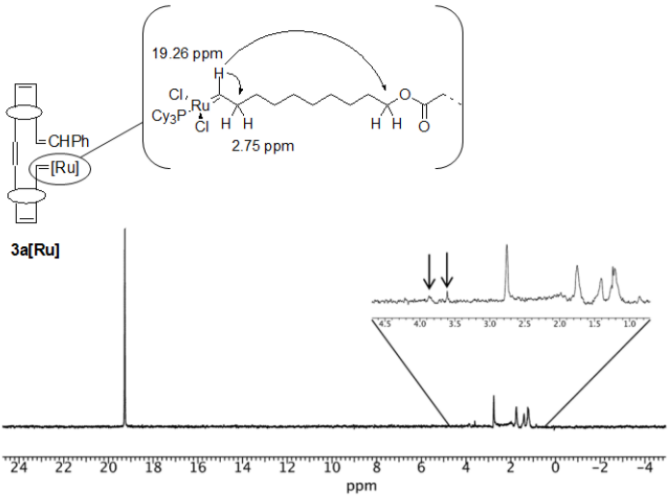

Figure 4.1. 1D TOCSY (600 MHz, $CDCl_3$, 25 °C, mixing time 150 ms) spectrum of the proton at 19.26 ppm; the arrows point to the methylene protons bound to the oxygen atom of the resorc[4]arene.

In the ^{31}P NMR spectrum of the mixture, two distinct resonances at 53.37 and 52.68 ppm are detected, whose integrated areas are in agreement with those detected in the ^{1}H NMR spectrum for the two signals centered at 19.98 ppm and 19.26 ppm, respectively (see Figure S2 of Section A4.2.7).

The increase of the ^{1}H resonance at 19.26 ppm during the reacting time is followed by a congruent increase of signals (partially superimposed to the aromatic resorc[4]arene signals), and centered at 6.35 and 6.20 ppm. They were attributed to the two protons of the -HC=CHPh system installed on the resorc[4]arene, as clearly

demonstrated by the reciprocal scalar correlation and the dipole-dipole interactions detected between such protons and the phenyl (ortho protons) resonance at 7.31 ppm in the 2D ROESY spectrum (see Figure S3 of Section A4.2.7). These olefin resonances are *J*-coupled to the allylic methylene protons at 2.17 ppm (CH_2 at 33.0 ppm, gHSQC). Their connection to the resorc[4]arene core unit was confirmed by TOCSY correlations produced by the signal centered at 2.17 ppm and the methylene protons directly bound to the oxygen of the resorc[4]arene pendants (see Figure S4 of Section A4.2.7).

In the double bonds region ranging from 5.45 to 5.20 ppm, a new resonance at 5.38 ppm appears, which is not present in the ^{1}H NMR spectrum of **2a** (Figure 4.2a). Moreover, the signals in this spectral region have a minor integrated area than that generated by the methine protons on the resorc[4]arene bridges (5.02 ppm). Interestingly, the lack of integrated area to achieve a 1 to 1 ratio (as in **2a**) between these two regions (olefin/methine bridge protons) is correlated to the integrated area of olefin protons at 6.35 ppm and 6.20 ppm bound to the phenyl moiety. Such new kinds of double bond signals (5.38 ppm and 6.35/6.20 ppm) are formed during the reaction at the expense of the internal vinyl protons of the resorc[4]arene core (5.31 ppm and 5.33 ppm, Figure 4.2b-c).

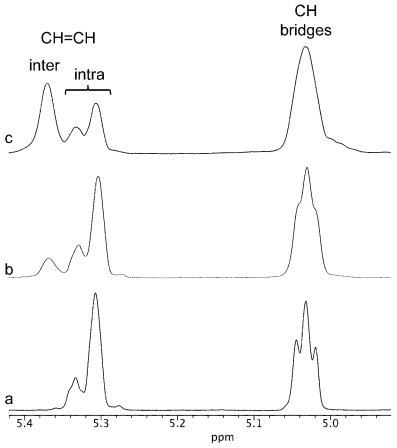

Figure 4.2. Expansion of the 5.45–4.70 ppm region in the ^{1}H NMR (600 MHz, $CDCl_3$, 25 °C) spectra of **2a** (a), freshly prepared 1:1 resorc[4]arene **2a**/G_1ST reaction mixture (b) and after 6.5 h reaction time (c).

As far as the proton(s) resonating at 5.38 ppm, they gave the ^{1}H-^{13}C correlation at 130.3 ppm, which is typical of olefin protons, and in the 1D TOCSY experiment correlations are detected with the allylic methylene at 1.93 ppm (36.3 ppm in the ^{13}C NMR spectrum) to methylene protons directly bound to the oxygens of the resorc[4]arene pendants (see Figure S5 of Section A4.2.7). This new signal corresponds to the internal double bond formed during an intermolecular reaction leading to dimer or trimer aggregates.

We found that the species linked to the metal (both the catalyst and the Ru-resorc[4]arene complexes) were subjected to degradation: in the ^{1}H NMR spectrum recorded after 22 h from the beginning of the

reaction, the singlets at 19.98 and 19.26 ppm disappeared, as well as the corresponding ^{31}P NMR resonances (namely, 53.37 and 52.68 ppm), and several new phosphorous signals were detected (see Figure S6 of Section A4.2.7). After degradation, an average diffusion coefficient of 1.7×10^{-10} m^2s^{-1} was measured in the DOSY map (see Figure S7-S8 of Section A4.2.7), to be compared to the value of 4.5×10^{-10} m^2s^{-1} measured for the starting resorc[4]arene olefin **2a**. This value confirmed the formation of dimer-to-trimer aggregates.

The experimental conditions reported up to now allowed us to carry out a qualitative characterization of the ruthenium-carbene-resorc[4]arene **3a[Ru]** complex, but the instability of the G_1ST catalyst in $CDCl_3$ prevented a quantitative characterization of the reaction outcome. Therefore, we performed several experiments in different solvents and C_6D_6 was selected as the optimum for the more stability of the G_1ST catalyst (Bielawski and Grubbs, 2007).

A4.1.2 Quantitative characterization of the reaction outcome

The metathesis reaction of resorc[4]arene bicyclic olefin **2a** was carried out in benzene in static conditions. Two different ratios were selected, involving an excess of olefin substrate relative to the catalyst (namely, **2a**/G_1ST 4:1 ratio) or the reverse (**2a**/G_1ST 1:4 ratio). Extensive purifications of the reaction mixtures by silica gel

column chromatography (DCM/ethyl acetate mixtures as eluents) led to isolate, among the reaction products, some pure compounds and some partially enriched mixtures. In both conditions, unreacted starting **2a** was recovered (35–40%), along with oligomeric products which were not isolated.

The reaction carried out in a 4:1 ratio (**2a**/G_1ST) led to the isolation, beside the known dimer **3a** (6%), of a new compound **4a** (2% yield, Figure 4.3), whereas the opposite condition (namely, 1:4 ratio **2a**/G_1ST) yielded again product **4a** (12.5%), a new compound **5a** (6%), and two enriched mixtures named **I** and **II** (*vide infra*). The characterization of both pure and enriched mixture products allowed us to develop an accurate NMR analytical protocol for the direct analysis of the crude reaction in a non-invasive fashion.

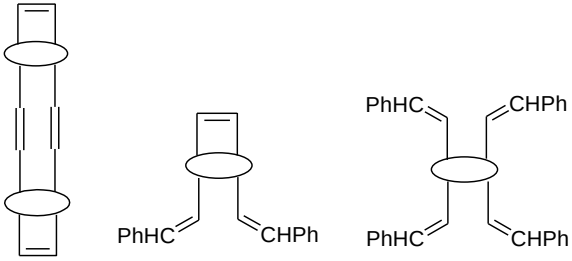

Figure 4.3. Schematic representation of the products isolated in the metathesis reaction of **2a** in benzene with G_1ST catalyst (**2a**/G_1ST = 4:1 and 1:4 ratio). For the chemical structures of compounds **3a**-**5a**, see A4.2.6 Section.

Compounds **4a** and **5a** proved to be monomers on the basis of their diffusion coefficients (D = 3.6 × 10^{-10} m^2s^{-1} and 3.8 × 10^{-10} m^2s^{-1}, respectively), which were quite similar to that measured for the starting olefin **2a** (D = 4.0 × 10^{-10} m^2s^{-1} in C_6D_6). For compound **3a**, a value of 2.6 × 10^{-10} m^2s^{-1} was obtained, according to a dimeric assembly.

Compound **4a** (for the structure, see Figure 4.4) shows a loss of the symmetry typical of **2a**, as well highlighted by inspection of the signals due to the resorc[4]arene core protons, the methine bridge protons, the O-bound and the C=C-bound methylene protons (Figure 4.4a-b). Two typical olefin signals centered at 6.38 ppm and 6.14 ppm and their integrated areas pointed out the presence of two CH=CHPh groups inserted on the resorc[4]arene skeleton. Furthermore, only one of the two intramolecular bridges initially present in **2a** was detected (5.37 and 5.45 ppm). Notably, the aromatic protons of A/A' rings, which are not involved in the formation of the intramolecular double bond between two side chains, are little affected, producing signals at 6.30 (H11/H23) and 6.85 (H25/H27) ppm. A strong perturbation was detected, instead, for the corresponding protons of B/B' rings. In particular, the signal for the H5/H17 protons centered at 6.08 ppm in the parent **2a** (Figure 4.4a) is splitted into two signals (1:1 ratio) at 6.07 (for H5) and 6.15 (for H17) ppm. In fact, proton H5 is in the same

environment as in **2a**, whereas H17 is surrounded by the two phenyl-bearing chains (see structure in Figure 4.4). The loss of symmetry for **4a** was confirmed by inspection of the methylene protons directly bound to the oxygen, which showed the original triplet (at 4.02 ppm), together with two strongly differentiated diastereotopic signals at 4.11 and 4.03 ppm (64.3 ppm in the ^{13}C NMR spectrum). The quartet at 2.12 ppm was diagnostic of the allylic methylene protons directly bound to the CH=CHPh terminal portion. The full NMR characterization of compound **4a** is given in Section A4.2.6.

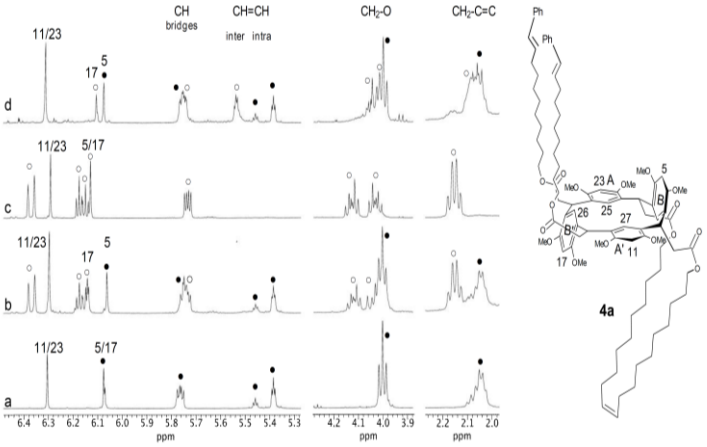

Figure 4.4. ^{1}H NMR (600 MHz, C_6D_6, 25 °C) spectra of compounds **2a** (a), **4a** (b), **5a** (c) and **3a** (d).
• = Signals belonging to B ring and its chains; ◦ = signals belonging to B' ring and its chains.

Compound **5a** showed the original symmetry featured by the starting bicyclic olefin **2a**, and the following patterns (Figure 4.4c): the lack of the signals for intramolecular double bonds; the aromatic protons H5/H17 of B/B' rings at the same chemical shift as observed for **4a**; a 2:1 olefin/methine bridge protons ratio, which suggests the presence of four open chains ending with CH=CHPh groups (Figure 4.3). The methylene protons directly bound to the oxygen and to the CH=CHPh moiety have the same spectral pattern found in **4a** (Figure 4.4b-c).

Compound **3a**, previously characterized, was identified for the signal at 5.53 ppm (130.4 ppm in the ^{13}C NMR spectrum), which confirmed the presence of an intermolecular double bond (Figure 4.4d). Any CH=CHPh moieties as in **4a** or **5a** were not detected. All the signals were in agreement with the structure already described (See Section A3.2.1).

Purification of the crude mixture obtained from the reaction carried out in a 1:4 ratio (**2a**/G_1ST) gave, beside compound **5a**, two additional reaction mixtures named **I** and **II**. To get a picture of the plausible structures of such mixtures we used the following two parameters (see Table 4.1): (*i*) the ratio between the integrated NMR areas of intermolecular double bonds (5.52 ppm) and olefin protons at 6.39 ppm (namely, inter/CH=CHPh ratio); (*ii*) the ratio between the intermolecular (5.52 ppm) and intramolecular (5.45

ppm and 5.37 ppm) double bonds (namely, inter/intra ratio). The combination of such parameters, which yielded the average number of CH=CHPh, intermolecular and intramolecular CH=CH groups, allowed the identification of three plausible dimers (namely, **6a-8a**) whose schematic structures are given in Figure 4.5. The average diffusion coefficient measured on the methine bridge protons of mixture **I** was 2.2×10^{-10} m^2s^{-1}, which suggests the prevalence of dimers in the mixture. In fact, the ratio between the integrated areas of the aromatic protons at 6.08 ppm, due to H5 proton of B ring included between intramolecularly bound chains, and the aromatic protons H11/H23 of A/A' rings at 6.32 ppm was 1:4. For mixture **II**, an average diffusion coefficient of 1.5×10^{-10} m^2s^{-1} was obtained, which suggests the presence of trimeric architectures built in a similar way as **6a-8a**.

Table 4.1. Ratios between the integrated NMR areas of the different types of double bonds expected for **2a**, **3a**, **6a-8a** and NMR experimental values found in mixtures **I** and **II** and in the reaction mixture with a 4:1 (**2a**/G_1ST) ratio.

Double bonds	**2a**	**3a**	**6a**	**7a**	**8a**	**I**	**II**	**2a**/G_1ST = 4:1
inter/CH=CHPh	0:0	2:0	1:2	1:1	1:4	1:1.8	1:1.1	1.7:1
inter/intra	0:2	1:1	1:2	2:1	1:1	1.5:1	3.2:1	1:3.6

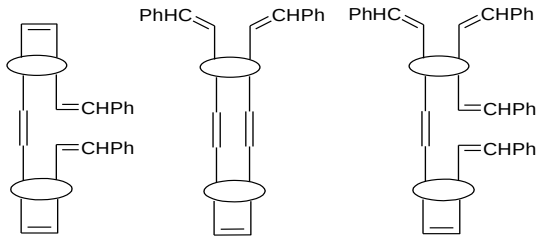

6a **7a** **8a**

Figure 4.5. Schematic representation of the plausible dimers formed in the metathesis reaction of **2a** in benzene with G_1ST catalyst (**2a**/G_1ST = 1:4 ratio).

The isolation of compounds **4a** and **5a** from the reaction mixture has been taken as an indirect proof of the formation of the ruthenium-carbene-resorc[4]arene complex **2a[Ru**] (Scheme 4.2), the first complex to be formed by ROM of the starting olefin **2a**, which rapidly evolves to **3a[Ru]**, by reaction with a second molecule. Indeed, when a 4-fold excess of the resorc[4]arene olefin **2a** is used, the ruthenium-carbene-resorc[4]arene complex **2a[Ru]** leads mainly to the self-metathesis product **3a** through a double CM with a second molecule of **2a** (see Scheme 4.3). When a 4-fold excess of catalyst is used, instead, the two carbene complexes **2a[Ru]** and **3a[Ru]** undergo a decomposition pathway typical of the G_1ST catalyst itself (Ulman and Grubbs, 1999), as outlined in Scheme 4.3.

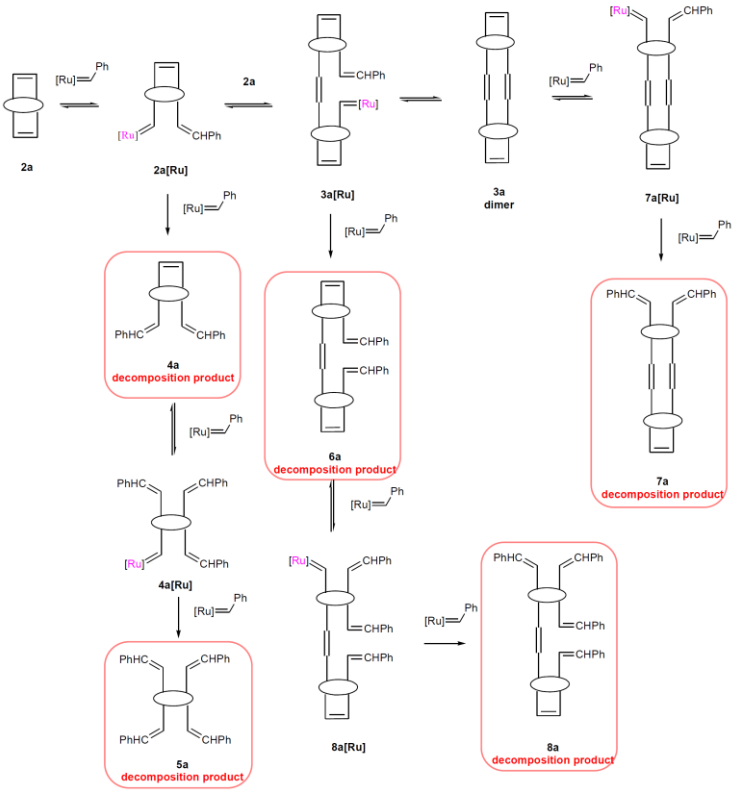

Scheme 4.3. General pathway for the decomposition of ruthenium-carbene-resorc[4]arene **2a[Ru]** and **3a[Ru]** complexes.

As a final refinement of our analytical NMR protocol, we decided to reproduce the same metathesis reaction carried out in benzene into the NMR tube, and selected, as probe reaction conditions, the 4:1 (**2a**/G_1ST) ratio.

The reaction proceeds with an increase of the species featuring an intermolecular double bond (Table 4.2), but the inter/CH=CHPh ratio was in favor of species like **3a** and **7a** (namely, 2:0 and 1:1, respectively, see Table 4.1).

Table 4.2. Integrated NMR areas of the double bonds at different reaction times (**2a**/G_1ST = 4:1).

Time	CH=CH intra	CH=CHPh	CH=CH inter
1 h	94.2	3.3	2.5
2.5 h	90.2	4.5	5.3
23 h	69.7	10.9	19.4

The decomposition of the catalyst was assessed to occur after 23 h of reaction time, on the basis of the complete disappearance of the ^{1}H NMR signals at 20.60 ppm and 19.80 ppm. As a consequence, the intra/inter ratio proved to be > 1 (see Table 4.1), indicating a high percentage of the starting olefin **2a**. Accordingly, the diffusion coefficient, measured on the intermolecular double bond (5.52 ppm), remains almost constant at 2.5×10^{-10} m^2s^{-1}, which is consistent with a dimeric structure, but the diffusion coefficient, measured on the protons of the resorc[4]arene bridges is higher ($D = 3.8 \times 10^{-10}$ m^2s^{-1}), in agreement with a high percentage of unreacted monomer. Moreover, an intermediate diffusion coefficient ($D = 3.0 \times 10^{-10}$ m^2s^{-1}), measured on the CH=CHPh

double bond, indicates the presence of monomer and dimer species containing CH=CHPh moieties.

These results proved to be in good agreement with those previously described for the reaction carried out in the same experimental conditions after work-up and purification.

A4.2 Experimental section

A4.2.1 General information

All manipulations were performed using a combination of glovebox and high vacuum under a nitrogen atmosphere. HPLC grade solvents were dried and degassed by standard procedures. First-generation Grubbs catalyst was purchased from Sigma Aldrich, together with QuadraSil AP silica gel and deuterated chloroform ($CDCl_3$, containing silver wire as stabilizer). Deuterated benzene (C_6D_6) was purchased from Deutero GmbH. Both solvents were employed without further purification.

A4.2.2 NMR and High-Resolution (HR) MS measurements

- NMR measurements were performed on a spectrometer operating at 600 MHz, 243 MHz and 150 MHz for ^{1}H, ^{31}P and ^{13}C nuclei, respectively. The temperature was controlled to ± 0.1 °C. The 2D NMR spectra were obtained by using standard sequences with the minimum spectral width required. Proton 2D gCOSY (gradient COrrelated SpectroscopY) spectra were recorded with 128-200 increments of 4-16 scans and 2K data points. The relaxation delay was 1 s. 2D TOCSY (TOtal Correlation SpectroscopY) spectra were recorded by employing a mixing

time of 80-120 ms. The pulse delay was 1 s; 256-512 increments of 16-32 scans and 2K data points each were collected. 1D TOCSY spectra were acquired with 1024-4096 scans in 32K data points with a 1 s relaxation delay and a mixing time ranging from 120 to 150 ms. The 2D ROESY (Rotating-frame Overhauser Enhancement SpectroscopY) experiments were performed by employing a mixing time ranging from 200 to 600 ms. The pulse delay was 1 s; 128-200 increments of 16-32 scans and 2K data points each were collected. 1D ROESY spectra were recorded using the selective pulse SEDUCE generated by means of the Agilent Pandora Software. The selective 1D ROESY spectra were acquired with 2048-8192 scans in 32K data points with a 1-5 s relaxation delay and a mixing time ranging from 300 to 600 ms. gHSQC (gradient Heteronuclear Single Quantum Coherence) and HMBC (Heteronuclear Multiple Bond Correlation) spectra were recorded by employing a pulse delay of 1 s and 128 or 200 increments of 32-128 scans. HMBC experiments were optimized for a long-range ^{1}H-^{13}C coupling constant of 8 Hz. DOSY (Diffusion Ordered SpectroscopY) experiments were carried out by using a stimulated echo sequence with self-compensating gradient schemes and 64K data points. Typically, g was varied in 20 steps (2-32 transients each) and Δ and δ were optimized in order to obtain an approximately 90-95% decrease in the resonance

intensity at the largest gradient amplitude. The baselines of all arrayed spectra were corrected prior to processing the data. After data acquisition, each FID was apodized with 1.0 Hz line broadening and Fourier transformed. The data were processed with the DOSY macro (involving the determination of the resonance heights of all the signals above a pre-established threshold and the fitting of the decay curve for each resonance to a Gaussian function) to obtain pseudo two-dimensional spectra with NMR chemical shifts along one axis and calculated diffusion coefficients along the other. Gradient amplitudes in DOSY experiments have been calibrated by using a standard sample of D_2O 99%.

- HR mass spectra were obtained using a Fourier-Transform Ion Cyclotron Resonance Mass Spectrometer (FT-ICR-MS), fitted with an electrospray ionization (ESI) source.

A4.2.3 Metathesis reaction into the NMR tube

Resorc[4]arene bicyclic olefin **2a** (20 mg, 0.014 mmol) was dissolved in $CDCl_3$ (0.35 mL) into a glovebox under a nitrogen atmosphere, and the solution was transferred into a NMR tube with a syringe. A solution of G_1ST [$Ru(=CHPh)Cl_2(PCy_3)_2$] catalyst (12 mg, 0.014 mmol) in $CDCl_3$ (0.35 mL) was then introduced, and the reaction course was

monitored, during the time, by ^{1}H NMR, ^{31}P NMR and DOSY spectroscopy.

A4.2.4 Metathesis reaction in benzene (2a/G_1ST = 4:1)

Resorc[4]arene bicyclic olefin **2a** (120 mg, 0.087 mmol) was dissolved in benzene (1.5 mL). The solution was exposed to a solution of the G_1ST [$Ru(=CHPh)Cl_2(PCy_3)_2$] catalyst (18 mg, 0.0218 mmol) in benzene (1.5 mL), previously prepared into the glovebox, to reach a 3×10^{-2} M substrate concentration. After stirring for 4 days at room temperature under a nitrogen atmosphere, the reaction mixture was kept heated to 50 °C for 6 h. Afterwards, it was cooled to room temperature, treated with QuadraSil AP metal scavenger (aminopropyl silica gel, 6 g) and left under stirring overnight. After filtration and evaporation, the residue was suspended in DCM and purified by silica gel column chromatography to give compounds **4a** (2.7 mg, 2%, with DCM-ethyl acetate, 97 : 3), **2a** (48.2 mg, 40%, with DCM-ethyl acetate, 97 : 3) and **3a** (7.3 mg, 6%, with DCM-ethyl acetate, 95 : 5).

This reaction was also reproduced into the NMR tube using C_6D_6 as the solvent and monitored, during the time, by ^{1}H NMR, ^{31}P NMR and DOSY spectroscopy.

A4.2.5 Metathesis reaction in benzene (2a/G_1ST = 1:4)

Resorc[4]arene bicyclic olefin **2a** (100 mg, 0.072 mmol) was dissolved in benzene (1.2 mL) and exposed to a solution of the G_1ST [Ru(=CHPh)Cl_2(PCy_3)$_2$] catalyst (237 mg, 0.288 mmol) in benzene (1.2 mL), previously prepared into the glovebox, to reach a 3×10^{-2} M substrate concentration. After four days stirring at room temperature under nitrogen atmosphere, the reaction mixture was heated at 50 °C for 6 h. After stirring for 4 days at room temperature under a nitrogen atmosphere, the reaction mixture was kept heated to 50 °C for 6 h. Afterwards, it was cooled to room temperature, treated with QuadraSil AP metal scavenger (aminopropyl silica gel, 6 g) and left under stirring overnight. After filtration and evaporation, the residue was suspended in DCM and purified by silica gel column chromatography to give compounds **5a** (7.7 mg, 6%, with DCM-ethyl acetate, 97 : 3), **4a** (14.2 mg, 12.5%, with DCM-ethyl acetate, 97 : 3), **2a** (35 mg, 35%, with DCM-ethyl acetate, 97 : 3) and two enriched mixtures products named **I** and **II** (with DCM-ethyl acetate, 90 : 10).

A4.2.6 NMR characterization of metathesis reaction products 2a–5a

Compound 2a. White powder. Mp: 191.4–190.4 °C. ^{1}H NMR (600 MHz, C_6D_6, 10 mM, 25 °C), δ (ppm) = 7.45 (2H, H26/H28, s), 6.87 (2H, H25/H27, s), 6.31 (2H, H11/H23, s), 6.08 (2H, H5/H17, s), 5.76 (4H, H2/H8/H14/H20, dd, $J_{CH\text{-}29}$ = 10.1 Hz, $J_{CH\text{-}29'}$ = 5.7 Hz), 5.45 (0.96H, CH=CH cis, t, ^{3}J = 5.1 Hz), 5.38 (3.04H, CH=CH trans, t, ^{3}J = 3.8 Hz), 4.01 (8H, O-CH_2, t, ^{3}J = 7.1 Hz), 3.52 (12H, OMe10'/OMe12'/OMe22'/OMe24', s), 3.21 (12H,OMe4'/OMe6'/OMe16'/OMe18', s), 3.13 (4H, H29', dd, $J_{29'\text{-}29}$ = 15.4, $J_{29'\text{-}CH}$ = 5.7), 3.06 (4H, H29, dd, $J_{29\text{-}29'}$ = 15.4, $J_{29\text{-}CH}$ = 10.1), 2.04 (8H, CH_2-C=C, m), 1.54-1.00 (56H, lateral chains, m). ^{13}C NMR (150 MHz, C_6D_6, 10 mM, 25 °C), δ (ppm) = 171.9 (CO), 157.2 (C4/C6/C16/C18), 156.1 (C10/C12/C22/C24), 131.1 (C=C cis), 130.4 (C=C trans), 128.3 (C3/C7/C15/C19), 127.0 (C25/C27), 126.2 (C26/C28), 122.6 (CC1/C9/C13/C21), 97.0 (C5/C17), 95.6 (C11/C23), 64.4 (O-CH_2), 55.4 (C10'/C12'/C22'/C24'), 55.3 (C4'/C6'/C16'/C18'), 40.1 (C29), 33.6 (C2/C8/C14/C20), 32.5 (CH_2 allylic), 30.2-26.3 (CH_2, lateral chains).

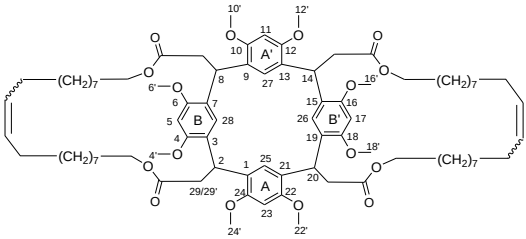

2a

Compound 3a. White powder. Mp: 167.4−166.4 °C. ^{1}H NMR (600 MHz, C_6D_6, 25 °C), δ (ppm) = 7.44 (4H, H26/H28, s), 6.86 (4H, H25/H27, s), 6.32 (4H, H11/H23, s), 6.11 (2H, H17, s), 6.08 (2H, H5, s), 5.75 (4H, H2/H8/H14/H20, dd, $J_{CH\text{-}29}$ = 6.2 Hz, $J_{CH\text{-}29'}$ = 2.4 Hz), 5.73 (4H, H2/H8/H14/H20, dd, $J_{CH\text{-}29}$ = 5.5 Hz, $J_{CH\text{-}29'}$ = 2.4 Hz), 5.53 (4H, CH=CH inter, m), 5.45 (1.08H, CH=CH cis, t, ^{3}J = 5.1 Hz), 5.37 (2.92H, CH=CH trans, t, ^{3}J = 3.7 Hz), 4.05 (8H, O-CH_2 of B' rings, m), 4.01 (8H, O-CH_2 of B rings, m), 3.53 (12H, OMe10'/OMe24' or OMe12'/OMe22', s), 3.52 (12H, OMe10'/OMe24' or OMe12'/OMe22', s), 3.23 (12H, OMe16'/OMe18', s), 3.21 (12H, OMe4'/OMe6', s), 3.13-2.99 (16H, H29/29' of B and B', m), 2.07 (8H, CH_2-C=C inter, m) 2.04 (8H, CH_2-C=C intra, m), 1.84-0.70 (112H, lateral chains, m). ^{13}C NMR (150 MHz, C_6D_6, 25 °C), δ (ppm) = 171.9 (CO), 171.8 (CO), 157.2 (C4/C6 or C16/C18), 157.1 (C4/C6 or C16/C18), 156.1 (C10/C24 or C12/C22), 156.0 (C10/C24 or C12/C22), 131.0 (C=C trans), 130.6 (C=C intermolecular), 130.7 (C=C cis), 126.2 (C26/C28), 127.0 (C25/C27), 122.6 (C3/C7 or C15/C19), 122.5 (C3/C7

or C15/C19), 96.9 (C5/C17), 95.6 (C11/C23), 64.3 (O-CH_2), 55.3 (C10'/C12'/C22'/C24'), 55.2 (C4'/C6'/C16'/C18'), 40.1 (C29), 33.1 (CH_2 allylic), 32.4 (CH_2 allylic), 40.3-19.9 (CH_2, lateral chains).

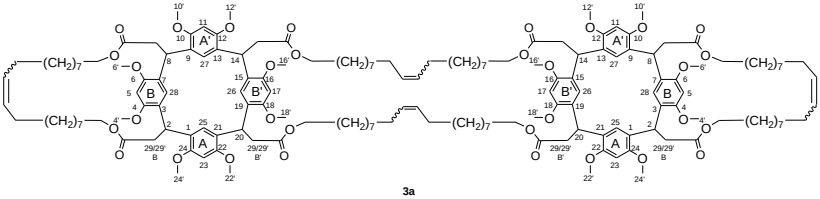

3a

Compound 4a. Yellow oil. ^{1}H NMR (600 MHz, C_6D_6, 25 °C), δ (ppm) = 7.43 and 7.42 (2H, H26/H28, s), 7.29 (4H, Ho, dd, $J_{o\text{-}m}$ = 8.0 Hz), 7.15 (4H, Hm, t, $J_{m\text{-}o}$ = $J_{m\text{-}p}$ = 8.0 Hz), 7.06 (2H, Hp, t, $J_{p\text{-}m}$ = 8.0 Hz), 6.85 (2H, H25/H27, s), 6.38 (2H, C=CH-Ph, d, $J_{CH\text{-}CH}$ = 15.9 Hz), 6.30 (2H, H11/H23, s), 6.17 (2H, -CH=C-Ph, dt, ^{2}J = 15.9 Hz, ^{3}J = 6.7 Hz), 6.15 (1H, H17, s), 6.06 (1H, H5, s), 5.75 (2H, H2/H8, m), 5.74 (2H, H14/H20, m), 5.45 (0.54H, CH=CH cis, t, ^{3}J = 5.2 Hz), 5.37 (1.46H, CH=CH trans, t, ^{3}J = 3.7 Hz), 4.11 (2H, O-C*H*H, dt, ^{2}J = 10.7 Hz, ^{3}J = 6.9 Hz), 4.04 (2H, O-CH*H*, dt, ^{2}J = 10.7 Hz, ^{3}J = 6.4 Hz), 4.02 (4H, O-CH_2, t, ^{3}J = 7.1 Hz), 3.52 (6H, OMe10'/OMe24' or OMe12'/OMe22', s), 3.50 (6H, OMe10'/OMe24' or OMe12'/OMe22', s), 3.26 (6H, OMe16'/OMe18', s), 3.20 (6H, OMe4'/OMe6', s), 3.17 (2H, H29 of B' ring, dd, ^{2}J = 15.7 Hz, ^{3}J = 5.3 Hz), 3.13 (4H, H29' of B ring, dd, ^{2}J = 15.3 Hz, ^{3}J = 6.1 Hz), 3.08 (2H, H29 of B ring, dd, ^{2}J = 15.3 Hz, ^{3}J = 3.6 Hz), 3.04 (2H, H29' of B' ring, dd, ^{2}J = 15.7 Hz, ^{3}J = 5.0 Hz), 2.12 (2H,

CH-C=C, q, ^{3}J = 7.6 Hz), 2.04 (2H, CH-C=C, q, ^{3}J = 6.1 Hz), 1.54-0.84 (56H, lateral chains, m). ^{13}C NMR (150 MHz, C_6D_6, 25 °C), □ (ppm) = 171.9 (CO), 171.8 (CO), 157.2 (C4/C16, C6/C20), 156.1 (C10/C24, C12/C22), 138.4 (Ar quaternary), 131.1 (*C*=C-Ph, C=C cis), 130.5 (C=*C*-Ph), 130.4 (C=C trans), 127.0 (C25/C27, Cp), 126.5 (Cm), 126.3 (Co), 126.2 (C1/C13, C9/C21, C26/C28), 122.7 (C3/C15, C7/C19), 96.9 (C5, C17), 95.6 (C11/C23), 64.4 (O-CH_2), 64.3 (O-CH_2), 55.4 (C10'/C24', C12'/C22'), 55.3 (C4'/C6', C16'/C18'), 40.2 (C29), 39.8 (C29), 33.6 (C2/C8/C14/C20), 33.5 (CH_2 allylic), 32.6 (CH_2 allylic), 37.7-23.0 (CH_2 lateral chains). HRMS (ESI- FT-ICR) m/z: [*M* + Na]$^{+}$ Calcd for $C_{98}H_{132}O_{16}Na$ 1587.94076 (monoisotopic mass), found 1587.94248.

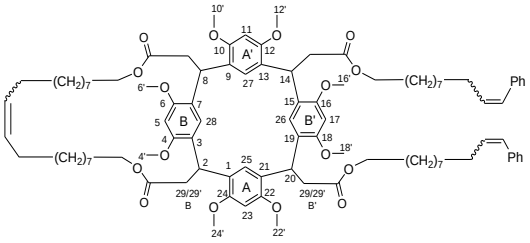

4a

Compound 5a. White oil. ^{1}H NMR (600 MHz, C_6D_6, 25 °C), δ (ppm) = 7.37 (2H, H26/H28, s), 7.25 (8H, Ho, dd, $J_{o\text{-}m}$ = 8.0 Hz, $J_{o\text{-}p}$ = 1.2 Hz), 7.11 (8H, Hm, t, $J_{m\text{-}o}$ = $J_{m\text{-}p}$ = 8.0 Hz), 7.01 (4H, Hp, tt, $J_{p\text{-}m}$ = 8.0 Hz, $J_{p\text{-}o}$ = 1.2 Hz), 6.79 (2H, H25/H27, s), 6.34 (4H, C=CH-Ph, d, $J_{CH\text{-}CH}$ = 15.7 Hz), 6.26 (2H, H11/H23, s), 6.13 (4H, -CH=C-Ph, dt, $J_{CH\text{-}CH}$ = 15.7 Hz,

J_{CH-CH2} = 6.9 Hz), 6.10 (2H, H5/H17, s), 5.69 (4H, H2/H8/H14/H20, dd, J_{CH-29} = 5.5 Hz, $J_{CH-29'}$ = 10.4 Hz), 4.08 (4H, O-CH_2, dt, ^2J = 10.5 Hz, $J_{CH2-CH2}$ = 6.8 Hz), 4.00 (4H, O-CH_2, dt, ^2J = 10.5 Hz, $J_{CH2-CH2}$ = 6.8 Hz), 3.47 (12H, H10'/H22', H12'/H24', s), 3.21 (12H, H4'/16', H6'/H18', s), 3.13 (4H, H29, dd, $J_{29-29'}$ = 15.8 Hz, J_{29-CH} = 5.5 Hz), 3.04 (4H, H29', dd, $J_{29'-29}$ = 15.8 Hz, $J_{29'-CH}$ = 10.4 Hz), 2.08 (8H, CH-C=C, q, J_{CH-CH} = J_{CH-CH2} = 7.10 Hz), 1.50-0.8 (56H, m). ^{13}C NMR (150 MHz, C_6D_6, 25 °C), □ (ppm) = 171.5 (CO), 156.8 (C4/C16, C6/C20), 155.7 (C10/C22, C12/C24), 138.0 (Ar quaternary), 130.7 (*C*=C-Ph), 130.1 (C=*C*-Ph), 126.7 (C25/C27, Cp), 126.0 (Co), 125.8 (C1/C13, C9/C21, C26/C28, Cm), 122.3 (C3/C15, C7/C19), 96.5 (C5/C17), 95.3 (C11/C23), 64.0 (O-CH_2), 55.0 (C4'/C16', C6'/C18', C10'/C22', C12'/C24'), 39.5 (C29), 33.2 (C2/C8/C14/C20), 33.1 (C allylic), 37.2-22.9 (lateral chains). HRMS (ESI-FT-ICR) m/z: [*M* + Na]$^+$ Calcd for $C_{112}H_{144}O_{16}Na$ 1768.03466 (monoisotopic mass), found 1768.03373 ± 7.02 10^{-4} u (mean value of 7 experiments).

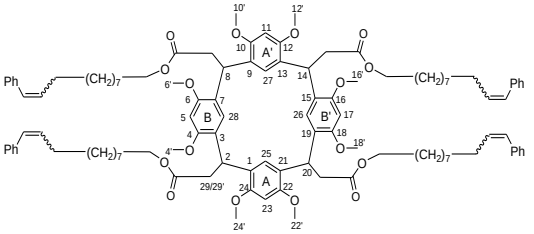

5a

A4.2.7 Supplementary figures

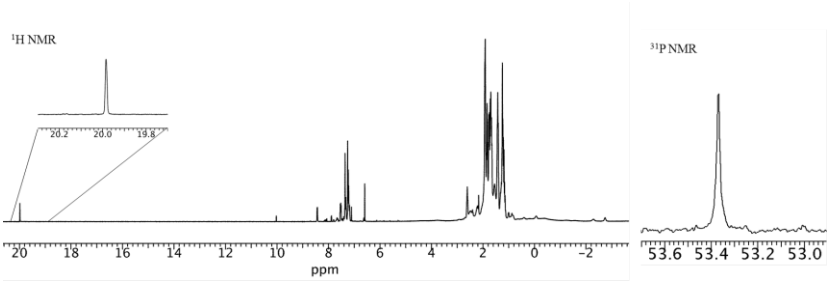

Figure S1. ^{1}H NMR (600 MHz, $CDCl_3$, 25 °C) and ^{31}P NMR (243 MHz, $CDCl_3$, 25 °C) spectra of the G_1ST catalyst (2 mM).

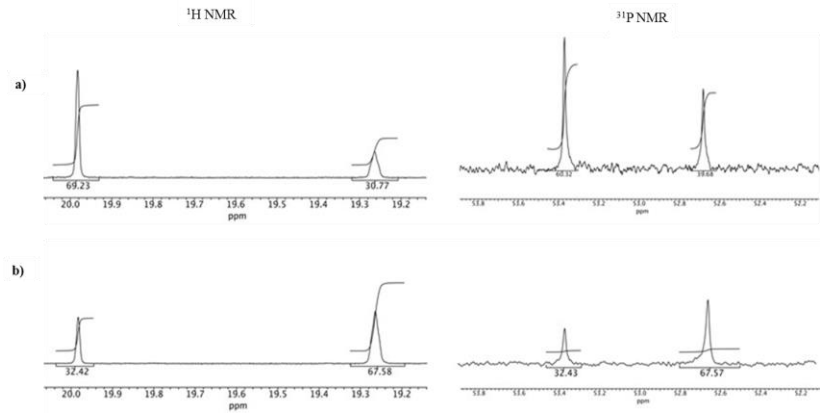

Figure S2. Expansion of the high-frequencies regions of ^{1}H NMR (600 MHz, $CDCl_3$, 25 °C) and ^{31}P NMR (243 MHz, $CDCl_3$, 25 °C) spectra of the reaction mixture of **2a** with G_1ST (a) immediately after preparation and (b) after 40 min.

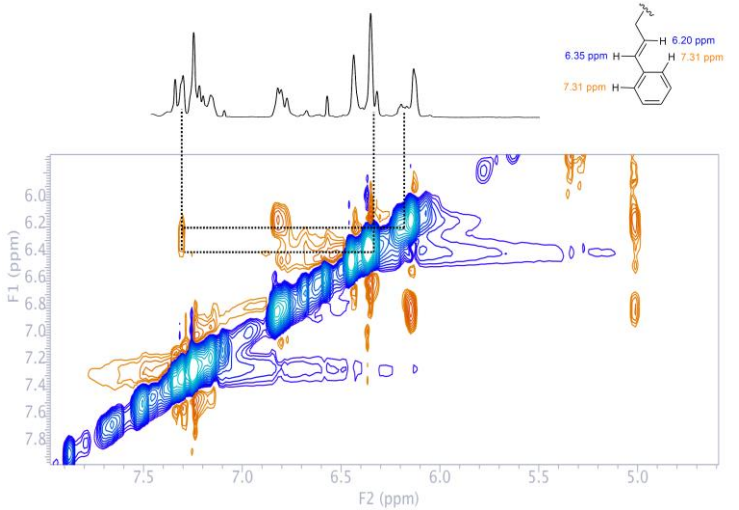

Figure S3. 2D ROESY (600 MHz, $CDCl_3$, 25 °C, mixing time 300 ms) map of the reaction mixture; expansion of the aromatic/olefin zone.

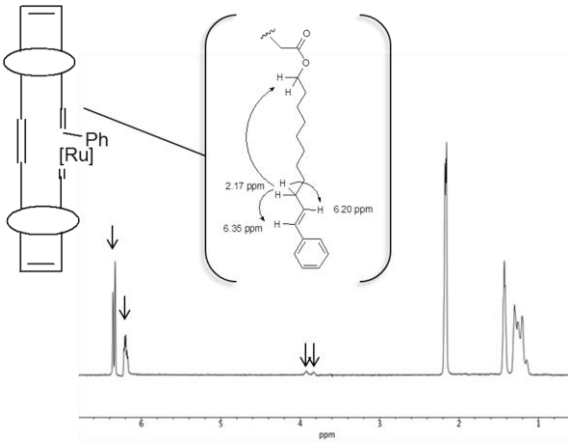

Figure S4. 1D TOCSY (600 MHz, $CDCl_3$, 25 °C, mixing time 150 ms) spectrum of the proton at 2.17 ppm. The arrows point the methylene protons bound to the oxygen and the olefin protons of the double bond directly bound to the phenyl moiety of the side chains.

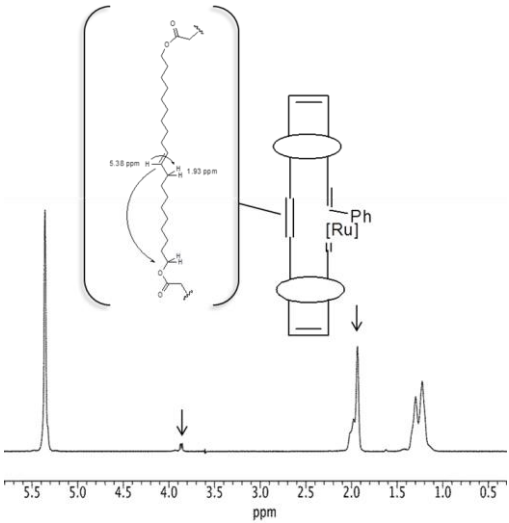

Figure S5. 1D TOCSY (600 MHz, $CDCl_3$, 25 °C, mixing time 150 ms) spectrum of the proton at 5.38 ppm. The arrows indicate the methylene protons bound to oxygen and the allylic protons at 1.93 ppm.

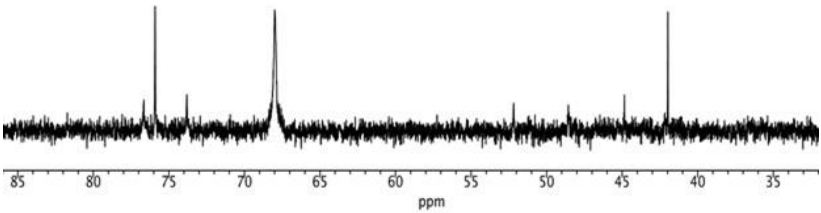

Figure S6. ^{31}P NMR (243 MHz, $CDCl_3$, 25 °C) spectrum of the reaction mixture after degradation.

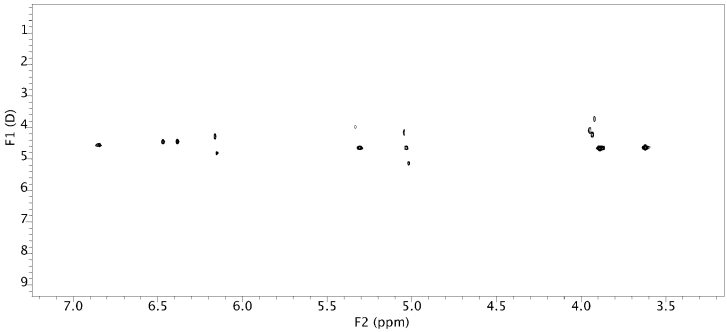

Figure S7. DOSY map (600 MHz, $CDCl_3$, 25 °C) of resorc[4]arene olefin **2a**.

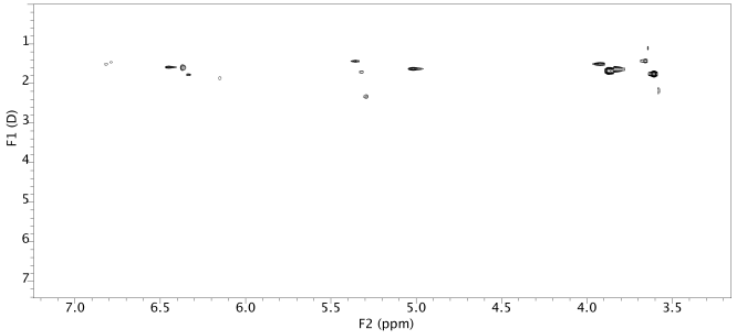

Figure S8. DOSY maps (600 MHz, $CDCl_3$, 25 °C) after 22 h reaction time.

Chapter A5

References

Abis L., Dalcanale E., Du Vosel A., Spera S., *J. Org. Chem.*, **1988**, *53*, 5475.

Ackermann L., Fürstner A., Weskamp T., Kohl F.J., Herrmann W.A., *Tetrahedron Lett.*, **1999**, 40, 4787.

Adlhart C., Chen P., *Helv. Chim. Acta*, **2000**, 83, 2192.

Adlhart C., Volland M.A.O., Hofmann P., Chen P., *Helv. Chim. Acta*, **2000a**, 83, 3306.

Adlhart C., Hinderling C., Baumann H., Chen P., *J. Am. Chem. Soc.*, **2000b**, 122, 8204.

Adlhart C., Chen P., *J. Am. Chem. Soc.*, **2004**, 126, 3496.

Aeilts S. L., Cefalo D.R., Bonitatebus P.J., Houser J.H., Hoveyda, R.R. Schrock, *Angew. Chem. Int. Ed.*, **2001**, 40, 1452.

Allcock H.R., Kellam E.C., III, Hofmann M.A., *Macromolecules*, **2001**, 34, 5140.

Arduengo A.J., *Acc. Chem. Res.*, **1999**, 32, 913.

Arduini A., Pochini A., Secchi A., Ugozzoli F., "Recognition of Neutral Molecules", In *Calixarenes* 2001, Asfari Z., Böhmer V., Harrowfield J., Vicens J. (Eds.), Kluwer Academic Publishers: Dordrecht, The Netherlands, **2001**, Chapter 25.

Asfari Z., Böhmer V., Harrowfield J., Vicens J., Eds. *Calixarenes 2001*, Kluwer Academic Publisher: Dordrecht, **2001**.

Astruc D., *New J. Chem*., **2005**, 29, 42.

Atiqullah M., Hammawa H., Hamid H., *Eur. Polym. J.*, **1998**, 34, 1511.

Baeyer A., *Ber. Dtsch. Chem. Ges.*, **1872a**, 5, 25.

Baeyer A., *ibid.*, **1872b**, 5, 280.

Banks R.L., Bailey G.C., *Int. Eng. Prod. Dev.*, **1964**, 3, 170.

Bazan G.C., Khosravi E., Scrock R.R., Feast W.J., Gibson V.C., O'Regan M.B., Thomas J.K., Davis W.M., *J. Am. Chem. Soc.*, **1990**, 112, 8378.

Bazan G.C., Oskam J.H., Cho H.N., Park L.Y., Schrock R.R., *J. Am. Chem. Soc.*, **1991**, 113, 6899.

Bielawski C.W., Grubbs R.H., *Prog. Polym. Sci.*, **2007**, 32, 1.

Blanchard M., Mortreux A., *Bull. Soc. Chim.*, **1972**, 4, 1641.

Blanchard M., Mortreux A., *J. Mol. Catal.*, **1975**, 1, 101.

Böhmer V., *Angew. Chem. Int. Ed.*, **1995**, 34, 713.

Botta B., Iacomacci P., Di Giovanni M.C., Delle Monache G. Gacs-Baitz E., Botta M., Tafi A., Corelli F., Misiti D., *J. Org. Chem.*, **1992**, 57, 3259.

Botta B., Delle Monache G., De Rosa M.C., Seri C., Benedetti E., Iacovino R., Botta M., Corelli F., Masignani V., Tafi A., Gács-Baitz E., Santini A., Misiti D., *J. Org. Chem.*, **1997**, 62, 1788.

Botta B., Cassani M., D'Acquarica I., Misiti D., Subissati D., Delle Monache G., *Curr. Org. Chem.*, **2005**, 9, 337.

Botta B., D'Acquarica I., Delle Monache G., Nevola L., Tullo D., Ugozzoli F., Pierini M., *J. Am. Chem. Soc.*, **2007**, 129, 11202.

Bourissou D., Guerret O., Gabbaï F. P., Bertrand G., *Chem. Rev.*, **2000**, 100, 39.

Bunz U.H.F., in Modern Arene Chemistry, ed. Astruc D., Wiley-VCH, *Weinheim*, **2002**, 217.

Bunz H.H.F., in Handbook of Metathesis, ed. Grubbs R. H., Wiley-VCH, *Weinheim*, **2003**, 3, 3, 10.

Calderon N., *Tetrahedron Lett.*, **1967**, 34, 3327.

Calderon N., *Acc. Chem. Res.*, **1972**, 5, 127.

Cao Y., Wang L., Bolte M., Vysotsky M.O., Böhmer V., *Chem. Commun.*, **2005**, 3132.

Casnati A., Sansone F., Ungaro R., *Acc. Chem. Res.*, **2003**, 36, 246.

Cavallo L., *J. Am. Chem. Soc.*, **2002**, 124, 8965.

Chatterjee A.K., Choi T.-L., Sanders D.P., Grubbs R.H., *J. Am. Chem. Soc.*, **2003**, 125, 11360.

Choi T.-L., Grubbs R.H., *Angew. Chem. Int. Ed.* **2003**, 42, 1743.

Conrad J.C., Eelman M.D., Duarte Silva J.A., Monfette S., Parnas H.H., Snelgrove J.L., Fogg D.E., *J. Am. Chem. Soc.*, **2007**, 129, 1024.

Connon S.J., Dunne A., Blechert S., *Angew. Chem. Int. Ed.*, **2002**, 41, 3835.

Cometti G., Dalcanale E., Du Vosel A., Levelut A.-M., *Liquid Crystals*, **1992**, 11, 93.

Conrad J.C., Fogg D.E., *Curr. Org. Chem.*, **2006**, 10, 185.

Dalla Cort A., Mandolini L., "Calixarenes As Hosts for Quats", in *Calixarenes in Action*, Mandolini L., Ungaro R. (Eds.), Imperial College Press, London, **2000**, Chapter 5.

Dias E.L., Nguyen S.T., Grubbs R.H., *J. Am. Chem. Soc.*, **1997**, 119, 3887.

Dubberley S.R., Romero P.E., Piers W.E., McDonald R., Parvez M., *Inorg. Chim. Acta*, **2006**, 359, 2658.

Dunne A.M., Mix S., Blechert S., *Tetrahedron Lett.*, **2003**, 44, 2733.

Egberink R.J.M., Cobben P.L.H.M., Verboom W., Harkema S., Reinhoudt D.N. J., *Inclusion Phenom.*, **1992**, 12, 151.

Eleuterio H.S., German Pat. 1072811, **1960**.

Eleuterio H.S., *J. Mol. Catal.*, **1991**, 65, 55.

Erdtman H., Högberg S., Abrahamsson S., Nilsson B., *Tetrahedron Lett.*, **1968**, 9, 1679.

Falana O.M., Al-Farhan E., Keehn P.M., Stevenson R., *Tetrahedron Lett.*, **1994**, 35, 65.

Fischer E.O., *Angew. Chem. Int. Ed.*, **1964**, 580.

France M.B., Grubbs R.H., McGrath V., Paciello R.A., *Macromolecules*, **1993**, 26, 4742.

Fürstner A., Dierkes T., Thiel O.R., Blanda G., *Chem. Eur. J.*, **2001**, 7, 5286.

Gerkensmeier T., Mattay J., Näther C., *Chem. Eur. J.*, **2001**, 7, 465.

Ghirga F., D'Acquarica I., Delle Monache G., Toscano S., Mannina L., Sobolev A.P., Ugozzoli F., Crocco D., Antiochia R., Botta B., *RSC Adv.*, **2013**, 3, 17567.

Ghosh S., Ghosh S., Sarkar N., *J. Chem. Sci.*, **2006**, 118, 223.

Grela K., Ignatowska J., *Org. Lett.*, **2002**, 4, 3747.

Grela K., Harutyunyan S., Michrowska A., *Angew. Chem. Int. Ed.*, **2002**, 41, 4038.

Grubbs R.H., *J. Am. Chem. Soc.*, **1972**, 94, 2538.

Grubbs R.H., Burk P.L., Carr D.D., *J. Am. Chem. Soc.*, **1975**, 97, 3265.

Grubbs R.H., Tumas W.J., *Science*, **1989**, 243, 907.

Grubbs R.H., Chang S., *Tetrahedron*, **1998**, 54, 4413.

Grubbs R.H., Handbook of Metathesis; Ed.; Wiley-VCH: Weinheim, Germany, **2003**.

Guerchais V., Astruc D., *J. Chem. Soc. Chem. Commun.*, **1985**, 835.

Gutsche C.D., *Acc. Chem. Res.*, **1983**, 16, 161.

Gutsche C.D., Calixarenes, Monographs in Supramolecolar Chemistry, Stoddart, J.F., Ed.; Royal Society of Chemistry: Cambridge, **1989**, 1.

Gutsche C.D., *Aldrichimica Acta*, **1995**, 28, 3.

Gutsche C.D., in *Calixarenes Revisited*, Stoddart J.F. (Ed.); The Royal Society of Chemistry, Cambridge, **1998**.

Green M.L.H., Mitchard L.C., Swanwick M.G., *J. Chem. Soc. A*, **1971**, 794.

Hansen S.M., Rominger F., Metz M., Hofmann P., *Chem.-Eur. J.*, **1999**, 5, 557.

Hérisson J.-L., Chauvin Y., *Makromol. Chem.*, **1971**, 141, 161.

Herrmann W.A., Köcher C., *Angew. Chem. Int. Ed.*, **1997**, 109, 2256.

Hinderling C., Adlhart C., Chen P., *Angew. Chem. Int. Ed.*, **1998**, 37, 2685.

Högberg A.G.S., *J. Am. Chem. Soc.*, **1980a**, 102, 6046.

Högberg A.G.S., *J. Org. Chem.*, **1980b**, 45, 4498.

Honda T., Namiki H., Kaneda K., Misutani H., *Org. Lett.*, **2004**, 6, 87.

Hoveyda A.H., Schrock R.R., *Angew. Chem. Int. Ed.*, **2001**, 40, 1452.

Huc V., Weihofen R., Martin- Jimenez I., Oulie´ P., Lepetit C., Lavigne G., Chauvin R., *New J. Chem.*, **2003**, 27, 1412.

Jerschow A., Mueller N., *J. Magn. Reson. A*, **1997**, 125, 372.

Katsuhiko A., Toyoki K., *Supramolecular Chemistry-Fundamentals and Application*, Iwanami Shoten Publishers, Tokyo, Springer, **2006**.

Keitz B.K., Endo K., Patel P.R., Herbert M.B., Grubbs R.H., *J. Am. Chem. Soc.*, **2012**, 134, 693.

Kingsbury J.S., Harrity J.P.A., Bonitatebus P.J., Hoveyda A.H., *J. Am. Chem. Soc.*, **1999**, 121, 791.

Konishi H., Iwasaki Y., Morikawa O., Okano T., Kiji J., *Chem. Express*, **1990**, 5, 869.

Lee C.W., Grubbs R.H., *Org. Lett.*, **2000**, 2, 2145.

Leitao E.M., v.d. Eide E.F., Romero P.E., Piers W.E., McDonald R., *J. Am. Chem. Soc.*, **2010**, 132, 2784.

Loupy A., Tchoubar B., Astruc D., *Chem. Rev.*, **1992**, 92, 1141.

Love J.A., Sanford M.S., Day M.W., Grubbs R.H., *J. Am. Chem. Soc.*, **2003**, 125, 10103.

Ludwig R., *Microchim. Acta*, **2005**, 152, 1.

Mandolini L., Ungaro, R., Eds., *Calixarenes in Action*, Imperial College Press, **2000**.

McEleney K., Allen D.P., Holliday A.E.,. Crudden C.M., *Org. Lett.*, **2006**, 8, 2663.

Meek S.J., O'Brien R.V., Llaveria J., Schrock R.R., Hoveyda A.H., *Nature* **2011**, 471, 461.

Meng D., Bertinato P., Balog A., Su D.-S., Kamenecka T., Sorensen E.J., Danishefsky S.J., *J. Am. Chem. Soc.*, **1997**, 119, 10073.

Monfette S., Fogg D.E., *Chem. Rev.*, **2009**, 109, 3783.

Monfette S., Crane A.K., Duarte Silva J.A., Facey G.A., dos Santos E.N., Araujo M.H., Fogg D.E., *Inorg. Chim. Acta*, **2010**, 363, 481.

Morril C. , Grubbs R.H., *J. Org. Chem.*, **2003**, 68, 603.

Mortreux A., Delgrange J.C., Blanchard M., Lubochinsky B., *J. Mol. Catal.*, **1977**, 2, 73.

Mortreux A., Petit F., Blanchard M., *Tetrahedron Lett.*, **1978**, 49, 4967.

Mortreux A., Petit F., Petit M., Szymanska-Buzar T., *J. Mol. Catal. A: Chem.*, **1995**, 96, 95.

Michrowska A., Bujok R., Harutyunyan S., Sashuk V., Dolgonos G., Grela K., *J. Am. Chem. Soc.*, **2004**, 126, 9318.

Natta G., *Angew. Chem. Int. Ed.*, **1964**, 3, 723.

Natta G., Dall'Asta G., Porri L., *Makromol. Chem.*, **1965**, 81, 253.

Nguyen S.T., Johson L.K., Grubbs R.H., Ziller J.W., *J. Am. Chem. Soc.*, **1992**, 114, 3974.

Novak B.M., Grubbs R.H., *J. Am. Chem. Soc.*, **1988**, 110, 7542.

Occhipinti G., Bjørsvik H.-R., Jensen V.R., *J. Am. Chem. Soc.*, **2006**, 128, 6952.

Perrin M., Oehler D., in Calixarenes. A Versatile Class of Macrocyclic Compounds (Eds: Vicens J., Böhmer V.), KLUWER Academic Publishers, Dordrecht, The Netherlands, **1991**, 65.

Prunet J., *Angew. Chem. Int. Ed.*, **2003**, 42, 2826.

Randall M.L., Tallarico J.A., Snapper M.L., *J. Am. Chem. Soc.*, **1995**, 117, 9610.

Randall M.L., Snapper M.L., *J.Mol. Catal. A*, **1998**, 133, 29.

Romero P.E., Piers W.E., McDonald R., *Angew. Chem. Int. Ed.*, **2004**, 43, 6161.

Romero P.E., Piers W.E., *J. Am. Chem. Soc.*, **2005**, 127, 5032.

Rouhi M.R., *Chem. Eng. News*, **2002**, 29.

Sanford M.S., Ulman M., Grubbs R.H., *J. Am. Chem. Soc.*, **2001**, 123, 749.

Schinzer D., Limberg A., Bauer A., Bohm O.M., Cordes M., *Angew. Chem. Int. Ed.*, **1997**, 36, 523.

Schinzer D., Bauer S., Bohm L., Limberg A., Cordes M., *Chem. Eur. J.*, **1999**, 5, 2483.

Schneider M.F., Blechert S., *Angew. Chem. Int. Ed.*, **1996**, 35, 411.

Schneider M.F., Lucas N., Velder J., Blechert S., *Angew. Chem. Int. Ed.*, **1997**, 36, 257.

Scholl M., Trnka T.M., Morgan J.P., Grubbs R.H., *Tetrahedron Lett.*, **1999a**, 40, 2247.

Scholl M., Ding S., Lee C.W., Grubbs R.H., *Org. Lett.*, **1999b**, 1, 953.

Schrock R.R., Rocklage S.M., Wengrovius J.H., Rupprecht G., Feldmann J., *J. Mol. Catal.*, **1980**, 8, 73.

Schrock R.R., Murdzek J.S., Bazan G. C., Robbins J., DiMare M., O'Regan M., *J. Am. Chem. Soc.*, **1990**, 112, 3875.

Schwab P., France M.B., Ziller J. W., Grubbs R.H., *Angew. Chem. Int. Ed.*, **1998**, 37, 1124.

Smith D.W., Wagener K.B., *Macromolecules*, **1993**, 26, 1633.

Smith A.B., III, Kozmin S.A., Adams C.M., Paone D.V., *J. Am. Chem. Soc.*, **2000**, 122, 4984.

Smith A.B., III, Adams C.M., Kozmin S.A., Paone D.V., *J. Am. Chem. Soc.*, **2001**, 123, 5925.

Steed J.W., Atwood J.L., *Supramolecular Chemistry, 2nd edition*, John Wiley & Sons, Ltd, **2009**.

Tallarico J.A., Bonitatebus P.J., Snapper M.L., *J. Am. Chem. Soc.*, **1997a**, 119, 7157.

Tallarico J.A., Randall M.L., Snapper M.L., *Tetrahedron*, **1997b**, 53, 16511.

Teng X., Cefalo D.R., Schrock R.R., Hoveyda A.H., *J. Am. Chem. Soc.*, **2002**, 124, 10779.

Thoden van Velzen E.U., Engbersen J.F.J., Reinhoudt D.N., *J. Am. Chem. Soc.*, **1994**, 116, 3597.

Timmerman P., Verboom W., Reinhoudt D.N., *Tetrahedron*, **1996**, 52, 2663.

Tindall D., Pawlow J.H., Wagener K.B., in Topics in Organometallic Chemistry, Vol. 1 (Ed: A. Fürstner), SPRINGER-VERLAG, Berlin, **1998**, 183.

Truett W.L., Johnson D.R., Robinson I.M., Montague B.P., *J. Am. Chem. Soc.*, **1960**, 82, 2337.

Trnka T.M., Morgan J.P., Sanford M.S., Wilhelm T.E., Scholl M., Choi T.L., Ding S., Day M.W., Grubbs R.H., *J. Am. Chem. Soc.*, **2003**, 125, 2546.

Tsang W.C.P., Jernelius J.A., Cortez G.A., Weatherhead G.S., Schrock R.R., Hoveyda A.H., *J. Am. Chem. Soc.*, **2003a**, 125, 2591.

Tsang W.C.P., Hultzsch K.C., Alexander J.B., Bonitatebus P.J., Schrock R.R., *J. Am. Chem. Soc.*, **2003b**, 125, 2652.

Tsuzuki S., Honda K., Uchimaru T., Mikami M., Tanabe K., *J. Am. Chem. Soc.*, **2000**, 122, 3746.

Tunstad L.M., Tucker J.A., Dalcanale E., Weiser J., Bryant J.A., Sherman J.C., Helgeson R.C., Knobler C.B., Cram D.J., *J. Org. Chem.*, **1989**, 54, 1305.

Urbina-Blanco C.A., Poater A., Lebl T., Manzini S., Slawin A.M.Z., Cavallo L., Nolan S.P., *J. Am. Chem. Soc.*, **2013**, 135, 7073.

Ulman M., Grubbs R.H., *Organometallics*, **1998**, 17, 2484.

Ulman M., Grubbs R.H., *J. Org. Chem.*, **1999**, 64, 7202.

Volland M.A.O., Ansen S.M., Rominger F., Hofmann P., *Organometallics*, **2004**, 23, 800.

Wagener K.B., Smith D. W., *Macromolecules*, **1991**, 24, 6073.

Wagener K.B., Boncella J.M., Nel J.G., *Macromolecules*, **1991a**, 24, 264.

Wagener K.B., Nel J.G., Duttweiler R.P., Hillmyer M.A., Boncella J.M., Konzelman J., Smith D.W., Puts R., Willoughby L., *Rubber Chem. Technol.*, **1991b**, 64, 83.

Wagener K.B., Brzezinska K., Anderson J.D., Younkin T.R., Steppe K., DeBoer W., *Macromolecules*, **1997,** 30, 7363.

Wakamatsu H., Blechert S., *Angew. Chem. Int. Ed.*, **2002a**, 41, 794.

Wakamatsu H., Blechert S., *Angew. Chem. Int. Ed.*, **2002b**, 41, 2403.

Wengrovius J.H., Schrock R.R., Churchill M.R., Missert J.R., Youngs W.J., *J. Am. Chem. Soc.*, **1980**, 102, 4515.

Wetskamp T., Schattenmann W.C., Herrmann W.A., *Angew. Chem. Int. Ed.*, **1998**, 37, 2490.

Yang Y., Swager T.M., *Macromolecules*, **2007**, 40, 7437.

Yang H.-C., Huang Y.-C., Lan Y.-K., Luh T.-Y., Zhao Y., Truhlar D.G., *Organometallics*, **2011**, 30, 4196.

Yu T., Guo M., *Prog. Polym. Sci.*, **1990**, 15, 825.

Zhang W., Kraft S., Moore J.S., *Chem. Commun.*, **2003**, 832.

Zhang W., Kraft S., Moore J.S., *J. Am. Chem. Soc.*, **2004**, 126, 329.

Zhang W., Moore J.S., *J. Am. Chem. Soc.*, **2004**, 126, 12796.

Part B

Metabolomics Studies by NMR Spectroscopy

Chapter B1

General Introduction

B1.1 Metabolomics overview

Metabolomics is a natural extension of genomics, transcriptomics, and proteomics (Figure 1.1), but instead of monitoring changes in the expression of genes or proteins, metabolomics monitors changes in the concentration of the low-molecular-weight (<1 kDa) compounds (metabolites) present in a cell, tissue, organ, organism, or biofluid (urine, plasma, cerebrospinal fluid, etc.) (Oliver et al., 1998; Nicholson et al., 1999).

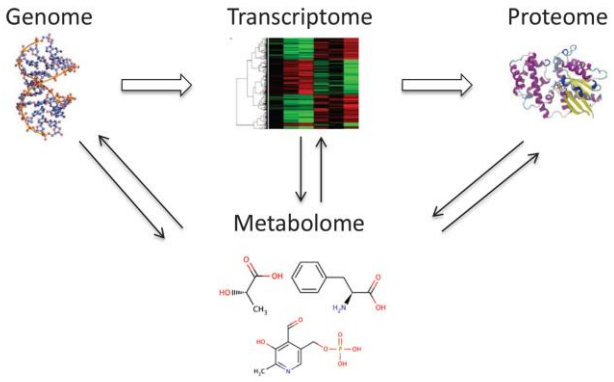

Figure 1.1. The metabolome is tightly connected with other "omes". The metabolome interacts and reflects the activity of the genome, transcriptome, and proteome. (Reproduced from Stringer et al., 2016)

The metabolome is the entire collection of small molecules or metabolites within a biological sample that may include amino acids, carbohydrates, cofactors, fatty acids, nucleotides, and even

xenobiotics that includes drugs and drug-associated metabolites. Importantly, changes in the metabolome or in a specific metabolite are a direct result of changes in the biological activity of an enzyme or protein, as they are down-stream products of gene transcription and translation. Correspondingly, metabolomics approaches, compared to other "omics" techniques, can provide a clearer picture of the phenotype of the cell or biological system: the changes in the metabolome capture how the system responds to environmental or genetic stress (Fiehn, 2002). Specifically, a drug or an active chemical lead would be expected to perturb the metabolome of a cell or tissue upon treatment. Targeted and untargeted metabolomics are two distinctly different approaches to investigating the metabolome. In particular, a targeted metabolomics approach follows changes to a specific metabolite or set of metabolites based on some prior information or hypothesis. The identified or targeted metabolites are expected to respond to a drug treatment, disease state, genetic modification, or some other environmental stressor. This approach takes advantage of the comprehensive understanding of a vast array of metabolic enzymes, their kinetics, end products, and the known biochemical pathways to which they contribute. Conversely, untargeted metabolomics is discovery based. The main aim of untargeted metabolomics is to monitor the entirety of the metabolome in order to identify the

affected metabolites and pathways. This approach requires the identification of unknown metabolites using either *in silico* libraries or experimental investigation through analytical chemistry. In either case, the metabolome extracted from cells or biofluids are compared before and after the addition of the stress factor (drug treatment, genetic mutation, disease, etc.). A variety of analytical technics are used to identify changes in the concentrations and fluxes of endogenous metabolites, but the high precision of mass spectrometry (MS) and the reproducibility of nuclear magnetic resonance (NMR) spectroscopy combined with their ability to elucidate chemical structures have resulted in these being the two most commonly employed methods.

B1.1.1 Important issues related to metabolomics

Metabolomics is a valuable tool of chemical and systems biology, and its application has been rapidly expanding. Recent developments in the use of metabolomics involve the characterization and interpretation of the cell metabolome, starting from prokaryotes (especially *Escherichia coli*) to eukaryotes cell lines (yeast or mammalian cells) (Tang, 2011; Cuperlovic-Culf et al., 2010). Complementary to the classic biofluid analyses, the metabolomic profiles of cells represent a powerful tool to

understand how the local metabolism and biochemical pathways are influenced by pathologies and by external or internal stimuli. In particular, the metabolome analysis of cells grown *in vitro* provides important information for the development of models of biological pathways and networks. *In vitro* cell metabolomics analysis offers several advantages: experimental variables are easier to control, higher reproducibility, less expensive and easier to interpret than analysis of animal models and human subjects (Zhang et al., 2013a). The use of mammalian cells is emerging in the metabolomics field in order to understand the molecular mechanism of disease progression, the cellular response to drug treatments (Bai et al., 2011) and the cell culture monitoring (Panopoulos et al., 2012). In particular, the identification and characterization of cancer cell metabolomic signature may play an important role in the early diagnosis as well as in the following therapeutic response, making it possible to map the drug action into metabolic pathways (Serkova and Glunde, 2009).

The ease of use and general utility has contributed to the continually increasing number of metabolomics studies, also making it easy to apply incorrectly. Untargeted metabolomics consists of acquiring one-dimensional (1D) ^{1}H NMR spectra for a set of cell lysates or biofluid samples that are then analysed using standard multivariate statistical analysis techniques (Worley and Powers,

2013). The 1D ^{1}H NMR spectra provides a fingerprint of the state of the metabolome, where multivariate analyses, such as principal component analysis (PCA), partial-least-squares (PLS), and orthogonal projection to latent structures discriminant analysis (OPLS-DA), determine if the metabolomes differentiate between the multiple classes (e.g., drug treated *vs* untreated cells). PLS and OPLS-DA S-plots and loading plots are then used to identify the spectral features (i.e., chemical shifts and associated metabolites) that primarily contribute to these observed class differentiations. The incorrect pre-analytical procedures, involving sample preparation, collection and storage, may lead to biologically irrelevant changes to the metabolome (Zhang et al., 2013b). Thus, inappropriate data processing and analysis protocols may bias the metabolomics data set, causing an erroneous interpretation (van den Berg et al., 2006; Craig et al., 2006). The lack of model validation may imply a class separation in a scores plot that are not statistically justified (Kjeldahl and Bro, 2010; Werth et al., 2010; Worley et al., 2013). Therefore, a current challenge in the field of metabolomics is optimizing and standardizing protocols (Sansone et al., 2007; Salek et al., 2013).

Unlike genomics or proteomics samples, metabolomics samples are not static and will change with time and from the handling and processing procedures (Canelas et al., 2008): the proof that the

observed changes in a metabolomics sample are biologically relevant is critical to a successful metabolomics study. Thus, multiple replicates of cell samples are grown, harvested, and lysed under identical conditions as is practically possible and as quickly as possible. Importantly, processing of samples should be completely randomized because, at a minimum, a time-bias will be imprinted on the samples if each class was processed sequentially. In the same way, each step of the process should be performed by the same individual. Despite these efforts, significant within class variability will occur because of the intrinsic nature of biological samples. Thus, it is also critical to prepare enough replicates per class in order to obtain statistical relevance to any observed class discrimination. Typically, a minimum of 5−10 replicates of cell lysates is required, but the sample size increases significantly for a clinical study (Blaise, 2013).

Acquiring and processing the NMR spectra for each cell lysate can also induce unintended perturbations in the metabolomics data set. Randomizing the NMR data collection, utilizing automation, and obtaining efficient solvent (water) suppression minimizes these issues. Specifically, high-quality water suppression is required to avoid baseline correcting the NMR spectrum: water suppression through presaturation has to be employed to reduce the water signal in the NMR spectrum, helping observation of the dynamic

range of the metabolite concentrations efficiently. A minimal and uniform approach to processing the NMR spectrum (Fourier transformation and phase correction) is preferred because baseline correction, applying a window function, zero filling, and other processing steps will modify the data in a biologically irrelevant manner. Proper preprocessing of the metabolomics data set, which includes removing noise (Halouska and Powers, 2006), normalization, scaling, and aligning (or binning), is also necessary for a reliable PCA, PLS, or OPLS-DA model and meaningful interpretation of the metabolomics data:

- Removing noise regions eliminates the possibility that serendipitous covariant noise peaks may contribute to irrelevant class separation;
- Normalization corrects for the variability in total metabolite concentration or NMR sensitivity due to experimental differences in the total number of cells harvested, in the efficiency in extracting the metabolomes, and potentially due to changes in instrument performance;
- Scaling accounts for large differences in metabolite concentrations within a given sample (dynamic range issue) and prevents intense peaks from dominating the multivariate statistical analysis;

- Binning or aligning the spectra corrects for small variations in peak position and peak shape due to differences in sample conditions (pH, ionic strength, concentration, etc.) and instrument variability between replicates.

B1.1.2 Applying metabolomics to cancer research

The first suitable metabolomic approach for cancer was developed in 2003 (Griffiths and Stubbs, 2003). Since then, different types of tumors have been studied using this method either to elucidate metabolic mechanism or to identify biomarkers (Bu et al., 2012; Claudino et al., 2012; Wei et al., 2014; Brunelli et al., 2016). A cancer biomarker can be a metabolite (secreted by tumor, metabolic pathway or process) that may be employed to diagnose cancer, predict patient response towards therapies and monitor recurrence. Markers can be employed for diagnosis (to identify early stage), prognosis (assess the lethality) and prediction (of patient's response to treatment) of cancer. Biomarkers have been identified for many types of tumors including but not limited to cancers of the prostate (Sreekumar et al., 2009; Trock, 2011; Teahan et al., 2011), breast (Crooke et al., 2006; Riscuta and Dumitrescu, 2012; Simpson et al., 2012), ovary (Zhang et al., 2012), colorectum (Yoshie et al., 2012; Cheng et al., 2012; Leichtle et al., 2012), colon (Denkert et al.,

2008), kidney (Clyne, 2012), lung (Hori et al., 2011) and bladder (Hyndman et al., 2011) as well as leukemia (Tiziani et al., 2009) and head (Wei et al., 2014). Various biological matrices, such as plasma, serum, urine, cell lines and cells were analysed in these studies. It is well known that cancer metabolism differs from that of normal tissue. Cancer cells rely on anaerobic metabolism as the source for energy, even under physiological oxygen levels. The best studied feature of cancer metabolism is central carbon metabolism (CCM) and the relationship between glycolysis, the tricarboxylic acid (TCA) cycle and oxidative phosphorylation. The general metabolic characteristics observed in cancers are summarized in Table 1.1.

Table 1.1. General features related to cancer metabolism.

Feature	References
High glycolytic enzyme activities	Weljie et al., 2010
Expression of the pyruvate kinase isoenzyme type M2	Vander Heiden et al., 2010
High phosphometabolite levels	Mazurek and Eigenbrodt, 2003
High rate of channeling of glucose carbons to synthetic processes	Mazurek, 2007
High rate of pyrimidine and purine *de novo* synthesis	Jahns-Streubel et al., 1997
High rate of fatty acid *de novo* synthesis	Brunet et al., 2008
Low (ATP+GPT)/(CTP+UTP) ratio	Fleming et al., 1983
Low AMP levels	Warrington et al., 2010
A high glutaminolytic capacity	Mazurek et al., 1996
Release of immunosuppressive metabolites	Adams et al., 2012
High level of methionine dependency	Crott et al., 2001

Cells are used extensively in disease research for understanding the molecular mechanism of disease progression, response, and resistance to therapeutics. Cultivated cell lines, although phenotypically and genetically not identical to the original cancer types, are still useful models because of their unlimited availability, the broad range of cells available, and the flexibility in the design of treatment (experimental setup). Cell metabolomics is an emerging field that addresses fundamental biological questions and allows

observation of metabolic phenomena in cells. Pan et al. (Pan et al., 2011) exposed four brain cancer cell lines to cisplatin drug and subjected to ^{1}H NMR analysis. The result shed light on relation of glycosylated UDP compounds (uridine diphospho-N-acetylglucosamine and uridine diphospho-N-acetylgalactosamine) to cancer cell death following chemotherapeutic treatment. Serizawa et al. (Serizawa et al., 2014) employed Capillary Electrophoresis Time Of Flight Mass Spectrometer (CE-TOF/MS) to screen biomarkers for the early detection of resistance to these inhibitors, using PC-9ER cells (drug erlotinib-resistant non-small-cell lung cancer cell). Enhanced glutamine metabolism was observed in the cancer cells that can be explained by the multiple pathways for bioenergetics and biosynthesis in proliferating cells. Lefort et al. (Lefort et al., 2014) used ^{1}H NMR experiments to profile the effects of drugs and concluded that treatment of breast cancer cells (MDA-MB-231 and MCF-7) with dichloroacetate (a pyruvate dehydrogenase kinase inhibitor) and allopurinol (xanthine oxidase/dehydrogenase inhibitor) results in more pronounced changes in metabolites found in extracellular medium than intracellular pools. An elevation in phosphocholine, total choline and phosphocholine/glycerophosphocholine level was observed in cancer cells compared to control. Furthermore, cell lines have been frequently directed to apoptosis phenomenon. An increased

concentration of fructose 1,6-bisphosphate was detected in the apoptotic HL-60 human leukaemia cell line by Williams and colleagues as early as 1998 (Williams et al., 1998). A decrease in the phosphocholine concentration in the hamster cell line CHO-K1 was detected after treatment with different pro-apoptotic agents including camptothecin, ceramide, chelerythrine and etoposide (Williams et al., 1998). The accumulation of mobile lipids, which are more mobile than most cell lipids (Luciani et al., 2009), was described in 2005 as a characteristic of apoptosis in human prostate carcinoma (DU145) cells treated with phenylacetate and phenylbutyrate (Milkevitch et al., 2005), and in 2008 after induction of apoptosis by ionizing radiation and the administration of the antineoplastic drug doxorubicin in HL-60 cells (Rainaldi et al., 2008).

B1.2 The Hedgehog (HH) signaling pathway

Tumors are composed of a heterogeneous group of cells. Some tumor cell fractions have the ability to initiate tumors in xenograft models, whereas other fractions do not. These cells, capable of sphere-like growth *in vitro* and tumor formation *in vivo*, are defined as cancer stem cells (CSCs) and share similarities with normal neural stem cells (NSCs). It has been hypothesized that these cells are involved in radio- and chemo-resistance, as well as tumor

recurrence. Several signaling pathways that regulate normal stem cells can cause neoplastic proliferation when disregulated by mutation. In tumor initiating cells those pathways may be constitutively activated or improperly regulated through genetic and/or epigenetic changes, leading to uncontrolled growth. Nevertheless, targeting CSCs alone may not be sufficient to get effect cures or long-term remission for most cancers. A combinatorial therapy, using conventional chemotherapeutic drugs with an agent that can target CSCs may provide a good approach to eradicate both cancer cells and cancer stem cells.

❖ ***Cancer stem cells in tumors***

The theory that malignancies arise from a small subset of stem-cell-like cancer cells has received increasing attention during the past decade. These cells, referred to as CSCs or cancer-initiating cells (CICs), have been identified in many malignancies and are hypothesized to form the clonogenic core of tumor tissues (Figure 1.2) (Vermeulen et al., 2008). The origin of CSCs in human tumors is, however, not fully understood. Such cells could potentially originate from a more-differentiated cancer cell that acquires self-renewal properties, perhaps as a result of epithelial-to-mesenchymal transition (EMT) (Espinoza and Miele, 2013). Alternatively, CSCs might derive from a normal tissue stem cell that undergoes

transformation as a result of oncogenic somatic mutations, under the influence of extrinsic microenvironmental factors (Reya et al., 2001; Krivtsov et al., 2006).

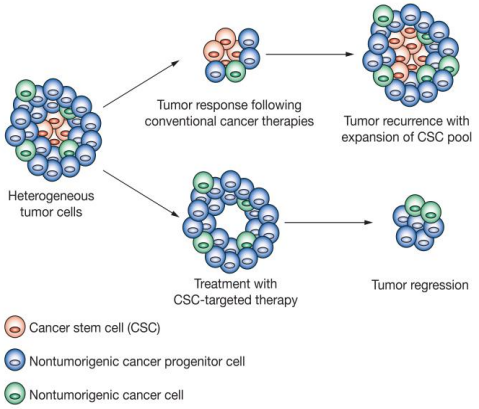

Figure 1.2. The cancer stem cell hypothesis. The cancer stem cell (CSC) hypothesis posits that tumor growth is driven by a subpopulation of cancer cells that are capable of proliferation and self-renewal. CSCs are also multipotent and can give rise to the diverse set of cells that make up a given tumor. Inherent within this hypothesis is the assumption that current treatments for cancer can considerably diminish tumor burden, but have a decreased effect on CSCs, which are later capable of driving tumor recurrence and regrowth. To achieve cancer remission or cure, therefore, it will be necessary to develop novel therapies that are cytotoxic to CSCs. (Reproduced from Das et al., 2008)

Although the co-occurrence of subpopulations of cancer cells with different tumorigenic properties within individual tumors is no longer in question (Pattabiraman et al., 2014), the CSC hypothesis remains controversial. This controversy arises as a consequence of the technical and logistical challenges in isolating and identifying CSCs from human solid tumors that contain heterogeneous cell populations, and the limited number of validated surrogate assays

currently available to substantively confirm stem-cell-like properties (Tirino et al., 2013). These cells tend to comprise a small fraction of total tumor mass and are, therefore, difficult to unequivocally identify histologically. Nonetheless, numerous researchers hypothesize that treatments targeting the CSC population could be more effective than existing therapies, and could dramatically transform treatment outcomes in oncology.

CSCs have been shown to have one or more aberrations in various signaling pathways; however, abnormal activity of pathways that control stem-cell self-renewal, and have important roles in embryonic development and differentiation (Notch, HH, and Wnt) are probably most crucial to the tumorigenicity of CSCs. Increasing evidence demonstrates that these embryonic pathways can interact with other cellular signaling pathways, such as those involving nuclear factor kappa-light-chain-enhancer of activated B cells (NFκB), mitogen-activated protein kinase (MAPK), phosphoinositide-3-kinase (PI3K), and epidermal growth factor (EGF). Therefore, these developmental pathways might be important therapeutic targets for blockade of CSC self‑renewal and proliferation, and tumor progression (Figure 1.2) (Merchant and Matsui, 2010).

❖ ***The pathway***

The HH signaling pathway is implicated in tissue-patterning during embryonic development and in normal tissues repair, and EMT transition (Beachy et al., 2010; Takebe et al., 2015). Binding of HH ligands (Sonic hedgehog (SHH), Indian hedgehog (IHH), or Desert hedgehog (DHH)) releases the inhibitory effect of their Patched (PTCH) transmembrane receptors on Smoothened (SMO), which is also located in the cell membrane (Figure 1.3) (Odoux et al., 2008).

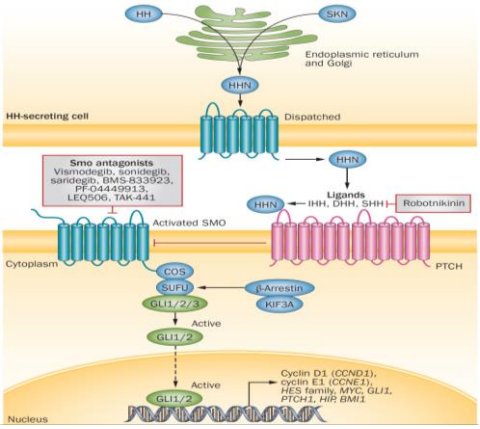

Figure 1.3. The canonical HH-signaling pathway and pharmacological inhibitors targeting this pathway that are under ongoing development as anticancer therapies. The HH-processing pathway involves HHC autocatalysis, and SKN and Dispatched proteins, which mediate the release of HHN ligands (IHH, DHH and SHH). In the absence of HHN binding, PTCH interacts with and inhibits the activity of SMO; HHN binding to PTCH releases its inhibitory effects on SMO, resulting in SMO accumulation and sequestration of COS and SUFU proteins in cilia, which releases the GLI transcription factors to exert their effects in the nucleus. KIF3A and β-arrestin are required for localization of SMO to cilia. GLI1/2 promote a gene-expression pattern relevant to tumorigenesis. Abbreviations: COS, Costal; DHH, Desert hedgehog; HH, Hedgehog; HHC, Hedgehog C-terminal domain; HHN, Hedgehog N-terminal domain; HIP, Hedgehog interacting protein; IHH, Indian hedgehog; Ptch, Patched; SHH, Sonic hedgehog; SKN, Skinny hedgehog; SMO, Smoothened; SUFU, suppressor of fused. (Reproduced from Takebe et al., 2015)

Progressively, the signaling cascade initiated by SMO leads to activation and nuclear localization of GLI transcription factors, which drive expression of HH target genes; most of the target genes are involved in proliferation, survival, and angiogenesis (Amakye et al., 2013). This cascade represents a novel target for cancer therapy, as aberrations in the HH-pathway contribute to tumorigenesis and tumor growth through several mechanisms. These mechanisms include mutations in the key members of the pathway, such as loss-of-function mutations in PTCH1 gene encoding Patched 1 and gain-of-function mutation in the SMO gene, that result in ligand-independent activation of the HH-pathway, as well as ligand-dependent signaling by either autocrine or paracrine routes (Amakye et al., 2013). Mutation-driven mechanisms of HH-pathway activation have been demonstrated in some tumors, such as basal-cell carcinoma (BCC) of the skin, medulloblastoma (MB), and rarely rhabdomyosarcoma (Ng and Curran, 2011). Indeed, PTCH1 mutations are associated with HH-pathway hyperactivation in >90% of BCCs and 30% of adult MB (Kool et al., 2014). The aetiology of rhabdomyosarcomas, although thought to originate by a similar mechanism, is controversial (Roma et al., 2012). Moreover, some studies have focused their attention to the role of HH-GLI signaling in glioma stem cells (GSCs) and found that it regulates self-renewal

and tumorigenic potential in GSCs (Clement et al., 2007; Uchida et al., 2011; Po et al., 2010; Hsieh et al., 2011; Liu et al., 2014).

Similarly to the Notch cascade, HH-signaling can involve canonical and noncanonical pathways. Canonical signaling follows the PTCH1-SMO-GLI axis (Figure 1.3), whereas noncanonical pathways can be SMO-independent (Amakye et al., 2013). The noncanonical signals are largely attributed to various tumor-associated signaling pathways integrating with HH-signaling, in part by influencing the activity of GLI transcription factors (Amakye et al., 2013).

❖ ***Resistance mechanism***

The most clinically advanced agent targeting the HH pathway is **vismodegib** (a direct cyclopamine-competitive SMO antagonist), which was approved by the US FDA in 2012 and by the European Medicines Agency (EMA) in 2013 for the treatment of metastatic BCC, or locally advanced BCC in patients who are not candidates for surgery or radiotherapy (Sekulic et al., 2012; Dirix, 2014).

To date, clinical efficacy has not been demonstrated in trials of SMO inhibitors, except in patients with tumors driven by mutations in components of the HH-signaling cascade, such as SMO and PTCH1 (Von Hoff et al., 2012). Primarily, possible reasons for the resistance to HH-inhibitor monotherapy and the lack of additional efficacy or benefit in combination with chemotherapy, compared with the

outcomes of chemotherapy alone, include insufficient drug concentrations in the stroma. This resistance mechanism has been discussed by Graham and colleagues (Graham et al., 2011), who described an unusual pharmacokinetic profile for vismodegib, owing to high-affinity, reversible binding to plasma proteins, solubility-limited absorption, and slow metabolic elimination. Moreover, a mutation in the gene SMO (D473H) was detected in a patient with MB after 3 months of treatment with vismodegib who harbored a PTCH1 mutation in both primary and metastatic lesion biopsies taken before therapy (Yauch et al., 2009). The SMO D473H mutation was present only after tumor progression and caused disruption of the vismodegib-binding site on SMO, and was, therefore, considered as the cause of the acquired resistance (Yauch et al., 2009). Compensatory upregulation of other signaling represents another potential resistance mechanism; for example, primary resistance to SMO inhibitors can be due to noncanonical activation of GLI transcription factors through pathways that bypass SMO and, in turn, the effects of SMO inhibitors (Ramaswamy et al., 2012). During the last decade, GLI factors are emerging as attractive targets for the development of novel anticancer drugs. A few GLI inhibitors have been identified, such as GANT61 (Lauth et al., 2007) and arsenic trioxide (ATO) (Kim et al., 2010) (Figure 1.4) and they have shown a good inhibitory effect on HH-dependent transcription

and MB growth *in vitro* and *in vivo*. However, none of these drugs have entered into clinical trials to date, mostly due to their potential toxicity or lack of specificity is still a major concern.

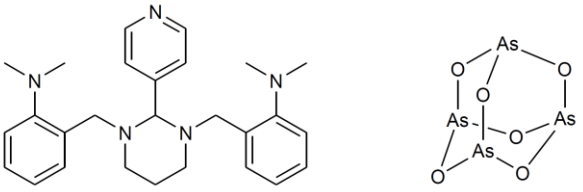

GANT 61 ATO

Figure 1.4. GANT 61 and ATO chemical structures.

B1.2.1 The role of HH-pathway in cancer cells metabolism

Cells of high-grade tumors, including MB and glioblastoma (GBM), must similarly balance energy metabolism with the need to synthesize the macromolecules essential for tumor growth. In most mammalian cells, glycolysis (literally lysis of glucose) is inhibited by the presence of oxygen, which allows mitochondria to oxidize pyruvate to CO_2 and H_2O (oxidative phosphorylation). This inhibition is termed the "Pasteur effect", after Louis Pasteur, who first demonstrated that glucose flux was reduced by the presence of oxygen (Racker, 1974). Cells with large ATP requirements are likely to be disadvantaged by aerobic glycolysis (conversion of glucose to

lactic acid in the presence of oxygen) because glycolysis generates less ATP per molecule of glucose than oxidative phosphorylation (2 ATP *vs* 38 ATP, respectively). Proliferating cells, however, may use aerobic glycolysis to satisfy the competing needs for both energy generation and the accumulation of biomass. This phenomenon (termed "Warburg effect") was first described by Warburg in the 1930s (Warburg, 1930), leading him to the hypothesis that cancer results from impaired mitochondrial metabolism (Figure 1.5). Unlike oxidative phosphorylation, aerobic glycolysis also generates metabolic intermediates that can be used for lipid (lypogenesis) and nucleic acid biosynthesis.

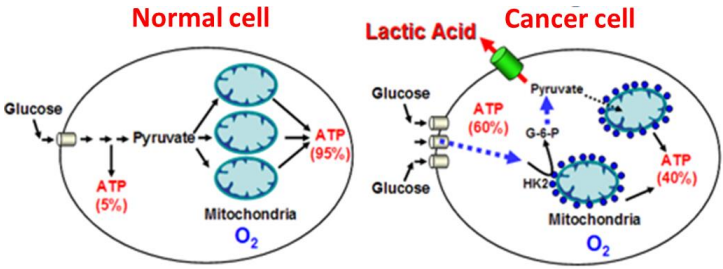

Figure 1.5. Cells metabolism. Warburg's theory on the origin of cancer postulates that tumor cells have defects in mitochondrial oxidative phosphorylation and therefore rely on high levels of aerobic glycolysis as the major source for ATP to fuel cellular proliferation. This was in contrast to normal cells, which primarily utilize oxidative phosphorylation for growth and survival.

In 2014, it has been demonstrated that HH-pathway activation in granule cell progenitors (GCPs), the cells from which MB arises, induces transcription of hexokinase 2 (HK2) and pyruvate kinase M2 (PKM2), two key gatekeepers of glycolysis (Di Magno et al., 2014). The process is mediated by the canonical activation of the GLI transcription factors by upregulanting PKM2 and HK2 mRNA levels and causes a robust increase of extracellular lactate concentration. These studies have shown by quantitative PCR analysis how both HK2 and PKM2 transcripts are significantly upregulated after treatment with SHH or the SMO agonist SAG (Figure 1.6), inducing a robust increase of the lactate released in the medium, that is conversely counteracted by ATO (direct GLI inhibitor). Since in metabolic tissues and fibroblasts the activation of SMO promotes Warburg-like effect (Teperino et al., 2012), through a rapid GLI-indipendent and AMPK-mediated activation of key glycolytic enzymes, further demonstration of GLI-dependent mechanism arises from the incubation of GCPs cells with purmorphamine, a SMO agonist that selectively activates the canonical GLI-dependent route (Di Magno et al., 2014). Importantly, aerobic glycolysis plays a key role also in GBM tumor that, like MB, shows high expression in Hk2 enzyme and high glucose uptake.

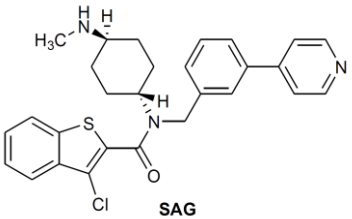

Figure 1.6. The SMO agonist SAG chemical structure.

In 2015, a joint investigation between our research group featuring a large expertise in the synthesis and isolation of natural products and experts in the molecular medicine of brain tumors was published, aimed at identifying the first naturally occurring small molecule capable of interfere with GLI activity (Infante et al., 2015). In particular, we identify the natural isoflavone Glabrescione B (GlaB) (Figure 1.7) as the first small molecule binding to GLI1 zinc-finger and impairing GLI1 activity by interfering with its interaction with DNA (Infante et al., 2015). Remarkably, as a consequence of its robust inhibitory effect on GLI1 activity, GlaB inhibited the growth of HH-dependent MB and BCC tumor cells both *in vitro* and in orthotopic xenograft mice and in allograft mice models, as well as the self-renewal ability and clonogenicity of tumor-derived stem cells (Infante et al., 2015).

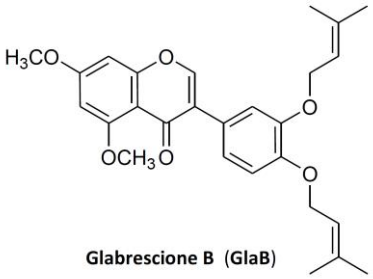

Figure 1.7. GlaB chemical structure.

On the basis of these evidences, targeted and untargeted NMR metabolomics analyses of HH-dependent tumor cells and the corresponding conditioned media would be able to figure out how the GlaB-treatment affects cell metabolism as a consequence of GLI1 inhibition.

Chapter B2
Cell Metabolomics: a Strategy to Study Crucial Pathways in Cancer Development

B2.1 Results and discussion

The present part of the thesis deals with a research activity carried out at the Centro di Risonanza Magnetica (CERM) at the Università degli Studi di Firenze, under the supervision of Prof. Paola Turano.

B2.1.1 Brain cancer cell models

Human cancer research heavily relies on molecular biology, which, among other methods, includes controlled studies in culture cell lines. Even though typical commercially available cell lines often differ from normal and cancer cells, difficult access to human tumor and/or human normal tissue makes them useful and popular experimental models. Two standard tumor brain cell lines DAOY, human MB cells, and GL261, murine glioma cells, are widely used in studies that employ experimental models of brain neoplastic disease.

MB, the most common malignant brain tumor in children, is a primitive neuroectodermal tumor arising in the cerebellum. The aggressive clinical behavior of the tumor along with the cognitive and endocrinological long-term side effects of current therapies mean that both the development of prognostic indicators for disease stratification and the identification of new therapeutic targets represent major goals. Current understanding of the

molecular biology of MB is limited. Cytogenetic studies have described consistent chromosomal aberrations, but molecular genetic studies have identified specific genetic and epigenetic abnormalities in only a small proportion of those tumors (Giangaspero et al., 2000; Ellison, 2002; Jones and Baylin, 2002). The DAOY cell line was established in 1985 by Jacobsen from the Royal Perth Hospital in Western Australia (Jacobsen et al., 1985). The line was derived from the biopsy material taken from a tumor in the posterior fossa of a four-year-old boy. Although the original tumor presented characteristics of both neuronal and glial phenotypes, these were not retained by the DAOY cell line. In the DAOY model, SHH consistently induced GLI1 mRNA, a biomarker of pathway activity (Scales and de Sauvage, 2009) and, therefore, these cells are useful for the pharmacological examination of the HH-pathway.

On the basis of the crystallographic structure of the zinc finger domain of GLI1 (GLI1ZF) in complex with DNA (Pavletich and Pabo, 1993), together with NMR studies as well as computational and experimental mutagenesis, we clarified the structural requirements of GLI1/DNA interaction and identified GlaB as a novel small molecule that binds GLI1ZF and interferes with its interaction with DNA (See Section B1.2.1). This small molecule turned out to be an efficient inhibitor of the growth of HH/GLI-dependent MB cells *in vitro* and *in vivo* (Infante et al., 2015). In the present study, the HH-

dependent DAOY tumor cells, belonging to the SHH MB subgroup, were taken into account as model to elucidate the direct effect of GlaB on GLI, knocking down GLI1 and GLI2 by siRNA. GlaB proved unable to repress PTCH1 mRNA levels in siGLI1/GLI2-knocked down DAOY cells, indicating that the presence of GLI factors is required for GlaB activity (Figure 2.1).

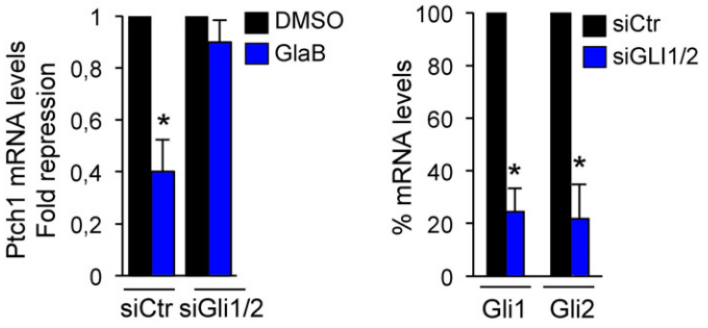

Figure 2.1. PTCH1 mRNA expression levels (left panel) were determined by qRT–PCR in DAOY cells transfected with siRNA specific for GLI1 and GLI2 (siGLI1/2) or a non-specific control siRNA (siCTR) and treated for 24 h with GlaB or DMSO as a control. (right panel) The graph shows GLI1 and GLI2 mRNA expression levels determined by qRT–PCR in DAOY cells transfected with siGLI1/2 or siCTR. Results are expressed as fold repression relative to control, and data were normalized to GAPDH and HPRT expression.

Moreover, to confirm the inhibitory effect of GlaB to impair MB tumor growth *in vivo*, the human MB DAOY cell system were implanted into the cerebellum of NOD/SCID mice. Tumor volume displayed a significant reduction of the tumor mass formed by DAOY cells in GlaB-treated mice compared to the control.

Gliomas are the most frequent and lethal cancers originating in the central nervous system (CNS) in adults. Despite current treatments consisting of surgery followed by adjuvant radiotherapy and chemotherapy, GBM patients display a median overall survival of only 14.6 months. Even though significant advances in cancer molecular targeting have been made, several promising preclinical results revealed poor translatability.

The application of suitable animal models in glioma research is necessary for the development of new therapeutic approaches. An ideal animal model of human glioma should reproduce the major features of this neoplasm: predictable and reproducible *in vitro* and *in vivo* growth patterns; infiltrative, but non-metastatic, tumor growth; and poor immunogenicity. A number of animal brain tumor models are being used; however, no model currently available simulates human high-grade gliomas exactly. Tumor models vary in their immunogenicity, growth patterns and invasiveness. For this reason, it is important to choose an appropriate animal model depending on the endpoint examined. Most models are derived from rat and several xenograft models, based on the intracerebral transplantation of human brain tumors into immune-deficient nude mice, are also available. Murine models of malignant brain tumors are used much less frequently, mainly because the number of available models is limited. One of the most frequently used murine

brain tumor models is GL261. The GL261 tumor was induced originally by intracranial injection of 3-methylcholantrene into C57BL/6 mice and maintained by serial intracranial and subcutaneous transplantations of small tumor pieces on the syngeneic mouse strain (Ausman et al., 1970). Perhaps, because of these serial passages, GL261 lacks the most important glial differentiation marker, such as the glial fibrillary acidic protein (Weiner et al., 1999). During the mid-1990s, *in vitro* growing cell cultures were established from the GL261 tumor, that was used in many immune therapeutic and gene therapeutic investigations. A subset of GBM tumors display enhanced HH-signaling, and this can be recapitulated *in vitro*, where some GBM cell lines proliferate in response to SHH treatment (Morgenroth et al, 2014). In particular, the GL261 cell model contains a small subpopulation of CSCs which overexpress the HH-pathway.

Since we observed that GLI1 is expressed in these cells and that its expression is reduced of about 20% if they were treated with GlaB 5 µM for 48 hours, the MTT assay was performed in order to estimate the toxicity of free GlaB on this cell system. As reported in Figure 2.2, a dose- and time-dependent reduction in cell viability was observed: cytofluorimetric cell count after 48 h revealed a reduction of total cell number of about 80% in samples seeded in the presence

of GlaB 5 µM and 10 µM and, after experimental times 72 h and 96 h, of about 50% at the same concentrations.

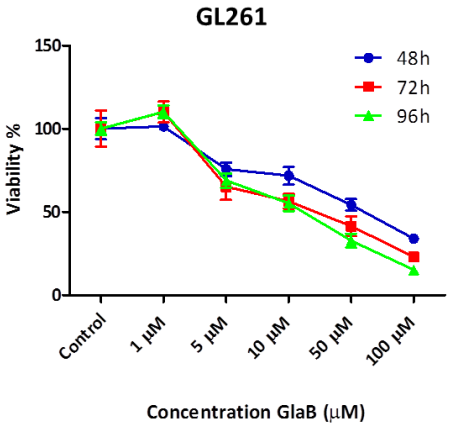

Figure 2.2. *In vitro* cytotoxicity of GlaB on GL261 cell line. Cells were incubated with GlaB for 48 h, 72 h and 96 h at increasing drug concentrations (1 – 100 µM). Cell viability, expressed as a percentage of control untreated cells, was determined by MTT assay after 48 h, 72 h and 96 h incubation with GlaB treatments.

Moreover, the analysis of early apoptosis in cells treated with GlaB 5 µM after 48 h, revealed by the double positivity to Annexin V and PI, showed a 10% increase of the percentage of apoptosis with respect to the untreated cells.

In vivo studies were also performed to evaluate the GlaB effect on tumor volume upon intraperitoneal and intranasal administrations, using murine GL261 glioma cells-bearing mice (8 week-old male mice, C57BL/6 strain, 20-25 g). The experimental data have shown

that intranasal and intraperitoneal GlaB administration reduced tumor volume compared to vehicle treated mice at 4.4 mg/Kg and 35 mg/Kg concentrations, respectively. Notably, the intranasal administration seems as effective as intraperitoneally at concentrations about 8 times lower.

B2.2 Cell metabolomics: protocol optimization and experimental design

Cell metabolomics has emerged as a promising tool with wide applications in many research areas (Zhang et al., 2013a). Metabolomics represents a very good approach to explore the cell phenotype and to have an overall portrait of the biological process under investigation. This analytical approach offers advantages with respect to animal models or to experiments involving human subjects. The advantages include an easier control of the experiments, a greater reproducibility and an easier and more direct interpretation of the results.

Many possible applications for cell metabolomics have been described, including studies aimed at characterising cellular responses to toxicity and environmental factors, as well as to expression of oncogenic molecules and treatment with drugs (Bayet-Robert et al., 2009; West et al., 2010; Kleinstreuer et al., 2011; Bai et al., 2011; Paglia et al., 2012; Chong et al., 2012).

A key condition for *in vitro* cell studies is to achieve reliable and reproducible models that are representative of the *in vivo* situation: sample preparation and metabolism quenching represent fundamental aspects (León et al., 2013). Depending on the experimental plan, the metabolomics analysis would be focused on the *endo*-metabolome (all the metabolites present inside the cell), the *exo*-metabolome (all the metabolites in the surrounding extracellular medium), or both.

In the present study, we analysed the effects of GlaB treatment on the *endo*- or/and on the *exo*-metabolome of two different cancer cell lines, the human MB DAOY and the GL261 cells, respectively. For this purpose, a simple, fast, and reproducible sample preparation protocol was developed, as reported in the Section B2.3.2; the analysis of the cellular lysates was performed to detect as many metabolites as possible and to avoid extraction procedures. Indeed, the metabolomics analysis of cellular extracts suffers from accuracy problems coming from differences in solubility of the various metabolites, variations in individual metabolite extraction efficiencies, and chemical destruction of some metabolites. In order to overcome all the inconveniences of the extraction procedures, the here developed protocol was performed by analysing the cellular cytosolic fraction using high-field profiling of standard solution of cell lysates. After an intense washing procedure to

remove the medium residues, the cells were detached from the dishes by mechanical scraping and quenching of the cellular activity was performed using protease and phosphatase inhibitors, in order to assure minimal changes in the metabolome and avoid misleading results. Subsequently, the cell lysis was carried out by sonication in multiple short bursts, while the sample was put into an ice bath, and the removal of all macromolecular waste products (cell membrane components and cellular debris) performed by centrifugation. The optimized protocol (Figure 2.3A) can be summarized in the following main steps: (i) growth of the cell culture; (ii) cell washing; (iii) cell scraping; (iv) quenching with protease and phosphatase inhibitors; (v) cell lysis by sonication; and (vi) centrifugation. Furthermore, the cell culture media are characterised by the presence of foetal bovine serum (FBS) thus, these samples were considered and analysed according to standard procedures for the NMR metabolomics analyses of human plasma and serum (Beckonert et al., 2007).

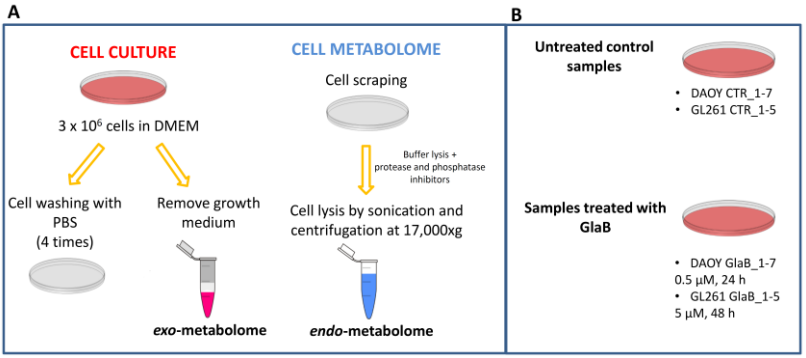

Figure 2.3. (A) General scheme describing the whole sample preparation protocol. **(B)** Overview of the experimental design.

In order to reduce bias in the interpretation of the experiments, it was decided to produce various biological replicates for each treated cell (from five to seven, namely with **GL261_GlaB_1-5** and **DAOY_GlaB_1-7**). Furthermore, the corresponding control samples for each cell system (untreated ones) were also collected (from five to seven, namely **GL261_CTR_1-5** and **DAOY_CTR_1-7**). Moreover, the culture medium of each cell growth was gathered for the *exo*-metabolome analysis and the produced samples were then analysed by high-resolution ^{1}H NMR spectroscopy. The whole design of experiment is summarized in Figure 2.3B. The most efficient dose and drug exposure duration time of cell culture were used on the basis of previous biological assays (see Section B.2.1.1).

B2.2.1 Metabolic profile

The 1D ^{1}H NMR spectra were acquired to determine the metabolic fingerprints of the treated and untreated cancer cells. The two cell lines used in this study revealed different metabolic signature. The cell lysates and the corresponding conditioned media were subjected to NMR analysis. The NMR spectra of cell lysates acquired 24 hours for the DAOY cell line and 48 hours for GL261 cell system after seeding are shown in Figure 2.4. As the ^{1}H NMR spectra from different measurements for each cell line displayed almost identical spectral profiles, only one of the replicates is shown in Figure 2.4. These observations indicated that metabolic profiles of the independently grown cell system were highly reproducible under the same culture conditions.

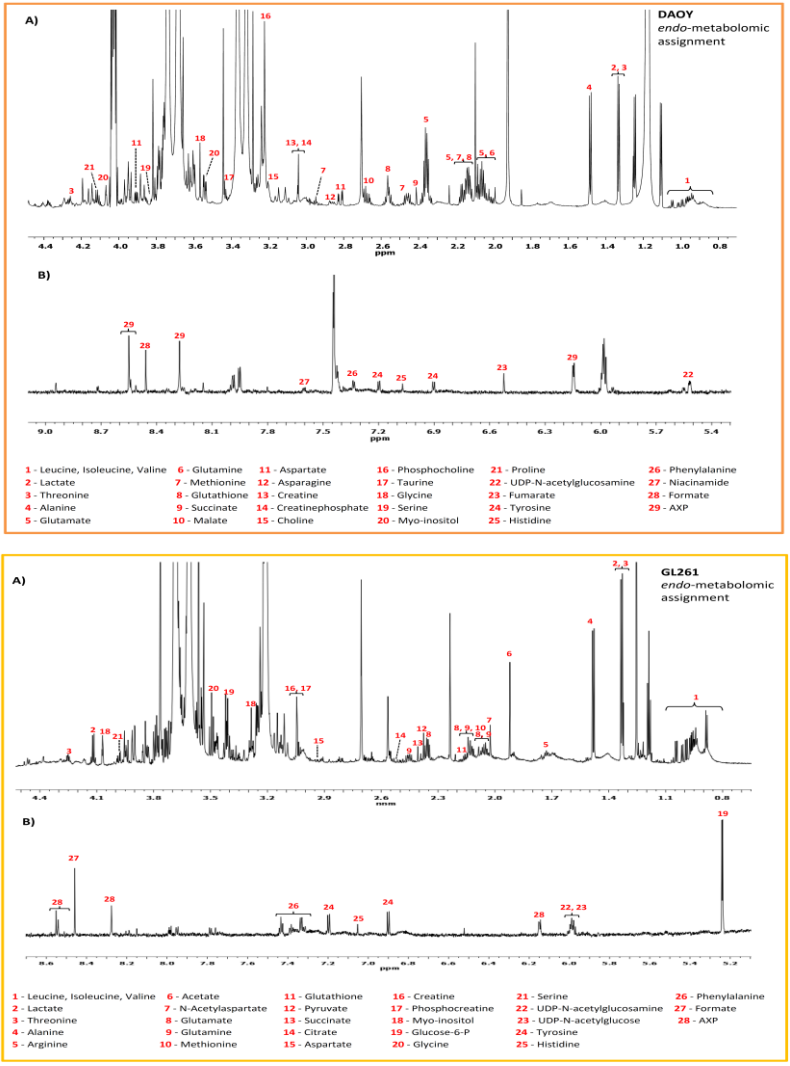

Figure 2.4. DAOY and GL261 cell lines assignment. (A) Upfield region (0.8 – 4.4 ppm) of the ^{1}H CPMG NMR spectrum along with the assignment of the most intense metabolites. **(B)** Downfield region (DAOY: 5.4–9.0 ppm; GL261: 5.2 –8.6 ppm) of the ^{1}H CPMG NMR spectrum along with the assignment of the less intense metabolites.

The resonance assignments of the major metabolites in the spectra were performed using a NMR spectra library of pure organic compounds (AMIX software), public databases (*i.e.* Human Metabolome Database-HMBD, http://www.hmdb.ca) storing reference NMR spectra of metabolites, spiking NMR experiment and using data available in literature. As a result, around 30 metabolites were identified, which provided information for assessing variations in metabolic profiles after drug administration.

The 1D ^{1}H NMR spectra were processed and studied using a completely untargeted and unbiased multivariate data analytical approach. The aim was to identify the perturbation in the metabolic signatures associated with response to treatment for each tested cell. For this purpose, a principal component analysis (PCA) was performed on the NMR spectra.

❖ ***DAOY cell line***

Our previous studies identified GlaB as an efficient inhibitor of the growth of HH/GLI-dependent tumors (in particular MB and BCC) and cancer stem cells in *vitro* and in *vivo*, indicating that GLI/DNA interference is an appealing therapeutic strategy to regulate the heterogeneous molecular changes leading to HH/GLI pathway activation in cancer (Infante et al., 2015). In this study we wished to

investigate whether a metabolomics approach could identify signatures associated with HH-pathway inhibition and whether this signatures provide new insight into the mechanism of action of this new molecule. We evaluated the metabolic changes induced by drug treatment after 24 h at the 0.5 µM concentration on MB DAOY cell line. Multivariate statistical modeling using PCA (unsupervised analysis) was performed on ^{1}H NMR spectra of seven independently grown replicates from cell lysates of treated and untreated cells. The scores plot, principal component 1 (PC1 72.9%) *vs* principal component 2 (PC2 9.59%), resulting from PCA revealed very clear discrimination between the intracellular metabolome before and after the drug administration (Figure 2.5A).

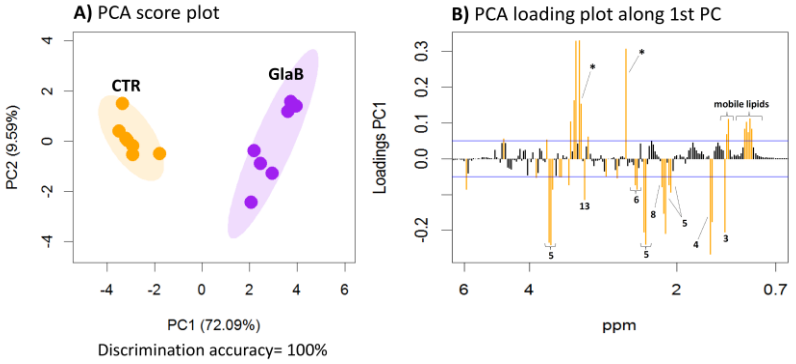

Figure 2.5. *endo*-Metabolomic phenotyping of DAOY cells. **A)** PCA score plot: *endo*-metabolomic profiles of native cell (orange dots) and GlaB-treated (purple dots) cell lysates. The discrimination accuracy value of the model is reported. Each dot represents a different cell lysate sample; **B)** PCA loading plot: section of the loading plot (0.7 – 6 ppm) obtained from the PCA analysis. The color in the plot can be used to identify the significant variables in the class separation.

It is noteworthy that the treatment with and without GlaB is separated along the first principal component. Importantly, even in the presence of the drug, reproducibility between replicates (7 for each treated and untreated sample) remained very high and the sample-to-sample variation within each group was significantly smaller (95% confidence interval location) than any variation arising from treatment or genetic variability. It must be emphasized that these differences were identified using an unsupervised analysis, *i.e.* any prior information about the samples. The discrimination accuracy of the model was assessed by the leave-one-out cross-validation method (LOOCV) and resulted to be about 100%. LOOCV method starts to split-sample cross-validation in forming training set and a test set. With LOOCV, however, the test set consists of only a single sample; the rest of the samples are placed in the training set. The sample in the test set is placed aside and not utilized at all in the development of the class prediction model.

The loading plot was used to identify the significant characteristic metabolites responsible for the clustering patterns. The plot for the first principal component of the comparison between the groups (treated *vs* untreated) identified threonine (**3**), alanine (**4**), glutamate (**5**), glutamine (**6**), glutathione (GSH, **8**), and the signals arising from mobile lipids and two unknown metabolites (*****) as major discriminators between the CTR and GlaB samples (Figure

2.5B). The metabolites **3**, **4**, **5**, **6**, **8** and **13** were lower in the treated cells, meanwhile the mobile lipids and unknown metabolites were high. The ability to distinguish the two groups so accurately represents a significant progress for profiling differing shared and non-shared drug responses.

Additionally, we calculated the relative integrals of the characteristic small molecules for the two groups and we focused on deregulated metabolites whose abundances changed significantly ($p<0.05$, Wilcoxon test). We found the significant alteration of 20 metabolites (see Figure S1 of Section 2.3.6). The administration of GlaB lowered the concentrations of the most of molecules, characterizing the DAOY *endo*-metabolic profile, including metabolites intimately associated with the TCA cycle, some amino acids and other metabolites, and induced a significant increase in concentration of two unknown compounds distinguished in the ^{1}H NMR spectra by a singlet centered at 2.56 ppm and two related doublet centered at 3.10 ppm and 3.15 ppm respectively, with a typical geminal proton-proton coupling constant (J= 16 Hz) (Figure 2.6).

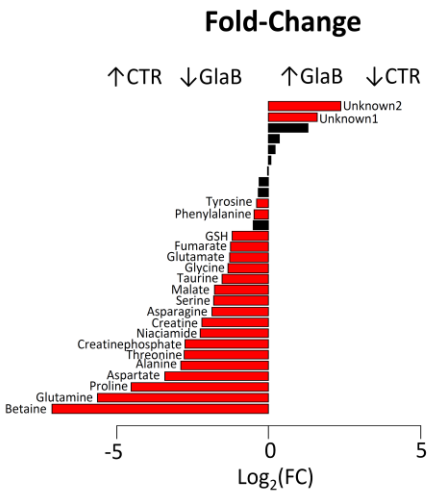

Metabolites	P-value (<0.05)
Threonine	0.002
Alanine	0.002
Glutamate	0.002
Glutamine	0.002
GSH	0.025
Aspartate	0.025
Asparagine	0.025
Creatine	0.002
Creatinephosphate	0.021
Taurine	0.006
Glycine	0.035
Serine	0.006
Proline	0.006
Fumarate	0.025
Tyrosine	0.013
Phenylalanine	0.025
Niacinamide	0.002
Unknown1, *s* 2.56 ppm	0.002
Unknown2, *d* 3.10 ppm *d* 3.15 ppm	0.002
Betaine	0.02

Figure 2.6. Altered metabolite levels in DAOY cells. Fold-change (FC) is calculated for each metabolite by dividing the treatment group (GlaB) by the reference treatment (CTR); the bars plot show the $Log_2(FC)$ (red and black bars refer to $p<0.05$ and $p>0.05$, respectively; Wilcoxon test was used). Abbreviations: *s*, singlet; *d*, doublet.

❖ *GL261 cell line*

To characterize the molecular mechanism induced by GlaB in GL261 cell line, we studied the metabolic changes introduced by the drug administration after 48 h at the 5 µM concentration. We analysed the effects of GlaB administration both on the *endo*- and on the *exo*-metabolome of this cell line. The separate analysis of the *exo*- and *endo*-metabolome provided complementary information for a

comprehensive picture of the cellular metabolic state and phenotype. To determine the differences in the metabolic profiles among the treated and untreated cells, respectively, we performed PCA to analyze the normalized ^{1}H NMR data. The results showed that all samples were located in the ellipse of the 95% confidence interval, and both the cell lysates and the conditioned media from untreated samples were perfectly separated from those treated with GlaB along the first principal component (PC1). The PCA scores plot displaying the two main PCs accounting for 87.08% of the variance (PC1 64.61%, PC2 22.47%) in the case of the *endo*-metabolome and for 99.92% (PC1 99.86%, PC2 0.06%) of the variance for the *exo*-metabolome, respectively (Figure 2.7A-B).

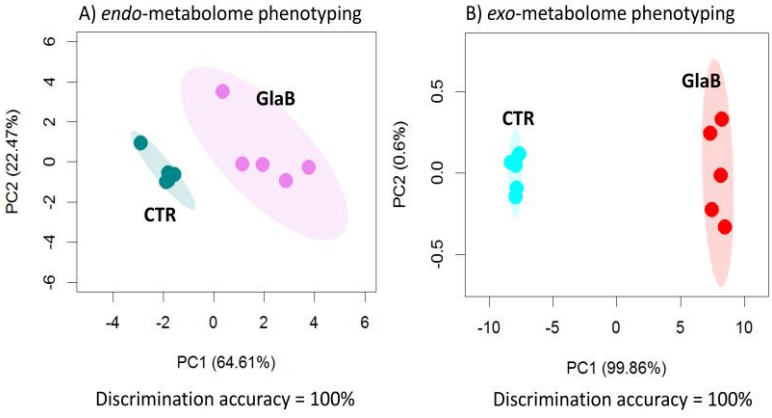

Figure 2.7. Metabolomic phenotyping of GL261 cells: scores plot of PCA analysis; discrimination of **A)** *endo*-metabolomic profiles of native cell (green dots) and GlaB-treated (purple dots) cell lysates; **B)** *exo*-metabolomic profiles of native cell (cyan dots) and GlaB-treated (red dots) cell lysates. The discrimination accuracy value of

each model is reported. Each dot represents a different cell lysate-conditioned medium sample.

The LOOCV method revealed that the two groups can perfectly be discriminated to each other with a discrimination accuracy of 100%.

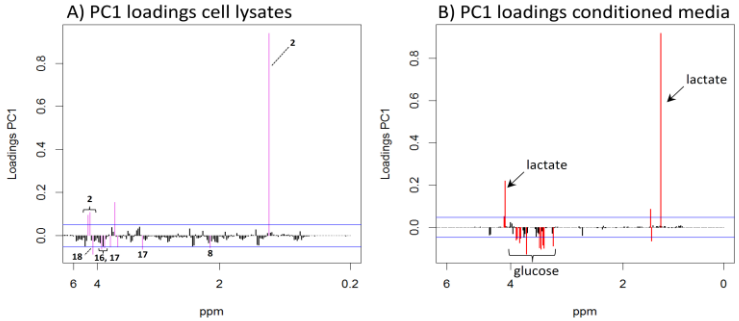

Figure 2.8. PCA loadings plot of cell lysates (A) and culture media (B) samples. The loading profiles correspond to first principal component (PC1). The color in the loadings plot can be used to identify the significant variables in the class separation.

The plot for the first principal component of cell lysates shows that samples treated with GlaB are characterized by an higher content of lactate (**2**) whereas the concentration of glutamate (**8**), myo-inositol (**18**), creatine (**16**) and phosphocreatine (**17**) are lower with the respect to the samples untreated (Figure 2.8A). The corresponding loadings plot of conditioned media along the first principal component exhibits higher content in lactate concentration in treated samples and the reverse lower amount in the glucose concentration, differing from the control samples (Figure 2.8B).

However, to better understand the effect of GlaB on the metabolism of the murine glioma cell line, a direct comparison of the average ^{1}H NMR spectra of the five replicates for both group of the intra- and extracellular samples was performed. Compared with the untreated group of cell lysates, the treated one showed a marked decrease in the relative intensities of the majority of metabolites such as alanine, NAA, glutamate, glutamine, aspartate, creatinephosphate and creatine, myo-inositol, glucose-6-P, UDP-glucose and UDP-N-acetylglucosamine and signal related to diphosphate nucleotides (XDP), and significantly increase levels of other metabolites, including lactate, succinate, citrate and signal related to monophosphate nucleotides (XMP) (Figure 2.9). The univariate statistical analysis of conditioned media revealed also essential differences in the metabolic pattern distribution between the two groups under consideration: in particular, the concentration of lactate increases after treatment and, on the contrary, the glucose and pyruvate concentrations decrease. Moreover, branched chain amino acids (BCAA), including isoleucine, leucine and valine and alanine were observed to increase upon treatment with GlaB; succinate increased and glycine, glutamine and citrate decreased significantly; choline and myo-inositol both decrease after treatment (see Figure S2 of Section 2.3.6).

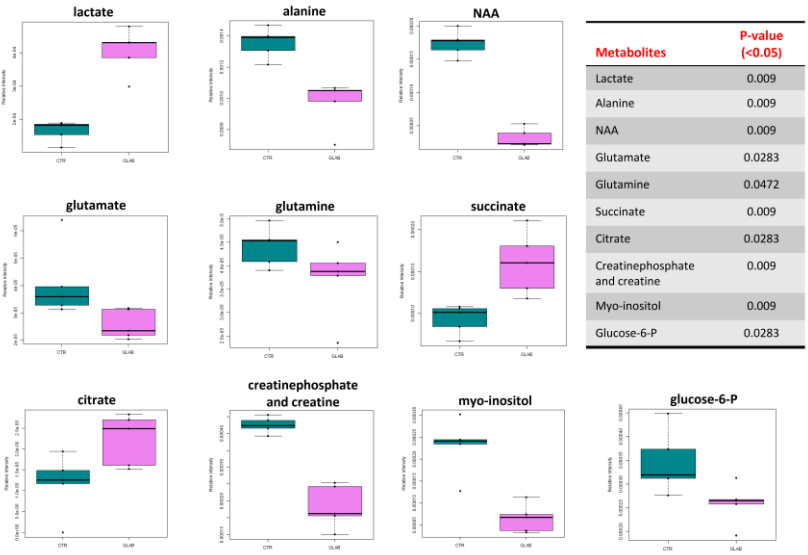

Metabolites	P-value (<0.05)
Lactate	0.009
Alanine	0.009
NAA	0.009
Glutamate	0.0283
Glutamine	0.0472
Succinate	0.009
Citrate	0.0283
Creatinephosphate and creatine	0.009
Myo-inositol	0.009
Glucose-6-P	0.0283

Figure 2.9. Univariate analysis of the relative integrals of characteristic metabolites inside the cells. The box plot shows the comparison of relative intensities of characteristic metabolites between the untreated (CTR, turquoise box) and treated (GlaB, violet box) samples of GL261 cell line. ($p<0.05$, Wilcoxon test was used).

B2.2.2 Metabolic pathway analysis

Cancer cell lines are well established models to study specific cellular mechanisms characteristic for different types of cancer, usually by monitoring specific proteins and their actions. Recent advances in "omics" technologies allow for more systematic investigations to characterize parameters like gene expression, protein and metabolite profiles (Blaise et al., 2006; Bundy et al.,

2007). The advantage of “omics” technologies lies in their multiparametric nature probing a large array of indicators at the same time. For the application of “omics” technologies to the understanding of drug action, it is essential that effects of drugs produce a sensitive response which can be reproduced with sufficiently high quality. Here we have shown that metabolic profiling of different cancer cells (human MB DAOY and murine GL261) can not only identify phenotypic differences between cell lines but can also sensitively detect and distinguish changes in metabolite concentrations after perturbation. It is important to mention that the GlaB administration caused a distinct reproducible profile which is observed in unsupervised PCA.

From the visual inspection of ^{1}H CPMG NMR spectra of DAOY cell line, there is a clear increase after 24 h of treatment with GlaB in the signals corresponding to the so-called mobile lipids (ML), represented mostly by triacylglycerides. These signals are attributed primarily to the methylene group ($-CH_2-$) at 1.3 ppm and to the methyl group ($-CH_3$) at 0.9 ppm of fatty acyl chains. ML apparently come from intracellular lipid bodies or membrane microdomains during the ongoing metabolic changes associated with programmed cell death (apoptosis phenomenon). Accordingly, in the PCA loading profile the signals arising from ML are some of the major

discriminators between the treated and untreated groups (see Figure 2.10).

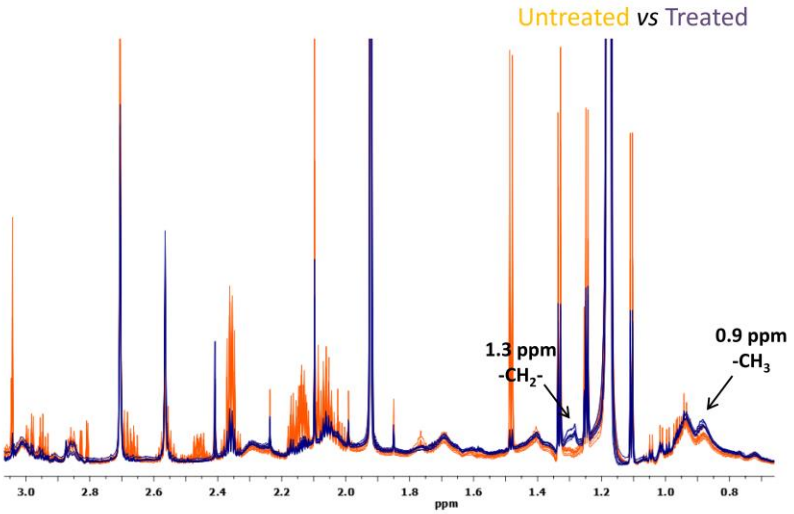

Figure 2.10. Superimposed ^{1}H NMR spectra of DAOY cell line before (orange) and after (purple) treatment with GlaB at 0.5 µM concentration. Notice a clear increase in the ML peaks intensity (indicative of apoptosis) at 0.9 ppm and 1.3 ppm over a 24 h incubation time.

Moreover, the altered amino acids (phenylalanine, tyrosine, leucine and valine) in tumor are mostly involved in TCA cycle anaplerosis (Tripathi et al., 2012) and protein biosynthesis (Owen et al., 2002) by being converted into fumarate and succinyl CoA, respectively (Dang, 2010). In our case, the treatment with GlaB induced a significant reduction in relative intensities of both phenylalanine and tyrosine amino acids and of TCA cycle intermediate fumarate.

Additionally, the treatment of DAOY cells for 24 h with GlaB lowered the concentration of glutamate and induced glutamine depletion resulting in aerobic respiration reduction. It has been known that glutamine has a prominent role in promoting oxygen consumption, because glucose depletion in the presence of glutamine enhanced oxygen consumption while glutamine depletion in the presence of glucose diminished oxygen consumption substantially (Alam et al., 2016). Through glutaminolysis process as a source of energy to fuel tumor growth, glutamine metabolite is the dominant respiratory substrate in tumor cells. Both glutamate and glutamine are the two most important amino acids in maintaining the nitrogen balance in the cell, supporting the central role of glutaminolysis and nitrogen anabolism to sustain cancer cell growth and proliferation. Furthermore, the metabolite GSH is also down-regulated in the treated group. As a ubiquitous intra- and extracellular protective antioxidant, GSH plays a key role in reducing reactive oxygen species (ROS) and combating increased oxidative stress. GSH is particularly vital in protecting cells from radiation damage, which has generated ROS. Rosi et al. found that a high level of this metabolite was correlated with radiation-induced apoptosis by MR spectra of cultured tumor cells (Rosi et al., 2007). Since GlaB after 24 h of treatment strongly diminished oxygen consumption

(glutamine depletion) and induced apoptosis, the GSH levels cannot supply the excessive ROS production induced by oxidative stress.

On the other hand, in GL261 cell line GlaB proved to be able to perturb the levels of the metabolites that are involved in mitochondrial activities, compared to the untreated control samples. In fact, among the detected metabolites, the increased levels of succinate indicate inhibition of Complex I of respiratory chain of mitochondria useful to convert succinate in fumarate. This process impairs TCA cycle and production of ATP. Moreover, mitochondrion dysfunctions are shown by prevented conversion of creatine to phosphocreatine that results in further impairment of urea cycle and amino acids synthesis. Furthermore, the level of glutamine was slight reduced after treatment: glutamine provides a crucial source of cellular energy and building blocks for cancer cells (Hensley et al., 2013) through glutaminolysis, which enters the TCA cycle by being converted into glutamate initially and then into α-ketoglutarate (Dang, 2010). In our case, the small reduction in glutamine concentration might be imply in down-regulation of anaplerotic flux. In addition, the GlaB administration to GL261 cells significantly induced a decrement in glutamate and NAA metabolites. Notably, N-acetylaspartate is the second most abundant amino acid derivative in the brain, second only to glutamate, and is the most abundant source of acetate (Mehta and

Namboodiri, 1995). NAA is synthesized in neuronal mitochondria (Goldstein, 1959) or endoplasmic reticulum (Lu et al., 2004) via acetylation of aspartate by the enzyme aspartate N-acetyl transferase. NAA may be converted to the dipeptide neurotransmitter N-acetylaspartylglutamate (NAAG) by the enzymes NAAG synthetase I and II (Becker et al., 2010; Collard et al., 2010) and it serves as a source of perisynaptic NAA and glutamate metabolites. Neverthless, the exact function of glutamate and NAA reduction remains unknown and requires further investigation. The other metabolites, such as lactate and myo-inositol, are metabolic markers frequently reported in cancers. Increased levels of lactate were detected in stomach cancer, oral cancer and rectal cancer tissues (Wang et al., 2013). Interestingly, the decreased level of lactate was observed in cells of head and neck squamous cell carcinoma, compared with those of normal human oral keratinocytes. It has also been found a decreased lactate level in glioma cell lines in the high-grade group. Lactate production, due to the high glycolytic rates in cancer cells, enhances intracellular acidosis, which in turn leads to apoptosis. Previous works (Baumann et al., 1992; Colen et al., 2011) have also demonstrated that glioma cells could rapidly discharge lactate into the nearby microenvironment through monocarboxylate transporters. Thus, the lactate up-regulation observed in both intra- and extracellular

metabolic profile might be associated with the capability of GlaB to promote the glycolytic rate as clear sign of apoptosis event and cell death. Furthermore, myo-inositol is associated with osmo-regulation and volume regulation (Duarte et al., 2013). In our study, the level of myo-inositol in the two groups was significantly different both in the intra- and extracellular media, implying that these metabolite might be involved in osmoregulation and volume regulation of GL261 cells upon treatment with GlaB.

B2.3 Experimental section

B2.3.1 Materials

- ***DAOY cell line***

DAOY cells were purchased from American Type Culture Collection (ATCC–Manassas, VA, USA), and maintained in Eagle's Minimum Essential Medium (MEM) purchased from Sigma Aldrich (St. Louis, MO, USA), plus L-Glutamine, antibiotics and 10% fetal bovine serum (FBS; ThermoFisher Scientific, Waltham, MA, USA). Trypsin-EDTA 1X in PBS (w/o Calcium, w/o Magnesium, w/o Phenol Red) was purchased from EuroClone S.p.A. (Milan, Italy). Leupeptin, Pepstatin, Sodium Orthovanadate, PMSF, Aprotinin were purchased from Sigma Aldrich.

RNA interference

DAOY cells were transfected with non-targeting siRNA as control or with double-stranded siRNAs targeting human GLI1 and GLI2 (On target-Plus SMARTpool reagents; Dharmacon, Lafayette,CO). Transfections were performed with HiPerFect transfection reagent (Qiagen, Hilden, Germany) according to the manufacturer's instructions.

- ***GL261 cell line***

GL261 cells were kindly provided by Dr. Serena Pellegatta, Neurological Institute "Carlo Besta", Italy. Cell culture medium (Dulbecco's modified minimum essential medium, DMEM), fetal bovine serum (FBS), penicillin G, streptomycin, glutamine, sodium pyruvate were from GIBCO Invitrogen (Carlsbad, CA). Phosphate buffer saline (PBS) (0.01 M Phosphate buffer, 0.0027 M KCl e 0.14 M NaCl, pH 7.4 at 25 °C) was purchased from Sigma-Aldrich (St. Louis, MO).

MTT viability assay

GL261 cells (5000/well) were seeded into 96 multi-well plates and treated with Glab 5 μM or vehicle for 4 days. MTT (500 μg/ml) was added into each well for 1.5 h. DMSO was then added to stop the reaction and the formazan produced was measured at 570 nm. Viability of cells was expressed relative to absorbance.

B2.3.2 Cell Culture and NMR sample preparation

- ***DAOY cell culture***

DAOY cells were grown in MEM, plus 10% FBS at 37 °C in a humidified atmosphere of 5% CO_2. In order to obtain the final desired number of cells (3 x 10^6) for each treatment (DMSO-d_6 0.5

µM and GlaB 0.5 µM solubilized in DMSO-d_6, respectively), the cell growth was carried out in parallel in multiple 100 mm tissue culture dishes (Corning). Upon achievement of 90% cellular confluency, the culture medium was removed and immediately stored at -80 °C, for the *exo*-metabolome analyses. In brief, the cells were washed with ice-cold phosphate-buffered saline (PBS 1X w/o Calcium, w/o Magnesium) in order to completely remove any residue of culture medium. For GlaB treated dishes, the cells were collected by adding 4 ml of PBS 1X and scraping with a rubber policeman. For DMSO-d_6 treated dishes, the cells were harvested by adding 1 ml of Trypsin-EDTA 1X in PBS (w/o Calcium, w/o Magnesium, w/o Phenol Red), then PBS 1X and scraping with a rubber policeman. Finally, the cells were counted and aliquoted 3 x 10^6 for each treatment replicate. Each replicate was lysed with 700 µl of Lysis Buffer (10 mM Tris-HCl, 5 mM EDTA, 120 mM NaCl) plus protease and phosphatase inhibitors (1 µg/µl Leupeptin, 0.5 ng/µl Pepstatin, 0.2 mM Sodium Orthovanadate, 0.1 mM PMSF, 0.1 mg/ml Aprotinin) and then sonicated 5 times (15s on – 15s off; 50% amplitude). The lysates were centrifuged two times at 17,000xg for 1 h and the last supernatant stored at -80 °C for the *endo*-metabolomic analysis.

- ***GL261 cell culture***

GL261 were cultured in DMEM supplemented with 20% heat-inactivated FBS, 100 IU/ml penicillin G, 100 µg/ml streptomycin, 2.5 µg/ml amphotericin B, 2 mM glutamine, and 1 mM sodium pyruvate. Cells were grown at 37 °C in a 5% CO_2 humidified atmosphere. Cells were subcultivated when confluent.

For metabolome analyses confluent GL261 cells were trypsinized, counted and plated (3 x 10^6) in 6 cm dishes containing 1% FBS medium. After 4 h the growth medium was changed and supplemented with GlaB 5 µM or vehicle (DMSO) for 48 h. Then the culture medium of each dish was collected, centrifuged (10,000xg for 10 minutes) and immediately stored at -80 °C until used. On the other side, cells were extensively washed (4 times) with ice-cold phosphate-buffered saline (PBS 1X), in order to completely remove any residue of culture medium, trypsinized and centrifuged. Afterwards, cells were dispersed in a buffer solution containing 10 mM Tris (pH 7.4), 5 mM EDTA, 120 mM NaCl, and protease inhibitors (Complete Protease inhibitor Cocktail tablet, Roche). Cell lysis was obtained by sonication and the cytosolic fraction containing the metabolites was obtained upon centrifugation at 17,000xg for 1 h at 4 °C. Subsequently, cytosols were collected for analysis and stored at -80 °C until used.

- ***NMR sample preparation***

NMR cell lysate samples were prepared in 5.00 mm NMR tubes (Bruker BioSpin srl) after the addition of 50 µl of $^{2}H_2O$ containing 10 mM sodium trimethylsilyl [2,2,3,3-$^{2}H_4$]propionate (TMSP) to 450 µl of cell lysate. The cell culture media samples were considered and analysed according to standard procedures for the NMR preparation of human plasma and serum. Frozen conditioned media samples were thawed at room temperature and shaken before use. An aliquot (300 µl) of a phosphate sodium buffer (70 mM Na_2HPO_4; 20% v/v $^{2}H_2O$; 0.025% v/v NaN_3; 0.8% w/v TMSP; pH 7.4) were added to 300 µl of each medium sample and the mixture was homogenized by vortexing for 30 seconds (s). The mixture was transferred into a 5.00 mm NMR tubes (Bruker BioSpin srl) for analysis.

2.3.3 NMR experiments

In order to study the possible metabolomic changes induced by GlaB treatment ^{1}H NMR spectra were acquired on both cell lysates and conditioned media verifying their feasibility and reproducibility. NMR spectra were recorded with a Bruker 900 MHz spectrometer equipped with CP TCI $^{1}H/^{13}C/^{15}N$ probe. The ^{1}H NMR spectra of cell lysates were acquired with the Carr-Purcell-Meiboom-Gill (CPMG)

sequence using a monodimensional spin–echo sequence with water presaturation (cpmgpr, Bruker). 256 scans over a spectral region of 18 kHz were collected into 110 K points, giving an acquisition time of 3.07 s. The spectra were recorded with the CPMG pulse sequence (Carr and Purcell, 1954) to impose a T_2 filter that allows selective observation of small molecular weight components. The total T_2 delay was set to 290 ms. The T_2 filtering in the CPMG pulse sequence, which contains trains of -(τ-180°-τ)- blocks repeated n= 256 times, was achieved with a total spin-echo delay (2nτ) of 80 ms. The acquisition of each spectrum required about 32 min. The raw data were multiplied by a 1 Hz exponential line broadening before Fourier transformation into 131 K points. The ^{1}H NMR spectra of conditioned media were acquired with a 1D nuclear Overhauser enhancement spectroscopy (NOESY)-presaturation pulse sequence (noesygppr1d, Bruker) with irradiation at the water frequency during the recycle and mixing time delays and a spoil gradient. A total of 64 scans with 110 K data points were collected using a spectral width of 17942 Hz, an acquisition time of 3.07 s, a relaxation delay of 4 s, and a mixing time of 100 ms. The NOESY spectra generally give the best overview over all types of molecules in biofluids. Transformed spectra were automatically corrected for phase and baseline distortions and calibrated (chemical shift was referenced to the proton of TMSP at δ 0.0 ppm) using TopSpin 3.5

(Bruker Biospin srl). We performed this type of experiments on various replicates (from five to seven) identifying the metabolomic fingerprints of both human MB DAOY and glioma murine GL261 cells and of those ones of the same cell lines treated with GlaB.

2.3.4 Spectral Analysis

Each spectrum in the region 10.00 – 0.2 ppm was segmented into 0.02 ppm chemical shift bins, and the corresponding spectral areas were integrated using the AMIX software (Bruker).

- ***DAOY spectra***

The area of each bin was normalized to the total spectral area, calculated with exclusion for the cell lysates of the regions 1.09 – 1.23, 1.85 – 1.97, 3.25 – 3.43, 3.63 – 3.71, 4.01 – 4.02 (which correspond to EDTA and Tris peaks, and the most intense peaks of the protease and phosphatase inhibitors used for sample preparation) and the water region (4.45 – 5.67 ppm).

- ***GL261 spectra***

The area of each bin was normalized to the total spectral area, calculated with exclusion for the cell lysates of the regions 2.55 – 2.57, 2.69 – 2.72, 3.6 – 3.65, 3.20 – 3.236, 3.67 – 3.72, 3.75 – 3.78,

3.79 – 3.82, 3.86 – 3.9, 7.65 – 7.70, 8.05 – 8.13 (which correspond to EDTA and Tris peaks, and the most intense peaks of the protease inhibitors used for sample preparation) and the water region (4.4 – 5.9 ppm); for the conditioned media exclusion regarded the water region 4.6 – 4.8 ppm.

2.3.5 Metabolite statistical analysis

The multivariate and univariate statistical techniques were applied on the obtained buckets using R 3.0.2 in house scripts.

Unsupervised PCA was used to obtain a preliminary outlook of the data (visualization in a reduced space, clusters detection, screening for out-layers). From the PCA score plot (PC1, PC2), a perfect discrimination between the two different groups tested (the treated and the untreated samples) was clearly visible indicating a strong differences on the cell metabolic profiles. The global accuracy for classification was assessed by means of a leave-one-out cross-validation scheme (LOOCV).

Around 30 metabolites, whose peaks in the spectra were well defined and resolved, were assigned and their levels analysed. The assignment procedure was made up using a NMR spectra library of pure organic compounds, public databases (such as Human Metabolome Database-HMBD) storing reference NMR spectra of

metabolites, spiking NMR experiment and using data available in literature. The relative concentrations of the various metabolites were calculated by integrating the corresponding signals in the spectra with an in house deconvolution script. The Wilcoxon test was used for the determination of the meaningful metabolites: a p-value of 0.05 was considered statistically significant. The concentration changes of the metabolites are also expressed as the Log_2(FC).

2.3.6 Supplementary figures

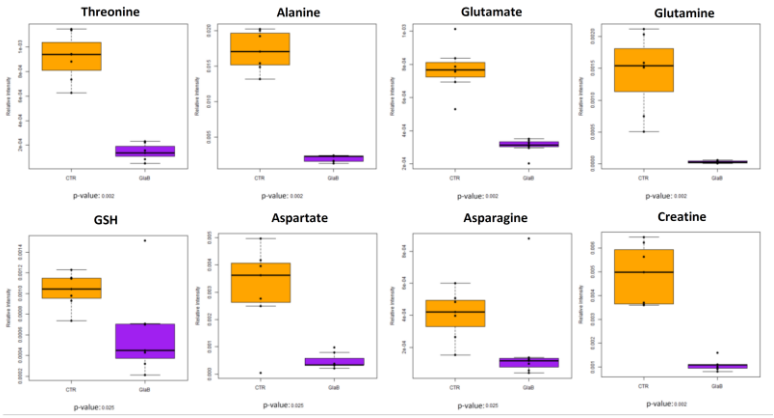

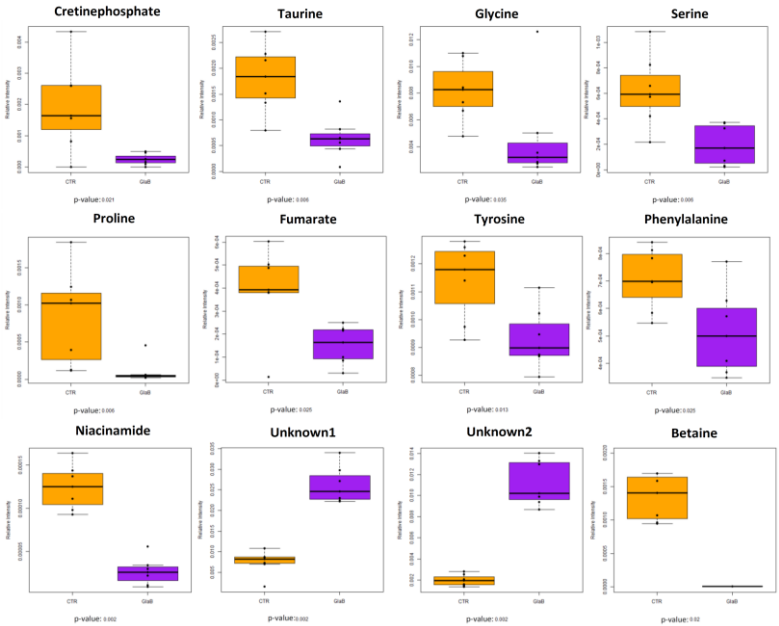

Figure S1. Univariate analysis of the relative integrals of characteristic metabolites inside the DAOY cells. The box plot shows the comparison of relative intensities of characteristic *endo*-metabolites between the untreated (CTR, orange box) and treated (GlaB, purple box) samples of DAOY cell line. ($p<0.05$, Wilcoxon test was used).

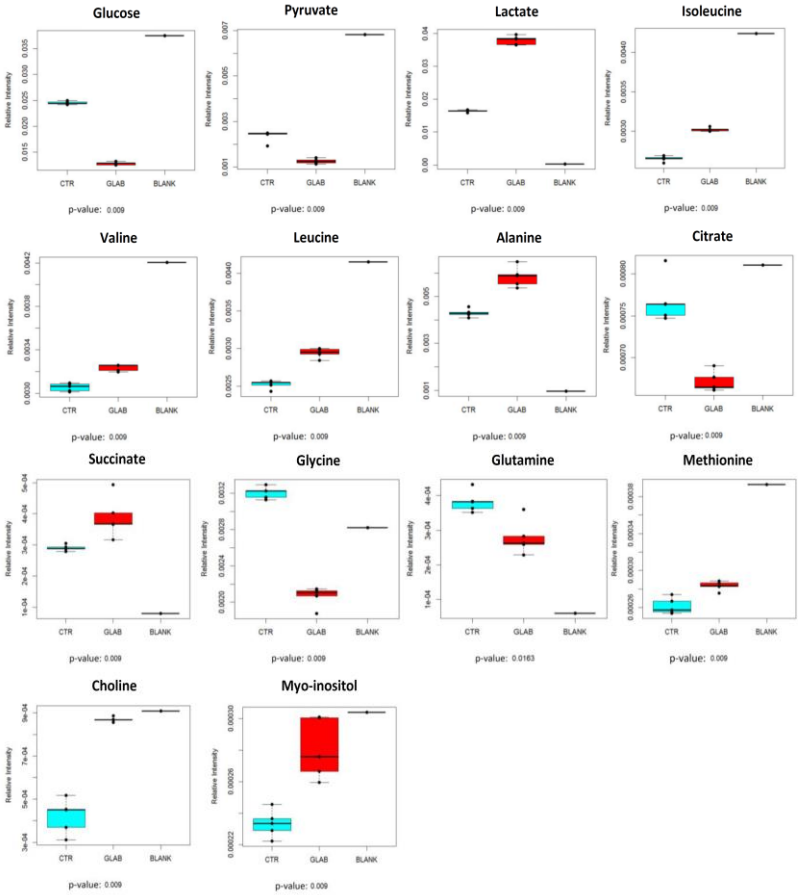

Figure S2. Univariate analysis of the relative integrals of characteristic metabolites outside the GL261 cells. The box plot shows the comparison of relative intensities of characteristic *exo*-metabolites between the untreated (CTR, cyan box) and treated (GlaB, red box) samples of GL261 cell line. ($p<0.05$, Wilcoxon test was used).

Chapter B3

References

Adams S., Braidy N., Bessesde A., Brew B.J., Grant R., Teo C., Guillemin G.J., *Cancer Res.*, **2012**, 72, 5649.

Alam M.M., Sohoni S., Kalainayakan S.P., Garrossian M., Zhang L., *B.M.C. Cancer*, **2016**, 16, 150.

Amakye D., Jagani Z., Dorsch M., *Nat. Med.*, **2013**, 19, 1410.

Ausman J.I., Shapiro W.R., Rall D.P., *Cancer Res.*, **1970**, 30, 2394.

Bai J., Wang M.X., Chowbay B., Ching C.B., Chen W.N., *Metabolomics*, **2011**, 7, 353.

Baumann M., DuBois W., Pu A., Freeman J., Suit H.D., *Int. J. Radiat. Oncol. Biol. Phys.*, **1992**, 23, 803.

Bayet-Robert M., Morvan D., Chollet P., Barthomeuf C.; *Breast Cancer Res. Treat.*, **2009**, 120, 613.

Beachy P.A., Hymowitz S.G., Lazarus R.A., Leahy D.J., Siebold C., *Genes Dev.*, **2010**, 24, 2001.

Becker I., Lodder J., Gieselmann V., Eckhardt M., *J. Biol. Chem.*, **2010**, 285, 29156.

Beckonert O., Keun H.C., Ebbels T.M.D., Bundy J., Holmes E., Lindon J.C., Nicholson J.K., *Nat. Protoc.*, **2007**, 2, 11.

Blaise B.J., *Anal. Chem.*, **2013**, 85, 8943.

Blaise B.J., Giacomotto J., Elena B., Dumas M.E., Toullhoat P., Ségalat L., Emsley L., *Proc. Natl. Acad. Sci. U.S.A.*, **2007**, 104, 19808.

Brunelli L., Caiola E., Marabese M., Broggini M., Pastorelli R., *Sci. Rep.*, **2016**, 6, 28398.

Brunet J., Vazquez-Martin A., Colomer R., Grana-Suarez B., Martin-Castillo B., Menendez J.A., *Mol. Carcinog.*, **2008**, 47, 157.

Bu Q., Huang Y., Yan G., Cen X., Zhao Y.L., *Comb. Chem. High Throughput Screening*, **2012**, 15, 266.

Bundy J.G., Iyer N.G., Gentile M.S., Hu D.E., Kettunen M., Maia A.T., Thorne N.P., Brenton J.D., Caldas C., Brindle K.M., *Cancer Res.*, **2006**, 66, 7606.

Canelas A., Ras C., ten Pierick A., van Dam J., Heijnen J., van Gulik W., *Metabolomics*, **2008**, 4, 226.

Carr H.Y., Purcell E.M., *Phys. Rev.*, **1954**, 94, 630.

Cheng Y., Xie G., Chen T., Qiu Y., Zou X., Zheng M., Tan B., Feng B., Dong T., He P., Zhao L., Zhao A., Xu L.X., Zhang Y., Jia W., *J. Proteome Res.*, **2012**, 11, 1354.

Chong W.P.K., Thng S.H., Hiu A.P., Lee D.-Y., Chan E.C.Y., Ho Y.S., *Biotechnol. Bioeng.*, **2012**, 109, 3103.

Claudino W.M., Goncalves P.H., di Leo A., Philip P.A., Sarkar F.H., *Criti. Rev. Oncol. Hematol.*, **2012**, 84, 1.

Clement V., Sanchez P., de Tribolet N., Radovanovic I., Ruiz I., Altaba A., *Curr. Biol.*, **2007**, 17, 165.

Clyne M., *Nat. Rev. Urol.*, **2012**, 9, 355.

Colen C.B., Shen Y., Ghoddoussi F., Yu P., Francis T.B., Koch B.J., Monterey M.D., Galloway M.P., Sloan A.E., Mathupala S.P., *Neoplasia*, **2011**, 13, 620.

Collard F., Stroobant V., Lamosa P., Kapanda C.N., Lambert D.M., Muccioli G.G., Poupaert J.H., Opperdoes F., Van Schaftingen E., *J. Biol. Chem.*, **2010**, 285, 29826.

Craig A., Cloareo O., Holmes E., Nicholson J.K., Lindon J.C., *Anal. Chem.*, **2006**, 78, 2262.

Crooke P.S., Ritchie M.D., Hachey D.L., Dawling S., Roodi N., Parl F.F., *Cancer Epidemiol. Biomarkers Prev.*, **2006**, 15, 1620.

Crott J., Thomas P., Fenech M., *Mutagenesis*, **2001**, 16, 317.

Cuperlovic-Culf M., Barnett D.A., Culf A.S., Chute I., *Drug Discov. Today,* **2010**, 15, 610.

Dang C.V., *Cell Cycle*, **2010**, 9, 3884.

Das S., Srikanth M., Kessler J.A., *Nat. Clin. Pract. Neuro.*, **2008**, 4, 427.

Denkert C., Budczies J., Weichert W., Wohlgemuth G., Scholz M., Kind T., Niesporek S., Noske A., Buckendahl A., Dietel M., Fiehn O., *Mol. Cancer*, **2008**, 7, 72.

Di Magno L., Manzi D., D'Amico D., Coni S., Macone A., Infante P., Di Marcotullio L., De Smaele E., Ferretti E., Screpanti I., Agostinelli E., Gulino A., Canettieri G., *Cell Cycle*, **2014**, 13, 3404.

Dirix L., *J. Clin. Oncol.*, **2014**, 32, 720.

Duarte I.F., Ladeirinha A.F., Lamego I., Gil A.M., Carvalho L., Carreira I.M., Melo J.B., *Mol. Pharm.*, **2013**, 10, 4242.

Ellison D., *Neuropathol. Appl. Neurobiol.*, **2002**, 28, 257.

Espinoza I., Miele L., *Cancer Lett.*, **2013**, 341, 41.

Fiehn O., *Plant. Mol. Biol*., **2002**, 48, 155.

Fleming H., Blumenthal R., Gurpide E., *Proc. Natl. Acad. Sci. U.S.A.*, **1983**, 80, 2486.

Giangaspero F., Bigner S.H., Kleihues P., Pietsch T., Trojanowski J.Q., *In tumors of the nervous system. Lyon: IARC*, Kleihues P., Cavenee W.K., eds., **2000**, 129.

Goldstein F.B., *Biochim. Biophys. Acta*, **1959**, 33, 583.

Graham R.A., Lum B.L., Cheeti S., Jin J.Y., Jorga K., Von Hoff D.D., Rudin C.M., Reddy J.C., Low J.A., Lorusso P.M., *Clin. Cancer Res.*, **2011**, 17, 2512.

Griffiths J.R., Stubbs M., *Adv. Enzyme Regul.*, **2003**, 43, 67.

Halouska S., Powers R., *J. Magn. Reson.*, **2006**, 178, 88.

Hensley C.T., Wasti A.T., DeBerardinis R.J., *J. Clin. Invest.*, **2013**, 123, 3678.

Hori S., Nishiumi S., Kobayashi K., Shinohara M., Hatakeyama Y., Kotani Y., Hatano N., Maniwa Y., Nishio W., Bamba T., Fukusaki E.,

Azuma T., Takenawa T., Nishimura Y., Yoshida M., *Lung Cancer*, **2011**, 74, 284.

Hsieh A., Ellsworth R., Hsieh D., *J. Cell. Physiol.*, **2011**, 226, 1118.

Hyndman M.E., Mullins J.K., Bivalacqua T.J., *Urol. Oncol.*, **2011**, 29, 558.

Infante P., Mori M., Alfonsi R., Ghirga F., Aiello F., Toscano S., Ingallina C., Siler M., Cucchi D., Po A., Miele E., D'Amico D., Canettieri G., De Smaele E., Ferretti E., Screpanti I., Uccello-Barretta G., Botta M., Botta B., Gulino A., Di Marcotullio L., *EMBO J.*, **2015**, 34, 200.

Jacobsen P.F., Jenkyn D.J., Papadimitriou J.M.J., *Neuropathol. Exp. Neurol.*, **1985**, 44, 472.

Jahns-Streubel G., Reuter C., Auf der Landwehr U., Unterhalt M., Schleyer E., Wörmann B., Büchner T., Hiddemann W., *Blood*, **1997**, 90, 1968.

Jones P.A., Baylin S.B., *Nat. Rev. Genet.*, **2002**, 3, 415.

Kim J., Lee J.J., Kim J., Gardner D., Beachy P.A., *Proc. Natl. Acad. Sci. U.S.A.*, **2010**, 107, 13432.

Kjeldahl K., Bro R., *J. Chemom.*, **2010**, 24, 558.

Kleinstreuer N.C., Smith A.M., West P.R., Conard K.R., Fontaine B.R., Weir-Hauptman A.M., Palmer J.A., Knudsen T.B., Dix D.J., Donley E.L., Cezar G.G., *Toxicol. Appl. Pharmacol.*, **2011**, 257, 111.

Kool M., Jones D.T., Jäger N., Northcott P.A., Pugh T.J., Hovestadt V., Piro R.M., Esparza L.A., Markant S.L., Remke M., Milde T., Bourdeaut

F., Ryzhova M., Sturm D., Pfaff E., Stark S., Hutter S., Seker-Cin H., Johann P., Bender S., Schmidt C., Rausch T., Shih D., Reimand J., Sieber L., Wittmann A., Linke L., Witt H., Weber U.D., Zapatka M., König R., Beroukhim R., Bergthold G., van Sluis P., Volckmann R., Koster J., Versteeg R., Schmidt S., Wolf S., Lawerenz C., Bartholomae C.C., von Kalle C., Unterberg A., Herold-Mende C., Hofer S., Kulozik A.E., von Deimling A., Scheurlen W., Felsberg J., Reifenberger G., Hasselblatt M., Crawford J.R., Grant G.A., Jabado N., Perry A., Cowdrey C., Croul S., Zadeh G., Korbel J.O., Doz F., Delattre O., Bader G.D., McCabe M.G., Collins V.P., Kieran M.W., Cho Y.J., Pomeroy S.L., Witt O., Brors B., Taylor M.D., Schüller U., Korshunov A., Eils R., Wechsler-Reya R.J., Lichter P., Pfister S.M., *Cancer Cell*, **2014**, 25, 393.

Krivtsov A.V., Twomey D., Feng Z., Stubbs M.C., Wang Y., Faber J., Levine J.E., Wang J., Hahn W.C., Gilliland D.G., Golub T.R., Armstrong S.A., *Nature*, **2006**, 442, 818.

Lauth M., Bergström A., Shimokawa T., Toftgård R., *Proc. Natl. Acad. Sci. U.S.A.*, **2007**, 104, 8455.

Lefort N., Brown A., Lloyd V., Ouellette R., Touaibia M., Culf A.S., Cuperlovic-Culf M., *J. Pharm. Biomed. Anal.*, **2014**, 93, 77.

Leichtle A.B., Nuoffer J.M., Ceglarek U., Kase J., Conrad T., Witzigmann H., Thiery J., Fiedler G.M., *Metabolomics*, **2012**, 8, 643.

León Z., García-Cañaveras J.C., Donato M.T., Lahoz A., *Electrophoresis*, **2013**, 34, 2762.

Liu Y., Liu X., Chen L.C., Du W.Z., Cui Y.Q., Piao X.Y., Li Y.L., Jiang C.L., *Neuroimmunol. Neuroinflammation*, **2014**, 1, 51.

Lu Z.H., Chakraborty G., Ledeen R.W., Yahya D., Wu G., *Molec. Brain Res.*, **2004**, 122, 71.

Luciani A.M., Grande S., Palma A., Rosi A, Giovannini C., Sapora O., Viti V., Guidoni L., *FEBS J.*, **2009**, 276, 1333.
Mazurek S., Hugo F., Failing K., Eigenbrodt E., *J. Cell Physiol.*, **1996**, 167, 238.

Mazurek S., Eigenbrodt E., *Anticancer Res.*, **2003**, 23, 1149.

Mazurek S., *Ernst Schering Found. Symp. Proc.*, **2007**, 4, 99.

Mehta V., Namboodiri M.A., *Mol. Brain Res.*, **1995**, 31, 151.

Merchant A.A., Matsui W., *Clin. Cancer Res.*, **2010**, 16, 3130.

Milkevitch M., Shim H., Pilatus U., Pickup S., Wehrle J.P., Samid D., Poptani H., Glickson J.D., Delikatny E.J., *Biochim. Biophys. Acta*, **2005**, 1734, 1.

Morgenroth A., Vogg A.T., Ermert K., Zlatopolskiy B., Mottaghy F.M., *Oncotarget*, **2014**, 5, 5483.

Ng J.M., Curran T., *Nat. Rev. Cancer*, **2011**, 11, 493.

Nicholson J.K., Lindon J.C., Holmes E., *Xenobiotica*, **1999,** 29, 1181.

Odoux C., Fohrer H., Hoppo T., Guzik L., Stolz D.B., Lewis D.W., Gollin S.M., Gamblin T.C., Geller D.A., Lagasse E., *Cancer Res.*, **2008**, 68, 6932.

Oliver S.G., Winson M.K., Kell D.B., Baganz F., *Trends. Biotechnol.*, **1998**, 16, 373.

Owen O.E., Kalhan S.C., Hanson R., *J. Biol. Chem.*, **2002**, 277, 30409.

Paglia G., Hrafnsdóttir S., Magnúsdóttir M., Fleming R.M.T., Thorlacius S., Palsson B.Ø., Thiele I., *Anal. Bioanal. Chem.*, **2012**, 402, 1183.

Pan X., Wilson M., Mirbahai L., McConville C., Arvanitis T.N., Griffin J.L., Kauppinen R.A., Peet A.C., *J. Proteome Res.*, **2011**, 10, 3493.

Panopoulos A.D., Yanes O., Ruiz S., Kida Y.S., Diep D., Tautenhahn R., Herrerías A., Batchelder E.M., Plongthongkum N., Lutz M., *Cell. Res.*, **2012**, 22, 168.

Pattabiraman D.R., Weinberg R.A., *Nat. Rev. Drug Discov.*, **2014**, 13, 497.

Pavletich N.P., Pabo C.O., *Science*, **1993**, 261, 1701.

Po A., Ferretti E., Miele E., De Smaele E., Paganelli A., Canettieri G., Coni S., Di Marcotullio L., Biffoni M., Massimi L., Di Rocco C., Screpanti I., Gulino A., *EMBO J.*, **2010**, 29, 2646.

Racker E., *Mol. Cell Biochem.*, **1974**, 5, 17.

Rainaldi G., Romano R., Indovina P., Ferrante A., Motta A., Indovina P.L., Santini M.T., *Radiat. Res.*, **2008**, 169, 170.

Ramaswamy B., Lu Y., Teng K.Y., Nuovo G., Li X., Shapiro C.L., Majumder S., *Cancer Res.*, **2012**, 72, 5048.

Reya T., Morrison S.J., Clarke M.F., Weissman I.L., *Nature*, **2001**, 414, 105.

Riscuta G., Dumitrescu R.G., *Methods Mol. Biol.*, **2012**, 863, 343.

Roma J., Almazan-Moga A., Sanchez de Toledo J., Gallego S., *Sarcoma*, **2012**, 2012, 695603.

Rosi A., Grande S., Luciani A.M., Palma A., Giovannini C., Guidoni L., Sapora O., Viti V., *Radiat. Res.*, **2007**, 167, 268.

Salek R.M., Haug K., Steinbeck C., *Gigascience*, **2013**, 2, 8.

Sansone S.-A., Fan T., Goodacre R., Griffin J.L., Hardy N.W., Kaddurah-Daouk R., Kristal B.S., Lindon J., Mendes P., Morrison N., Nikolau B., Robertson D., Sumner L.W., Taylor C., van d.W.M., van O.B., Fiehn O., *Nat. Biotechnol.*, **2007**, 25, 846.

Scales S.J., de Sauvage F.J., *Trends Pharmacol. Sci.*, **2009**, 30, 303.

Sekulic A., Migden M.R., Oro A.E., Dirix L., Lewis K.D., Hainsworth J.D., Solomon J.A., Yoo S., Arron S.T., Friedlander P.A., Marmur E., Rudin C.M., Chang A.L., Low J.A., Mackey H.M., Yauch R.L., Graham R.A., Reddy J.C., Hauschild A., *N. Engl. J. Med.*, **2012**, 366, 2171.

Serizawa M., Kusuhara M., Zangiacomi V., Urakami K., Watanabe M., Takahashi T., Yamaguchi K., Yamamoto N., Koh Y., *Anticancer Res.*, **2014**, 34, 2779.

Serkova N., Glunde K., *In Tumor Biomarker Discovery SE -20*; Tainsky M.A., Ed., **2009**, 520, 273.

Simpson N.E., Tryndyak V.P., Beland F.A., Pogribny I.P., *Breast Cancer Res. Treat.*, **2012**, 133, 959.

Sreekumar A., Poisson L.M., Rajendiran T.M., Khan A.P., Cao Q., Yu J., Laxman B., Mehra R., Lonigro R.J., Li Y., Nyati M.K., Ahsan A., Kalyana-Sundaram S., Han B., Cao X., Byun J., Omenn G.S., Ghosh D.,

Pennathur S., Alexander D.C., Berger A., Shuster J.R., Wei J.T., Varambally S., Beecher C., Chinnaiyan A.M., *Nature*, **2009**, 457, 910.

Stringer K.A., McKay R.T., Karnovsky A., Quémerais B., Lacy P., *Front. Immunol.*, **2016**, 7, 44.

Takebe N., Miele L., Harris P.J., Jeong W., Bando H., Kahn M., Yang S.X., Ivy S.P., *Nat. Rev. Clin. Oncol.*, **2015**, 12, 445.

Tang J., *Curr. Genom.*, **2011**, 12, 391.

Teahan O., Bevan C.L., Waxman J., Keun H.C., *Int. J. Biochem. Cell Biol.*, **2011**, 43, 1002.

Teperino R., Amann S., Bayer M., McGee S.L., Loipetzberger A., Connor T., Jaeger C., Kammerer B., Winter L., Wiche G., Dalgaard K., Selvaraj M., Gaster M., Lee-Young R.S., Febbraio M.A., Knauf C., Cani P.D., Aberger F., Penninger J.M., Pospisilik J.A., Esterbauer H., *Cell*, **2012**, 151, 414.

Tirino V., Desiderio V., Paino F., De Rosa A., Papaccio F., La Noce M., Laino L., De Francesco F., Papaccio G., *FASEB J.*, **2013**, 27, 13.

Tiziani S., Lodi A., Khanim F.L., Viant M.R., Bunce C.M., Gunther U.L., *PLoS ONE*, **2009**, 4, e4251.

Tripathi P., Kamarajan P., Somashekar B.S., MacKinnon N., Chinnaiyan A.M., Kapila Y.L., Rajendiran T.M., Ramamoorthy A., *Int. J. Biochem. Cell Biol.*, **2012**, 44, 1852.

Trock B.J., *Urol. Oncol.*, **2011**, 29, 572.

Uchida H., Arita K., Yunoue S., Yonezawa H., Shinsato Y., Kawano H., Hirano H., Hanaya R., Tokimura H., *J. Neurooncol.*, **2011**, 104, 697.

van den Berg R.A., Hoefsloot H.C., Westerhuis J.A., Smilde A.K., van der Werf M.J., *B.M.C. Genomics*, **2006**, 7, 142.
Vander Heiden M.G., Locasale J.W., Swanson K.D., Sharfi H., Heffron G.J., Amador-Noguez D., Christofk H.R., Wagner G., Rabinowitz J.D., Asara J.M., Cantley L.C., *Science*, **2010**, 329, 1492.

Vermeulen L., Sprick M.R., Kemper K., Stassi G., Medema J.P., *Cell Death Differ.*, **2008**, 15, 947.

Von Hoff D.E., Ervin T.J., Arena F.P., Chiorean E.G., Infante J.R., Moore M.J., Seay T.E., Tjulandin S., Ma W.W., Saleh M.N., Harris M., Reni M., Ramanathan R.K., Tabernero J., Hidalgo M., Van Cutsem E., Goldstein D., Wei X., Iglesias J.L., Renschler M.F., Piper V.G., *N. Engl. J. Med.*, **2013**, 369, 1691.

Wang H., Wang L., Zhang H., Deng P., Chen J., Zhou B., Hu J., Zou J., Lu W., Xiang P., Wu T., Shao X., Li Y., Zhou Z., Zhao Y.L., *Mol. Cancer*, **2013**, 12, 121.

Warburg O., Constable, London, **1930**.

Warrington N.M., Gianino S.M., Jackson E., Goldhoff P., Garbow J.R., Piwnica-Worms D., Gutmann D.H., Rubin J.B., *Cancer Res.*, **2010**, 70, 5717.

Wei H., Mo J., Tao L., Russell R.J., Tymiak A.A., Chen G., Iacob R.E., Engen J.R., *Drug. Discov. Today*, **2014**, 19, 95.

Weiner N.E., Pyles R.B., Chalk C.L., Balko M.G., Miller M.A., Dyer C.A., Warnick R.E., Parysek L.M., *J. Neuropathol. Exp. Neurol.*, **1999**, 58, 54.

Weljie A.M., Jirik F.R., *Int. J. Biochem. Cell Biol.*, **2010**, 43, 981.

Werth M.T., Halouska S., Shortridge M.D., Zhang B., Powers R., *Anal. Biochem.*, **2010**, 399, 56.
West P.R., Weir A.M., Smith A.M., Donley E.L.R., Cezar G.G., *Toxicol. Appl. Pharmacol.*, **2010**, 247, 18.

Williams S.N., Anthony M.L., Brindle K.M., *Magn. Reson. Med.*, **1998**, 40, 411.

Worley B., Halouska S., Powers R., *Anal. Biochem.*, **2013**, 433, 102.

Worley B., Powers R., *Curr. Metabolomics*, **2013**, 1, 92.

Yauch R.L., Dijkgraaf G.J., Alicke B., Januario T., Ahn C.P., Holcomb T., Pujara K., Stinson J., Callahan C.A., Tang T., Bazan J.F., Kan Z., Seshagiri S., Hann C.L., Gould S.E., Low J.A., Rudin C.M., de Sauvage F.J., *Science*, **2009**, 326, 572.

Yoshie T., Nishiumi S., Izumi Y., Sakai A., Inoue J., Azuma T., Yoshida M., *Cancer Sci.*, **2012**, 103, 1010.

Zhang T., Wu X., Yin M., Fan L., Zhang H., Zhao F., Zhang W., Ke C., Zhang G., Hou Y., Zhou X., Lou G., Li K., *Clin. Chim. Acta*, **2012**, 413, 861.

Zhang A., Sun H., Xu H., Qiu S., Wang X., *OMICS*, **2013a**, 17, 495.

Zhang B., Halouska S., Gaupp R., Lei S., Snell E., Fenton R.J., Barletta R.G., Somerville G.A., Powers R., *J. Integr. OMICS*, **2013b**, 2, 120.

Conclusions

NMR spectroscopy represents a versatile technique that is employed in diverse scientific areas, including life science, material science and medicine. It has proved to be a multifaceted tool both for monitoring the progression of olefin metathesis reaction, and for detecting variation in metabolic phenotype of cancer cell culture after drug treatment. In particular, in part A it has been described the detection of a ruthenium-carbene-resorc[4]arene complex produced, as a key intermediate, during an olefin metathesis reaction carried out on a resorc[4]arene bicyclic olefin (namely, **2a**) with $[Ru(=CHPh)Cl_2(PCy_3)_2]$ Grubbs first-generation (G_1ST) catalyst. Although the olefin metathesis reaction on the *chair* stereoisomer **1a** was carried out with the Grubbs second-generation catalyst (G_2ST), for the investigation of mechanistic pathway involved in the dimer **3a** formation from **2a** the G_1ST was used. It is well known that G_2ST initiated much slower than G_1ST, despite the much greater σ-donating ability of SIMes *versus* PCy_3. Instead, the origin of the higher rate of activity of second generation complexes was found to be due to the preference of second generation alkylidenes for alkene over phosphine. The complex was identified by high-resolution (600 MHz) ^1H, ^{31}P NMR and DOSY spectroscopy, in a non-invasive fashion. The singlet at 19.98 ppm (^1H NMR), attributed to

the alkylidene proton in the G_1ST catalyst and that at 53.37 ppm (^{31}P NMR), attributed to the phosphorus atom coordinated with the metal, were selected as probes for a kinetic analysis. They proved to decrease at the expense of the singlets at 19.26 (^{1}H NMR) and 52.68 ppm (^{31}P NMR), diagnostic for the formation of the ruthenium-carbene-resorc[4]arene complex **3a[Ru]**. Such resorc[4]arene activated olefin proved to behave as key propagating species leading to oligomers according to a ROMP pathway. Moreover, the high instability of G_1ST complex in $CDCl_3$, due to the residual acidity of the solvent, induces a fast degradation of the catalyst; a good stability was instead found in benzene-d_6 solutions, even if the reaction is faster in $CDCl_3$. Thank to this higher stability and to the slowness of the reaction, a quantitative analysis was performed, thus highlighting that, beside highly strained and unstrained olefins, macrocycles themselves could be appropriate substrates for a "macrocyclization" reaction, according to a ROM-CM mechanism, and the size of the macrocycles can be modulated by using appropriate substrate/catalyst ratios (**2a**/G_1ST = 4:1 and **2a**/G_1ST = 1:4, respectively). Such structures would have the advantage to share supramolecular properties (e.g., molecular recognition of appropriate guests, propensity to self-assembly) with the intrinsic ability to yield suitable materials for biomedical applications

(namely, drug delivery, tissue engineering and regenerative medicine).

The data presented in part B highlight the potential of ^{1}H NMR based profiling of drug response in cancer cells. Following other methods of functionally annotated profiling, the importance of metabolomics is that it describes the actual functional state of the cells. In the present work, we performed NMR-based metabolomic analysis on human MB DAOY and murine glioma GL261 cell lines before and after GlaB administration. A reliable sample protocol preparation was developed for each cell line in order to perform a trustworthy metabolomics NMR analysis. The procedures can be recapitulated in the following main steps: (i) growth of the cell culture; (ii) cell washing; (iii) cell scraping; (iv) quenching with protease and phosphatase inhibitors; (v) cell lysis by sonication; and (vi) centrifugation. In order to reduce the bias in the interpretation, from five to seven replicates (for both cell lysates and the corresponding conditioned media) were, consequently, analysed by high resolution ^{1}H NMR (900 MHz) spectroscopy. After the resonance assignment of major metabolites (≈ 30 metabolites), the untargeted and unbias multivariate data analytical approach (PCA) on the 1D ^{1}H NMR spectra revealed that both the cell lysates and the conditioned media were completely differentiated from those treated with GlaB along the first principal component (PC1). The

LOOCV method established a discrimination accuracy of the model of 100%. Moreover, we identified for both DAOY and GL261 cell lines characteristic metabolites contributing significantly to distinguishing the metabolic profiles between the treated and the untreated group. Although these are an ongoing studies at their initial stage of advancement, some promising results, summarized below, have been obtained so far: the *exo*- and *endo*-metabolomic phenotype of both the DAOY and GL261 cell line resulted to be completely changed after 24 h and 48 h of GlaB administration, respectively; GlaB administration in DAOY cells seems to promote changes in mitochondrial morphology, respiration and function; GL261 cells after GlaB treatment strongly increased the intake of glucose and the excretion of lactate. These data are not in agreement with the known GLI-mediated extracellular lactate concentration increment. It suggests the presence of a different mechanism of action in no HH/GLI-dependent manner; the levels of most metabolites decreased in both DAOY and GL261 cells after 24 h and 48 h incubation time, consistently with possible apoptosis phenomenon. In order to better evaluate the changes induced before apoptotic events, these data need to be combined with molecular and biological analyses performed on the same cells and the NMR metabolic profiling needs to be performed at different time points of treatment with GlaB (6 h and 12 h for DAOY cells; 12

h and 24 h for GL261 cells). Altogether, our results demonstrate that the metabolome characterisation of tumor cell lines ("oncometabolomics") provides important information about the metabolic changes accompanying cancer progression and response to different environmental conditions (like drugs), which help identify and characterise new therapeutic agents and diagnostic biomarkers.

List of publications

M. Mori; L. Tottone; D. Quaglio; N. Zhdanovskaya; C. Ingallina; M. Fusto; F. Ghirga; G. Peruzzi; M. E. Crestoni; F. Simeoni; F. Giulimondi; C. Talora; B. Botta; I. Screpanti; R. Palermo. *Identification of a novel chalcone derivative that inhibits Notch signaling in T-cell acute lymphoblastic leukemia*. Submitted to **Scientific Reports**.

F. Aiello, F. Balzano, F. Ghirga, I. D'Acquarica, B. Botta, G. Uccello-Barretta, D. Quaglio. *First detection of a ruthenium-carbene resorc[4]arene complex during the progress of a metathesis reaction*. Accepted manuscript online, **EUR. J. Org. Chem**.. DOI: 10.1002/ejoc.201601502.

P. Infante; R. Alfonsi; C. Ingallina; D. Quaglio; F. Ghirga; I. D'Acquarica; F. Bernardi; L. Di Magno; G. Canettieri; I. Screpanti; A. Gulino; B. Botta; M. Mori; L. Di Marcotullio. *Inhibition of Hedgehog-dependent tumors and cancer stem cells by a newly identified naturally occurring chemotype*. **Cell death & Disease** (2016) 7(9):e2376.

I. D' Acquarica; F. Ghirga; C. Ingallina; D. Quaglio; G. Zappia; G. Uccello-Barretta; F. Balzano; B. Botta. *Resorc[4]arenes as Preorganized Synthons for Surface Recognition and Host-Guest Chemistry*. In book: **Calixarenes and Beyond** (2016), pp. 175-193.

I. D'Acquarica; F. Ghirga; D. Quaglio; A. Cerreto; C. Ingallina; A. Tafi; B. Botta. *Molecular recognition of natural products by resorc[4]arene receptors*. **Curr. Pharm. Des.** (2016) 22(12):1715-29.

C. Ingallina; I. D'Acquarica; G. Delle Monache; F. Ghirga; D. Quaglio; P. Ghirga; S. Berardozzi; V. Markovic; B. Botta. *The Pictet-Spengler reaction still on stage*. **Curr. Pharm. Des.** (2016) 22(12):1808-50.

F. Ghirga; D. Quaglio; P. Ghirga; S. Berardozzi; G. Zappia; B. Botta; M. Mori; I. D'Acquarica. *The occurrence of enantioselectivity in nature: the case of (S)-norcoclaurine*. **Chirality** (2016) 28(3):169-80.

F. Ghirga; D. Quaglio; V. Iovine; B. Botta; M. Pierini, L. Mannina; A. P. Sobolev; F. Ugozzoli; I. D' Acquarica. *Synthesis of a Double-Spanned-Resorc[4]arene via Ring-Closing Metathesis and Calculation of Aggregation Propensity*. **J. Org. Chem.** (2014) 79(22):11051-60.

Acknowledgements

Foremost, I would like to express my sincere gratitude to my supervisor Professor Bruno Botta for the continuous support of my Ph.D study and research, for his patience, motivation, enthusiasm, and immense knowledge. His guidance helped me in all the time of research. I could not have imagined having a better supervisor and mentor for my Ph.D study.

In my later work of metabolomics, I am particularly indebted to Professor Paola Turano who provided me an opportunity to join her team as intern, and who gave access to the laboratory and research facilities. Without her precious support it would not be possible to conduct this research.

In addition, I gratefully acknowledge Professor Ilaria D'Acquarica, for her valuable guidance. She definitely provided me with the tools that I needed to choose the right direction and successfully complete my thesis.

I would like to thank Professor Luisa Mannina and Dr. Donatella Capitani (Istituto di Metodologie Chimiche CNR, Monterotondo, Italy) for performing 2D and solid state NMR spectra, respectively, Professor Franco Ugozzoli (Dipartimento di Chimica, Università degli Studi di Parma, Italy) for providing X-ray diffraction data, and Professor Gloria Uccello Barretta (Dipartimento di Chimica e

Chimica Industriale, Università di Pisa) for planning the NMR spectroscopy studies.

A few people have helped and taught me immensely at the Dipartimento di Chimica e Tecnologie del Farmaco (Sapienza Università di Roma, Italy): all the Professor Botta's group, in particular Francesca Ghirga, who believed in me since the first time in the lab. She has been a source of love and energy ever since; Cinzia Ingallina, Simone Berardozzi and Patrizio Ghirga for their support, cooperation and of course friedship.

I would like to express my special thank to Veronica Nasta and Silvia Ciambellotti, for the time spent together and for the best moments ever. Their love, support, and belief in me were a treasure. Real friends treat you like family and they are like sisters to me.

I would also like to thank all of my friends, who supported me in writing, and incented me to strive towards my goal.

Last but not the least, I would like to thank my family: my parents and to my sister for supporting me spiritually throughout writing this thesis and my my life in general. Finally, my deepest gratitude goes to Alessandro for his unflagging love and unconditional support throughout my life and my studies.